Theoretical Advances in Understanding and Designing the Active Sites for Hydrogen Evolution Reaction

Fang Sun[a], Qing Tang*,[a], and De-en Jiang*,[b]

[a] School of Chemistry and Chemical Engineering, Chongqing Key Laboratory of Theoretical and Computational Chemistry, Chongqing University, Chongqing 401331, China

[b] Department of Chemistry, University of California, Riverside, California 92521, United States

*To whom correspondence should be addressed.

E-mail: qingtang@cqu.edu.cn; djiang@ucr.edu

Abstract: As a fundamental step of water splitting and the stepping stone toward exploring other multi-electron transfer processes, the electrocatalytic hydrogen evolution reaction (HER) is a poster child for both fundamental understanding and electrocatalyst design. Here, we review the fundamentals and recent developments of theoretical insights into HER, covering the mechanistic aspects, key activity descriptors, local environment considerations, and advances beyond the computational hydrogen electrode. Although it is experimentally challenging to explore the active sites and mechanisms in the electrocatalytic process, computational and theoretical advances show great potential in identifying active sites and reaction mechanisms. In this review we especially focus in depth on theoretical insights in revealing and designing the active sites for HER. Major challenges ahead will also be discussed at the end.

Keywords: density functional theory, hydrogen evolution reaction, activity descriptors, local environment, active sites

TOC Graphic

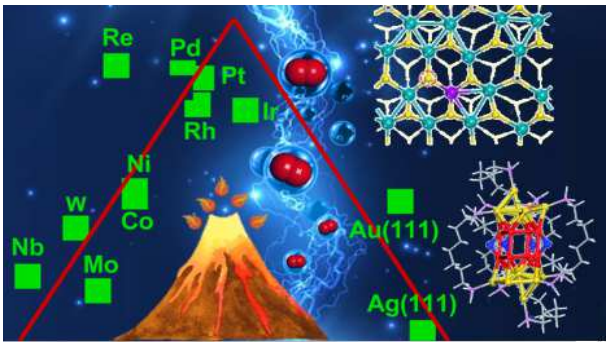

1. Introduction

Hydrogen is a green energy carrier for power and transportation.[1] Using renewable energy to split water and generate hydrogen via hydrogen evolution reaction (HER) is a vital clean-energy technology for a sustainable future. HER is also an important model reaction in understanding electrocatalysis and designing new electrocatalysts.[2] Despite its long history, the study of HER on electrode surfaces has recently gone through a renaissance due to rapid experimental progress at various fronts.[3, 4] In parallel, computational modeling based on density functional theory (DFT) has become a powerful tool in identifying active sites and exploring the mechanisms of catalytic processes at an atomic scale.[2, 5] The correlation between the electronic structure and the electrocatalytic activity can be constructed to achieve a comprehensive understanding of a particular electrocatalytic process.[3, 6, 7] Descriptors such as adsorption free energy of hydrogen, d-band center, and valence-band orbital levels have been widely used in the (semi-)quantitative assessment of the HER electrocatalysts, providing useful guidance for the rational design and synthesis of HER electrocatalysts. Particularly, a descriptor-based volcano plot of the exchange current density vs the adsorption energy[8-10] provides a convenient conceptual framework to rationalize the trends for many different types of electrocatalysts.[6, 11-13]

The computational hydrogen electrode model developed by Nørskov et al.[14] is an elegant way to probe reaction thermodynamics without the need to explicitly deal with the electrode/electrolyte interface.[3, 15, 16] However, the local electrochemical environment such as the electrode potential, the electric double layer, the ion solvation, and *pH* can be important factors during HER.[8, 17] An accurate electrochemical interface model is particularly important for describing these local factors surrounding the active site. In recent years, various methods have been proposed to simulate the electrochemical interfaces,[18-23] but first principles simulation of the electrochemical interface is still facing many challenges.[24, 25]

Several excellent reviews on electrocatalytic HER have been published.[2, 26, 27] They are more on the experimental progress. Here we review and highlight recent advances in the theoretical

understanding of electrocatalytic HER. First, we discuss several fundamental aspects of HER, including the proton–coupled electron transfer, the reaction mechanisms, the kinetic analysis, and some key activity descriptors. Then, we present the applications of DFT-based modeling in identifying HER active sites, considering important local environment such as electrode potential, solvation, *pH* effect, electric field, and H coverage. Finally, major challenges and prospects for future theoretical research are put forward.

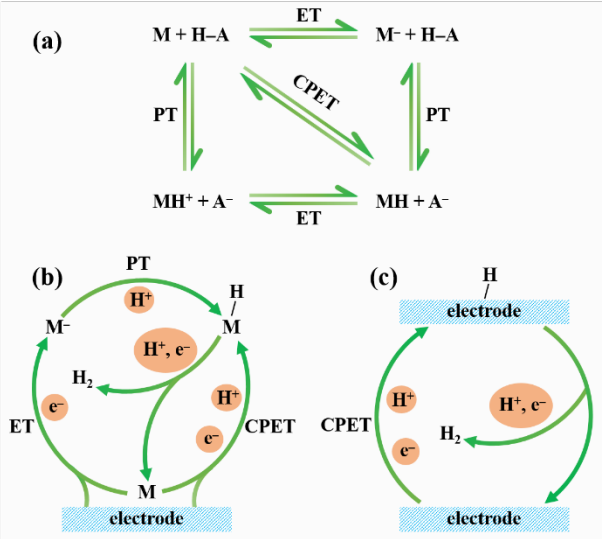

Figure 1. Schematic representations of proton-coupled electron transfer (PCET) processes between M and H-A to form MH and A^-: (a) various scenarios of PCET; (b) PCET in HER; (c) PCET in heterogeneous HER. ET, PT, and CPET represent electron transfer, proton transfer, and concerted proton-electron transfer, respectively.

2. Mechanistic aspects

2.1. Proton–coupled electron transfer. The proton-coupled electron transfer (PCET) plays a central role in many important chemical and biochemical reactions.[28, 29] In electrocatalytic HER, the elementary steps formally involve two proton transfers (PT) and two electron transfers (ET).[30-36] Stepwise ET-PT or PT-ET process and concerted proton-electron transfer (CPET) process are possible (**Figure 1a**). In homogeneous HER (**Figure 1b**), the formation of M-H* species is generally considered to be driven via the ET-PT or CPET mechanism.[37, 38] The heterogeneous HER on an electrode surface is most commonly through the concerted mechanism (**Figure 1c**).[37] In

general, the stepwise ET-PT route forms charged intermediates, while the CPET route tends to have a high barrier.[39] Extensive experimental and computational efforts have been devoted to understanding the kinetics of these processes.[34, 35, 40-47]

2.2. HER mechanisms. HER is the cathodic half-reaction of electrochemical water splitting. It follows a two-step reduction. The initial step is the Volmer reaction, followed by Tafel or Heyrovsky process (**Table 1 and Figure 2**). Solvated protons such as hydronium ions in aqueous systems are the dominant HER reactants in strong acidic solutions.[48-51] In the Volmer step (electrochemical adsorption), the adsorbed H_3O^+ from acidic electrolyte first couples with an electron on the surface to generate an adsorbed H*. Step 2 has two channels: if the H* concentration on the cathode surface is high, two nearby H* can combine to generate H_2 (Tafel step, chemical desorption); otherwise, H* will react with a new set of $H_3O^+ + e^-$ (via PCET) to form H_2 (Heyrovsky step, electrochemical desorption). The overall process is shown in **Figure 2a**. Likewise, the HER mechanism in aqueous alkaline electrolytes can be described as either Volmer-Tafel or Volmer-Heyrovsky pathway with water as the reactant (**Figure 2b**).

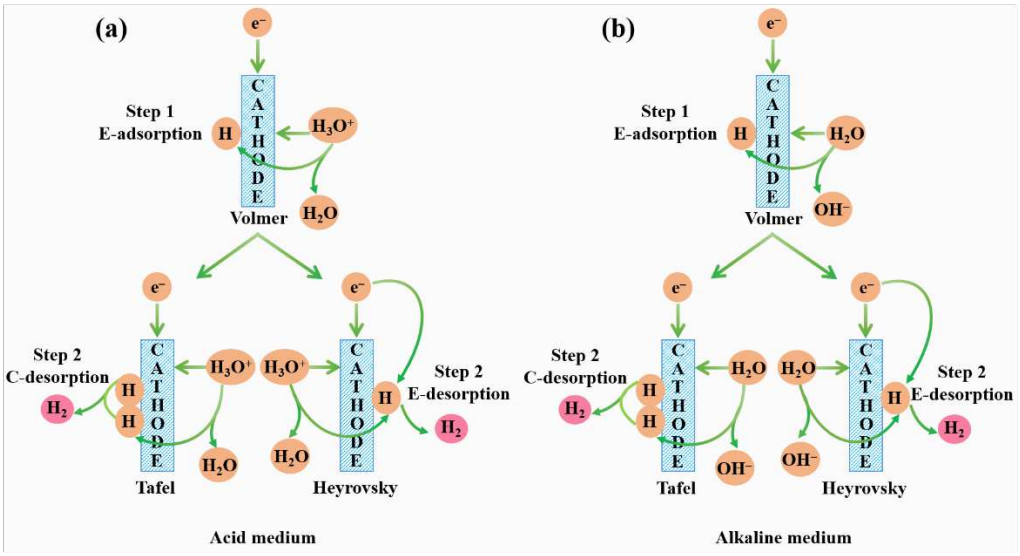

Figure 2. Volmer-Tafel and Volmer-Heyrovsky mechanisms of HER in acidic (a) and alkaline (b) conditions. E-/C- refers to electrochemical/chemical, respectively.

Table 1. Aqueous HER mechanisms (* refers to an active catalytic site).

Medium	Step 1	Step 2	
	Volmer	Tafel	Heyrovsky
Acidic	$H^+ + e^- + * = H^*$	$2H^* = H_2 + 2*$	$H^+ + e^- + H^* = H_2 + *$
Alkaline	$H_2O + e^- + * = H^* + OH^-$	$2H^* = H_2 + 2*$	$H_2O + e^- + H^* = H_2 + * + OH^-$

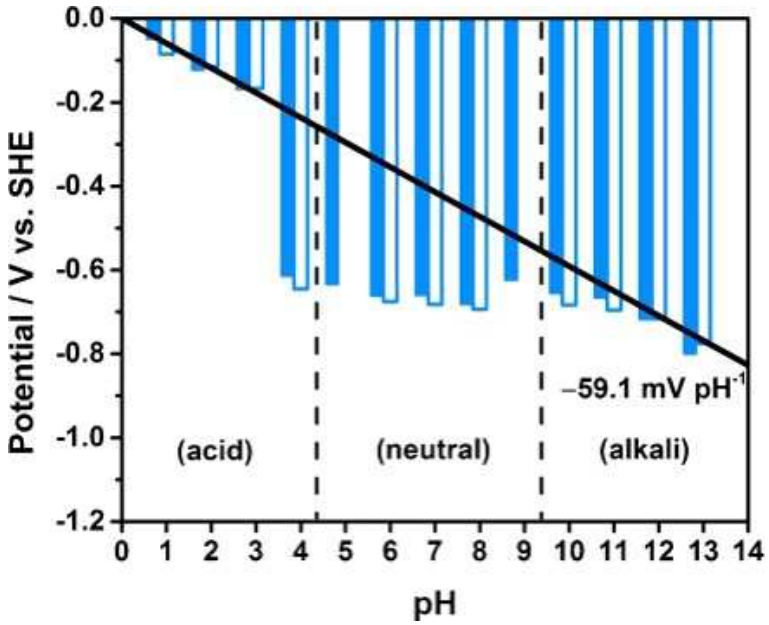

Figure 3. The *pH*-dependence of HER activity on Pt disk (solid) and Pt/C (open) electrodes in 0.5 M Na_2SO_4 electrolyte with H_2. Adapted with permission from ref [52]. Copyright 2014 Wiley.

HER mechanism under neutral and near-neutral conditions is more complex, due to the participation of both H_3O^+ ions and H_2O molecules; the activities depend on many factors, e.g., the type of reactants, buffer species, and concentration of electrolyte.[52-58] Two characteristics have emerged: at relatively low overpotential, H_3O^+ ions are the primary reactant of the first reduction step; at higher overpotential, the dominant reactant changes from H_3O^+ ions to H_2O in the second reduction step.[59] Conway et al.[60] first proposed the switching of reactant from H_3O^+ to H_2O for $pH > 5$. Later, Katsounaros et al. found significant *pH* difference between the electrode surface

and the bulk electrolyte in unbuffered or insufficiently buffered solutions.[61] Takanabe et al. conducted a comprehensive study of HER electrocatalysis in several near-neutral *pH* solutions and found that the required overpotential increases sharply at about *pH*=4, which can be attributed to the reactant switching from H_3O^+ to H_2O (**Figure 3**).[52-55] A feasible strategy for improving HER activity in neutral electrolytes is to facilitate the reductive dissociation of water molecules.

2.3. HER kinetics. Any of the elementary reaction (Volmer, Tafel, or Heyrovsky) could be the rate-determining step (RDS) in HER. Empirically, the Tafel relation $\eta = a + b\,log(i)$ holds, where η is overpotential, i is exchange current density, and b is the Tafel slope. The kinetic expressions and corresponding Tafel slopes are summarized in **Table 2**. In the Volmer-Tafel pathway, the Tafel slope is 118 mV dec^{-1} at 298K when the Volmer step is the RDS, which has been confirmed in experiment (e.g., on Pt and some Pt-group metals).[62] When the Tafel step is the RDS, its slope is 30 mV dec^{-1} at 298K. For the Volmer-Heyrovsky mechanism, the Tafel slopes are 118 mV dec^{-1} for the Volmer RDS and 39 mV dec^{-1} for the Heyrovsky RDS.

Table 2. Kinetic expressions and Tafel slopes for HER at 298 K for different rate-determining steps (RDS). η is overpotential; α and β are symmetric coefficients for HER, $\alpha = \beta = 0.5$.

Mechanism	RDS	Kinetic expression	Tafel slope, b	b at 298 K (mV dec^{-1})
Volmer-Tafel	Volmer	$i = 2i_0[-e^{\frac{-\alpha F}{RT}\eta} + e^{\frac{\beta F}{RT}\eta}]$	$\frac{2.303RT}{\alpha F}$	118
Volmer-Tafel	Tafel	$\eta = \frac{RT}{2F} ln\,(1 + \frac{i}{iT})$	$\frac{2.303RT}{2F}$	30
Volmer-Heyrovsky	Volmer	$i = 2i_0[-e^{\frac{-\alpha F}{RT}\eta} + e^{\frac{(1+\beta)F}{RT}\eta}]$	$\frac{2.303RT}{\alpha F}$	118
Volmer-Heyrovsky	Heyrovsky	$i = 2i_0[-e^{\frac{-(1+\alpha)F}{RT}\eta} + e^{\frac{\beta F}{RT}\eta}]$	$\frac{2.303RT}{(1+\alpha)F}$	39

2.4. Hydrogen adsorption

In HER, adsorption and desorption of H* intermediate on the electrode surface are competing. Based on the Sabatier principle, an excellent HER catalyst should form a strong enough bond with the adsorbed H* to facilitate the PCET, but not too strong to hinder formation and release of H_2.[63] The most ideal case is that ΔG_{H^*} is close to 0 eV.[2, 63] The thermodynamically derived ΔG_{H^*} can be correlated with the exchange current density (j_0, the rate of hydrogen evolution per surface area at the equilibrium potential).[11] Based on the micro-kinetic model, the theoretically calculated j_0 can be represented as:[9]

$$j_0 = Fk^0 C_{total}[(1-\theta)^{1-\alpha}\theta^{\alpha}] \quad (1)$$

where k^0, C_{total}, θ, and α refer to the standard rate constant, the total number of HER active sites on the electrode surface, the coverage of H* intermediate on the surface, and the relative slope of the energy curve at the intersection of initial state and final state, respectively. According to the Langmuir adsorption model, $\theta = (1+K)/K$, where K is the equilibrium constant and can be directly related to the calculated ΔG_{H^*}.

The correlation between ΔG_{H^*} and the experimental j_0 value, first proposed by Parsons, led to the so-called volcano curve, to correlate the energetics of H* intermediate and HER reaction rate.[64] The peak of the volcano corresponds to $\Delta G_{H^*} = 0$. Further, Trasatti found a similar curve between the j_0 value and the metal-H bond strength (**Figure 4a**).[10] Thanks to the rapid development of computing hardware and software in the past couple of decades, predictive modeling based on density functional theory (DFT) allows one to not only understand the HER mechanism and kinetics, but also design the active sites and discover new HER catalysts that can guide the experimental efforts.[2, 5]

3. Density functional theory in electrocatalytic HER

Simulations based on DFT have proven very successful in providing insights into the structure-property correlation of electrochemical processes at the microscopic level.[65] In this section, we focus on the extraordinary progress of DFT computation in electrocatalytic HER.

3.1. Computational hydrogen electrode (CHE). The computational hydrogen electrode (CHE)

introduced by Nørskov and coworkers revolutionized computational electrocatalysis with its computational efficiency and thermodynamic rigor.[14, 15] In the CHE model, the definition of zero voltage is based on the reversible hydrogen electrode (RHE), where the $H^+ + e^- \rightarrow \frac{1}{2} H_2$ reaction is defined as being at equilibrium at U=0, at all values of pH and temperatures. As such, the free energy of the proton-electron pair is half that of the standard H_2 state: $\mu(H^+) + \mu(e^-) = \frac{1}{2} \mu(H_2)$. The value of $\mu(H^+) + \mu(e^-)$ can be further adjusted as a function of the applied potential (U). Since RHE is defined as 0 V at all pH values, no pH correction is required. As such, the CHE approach allows U to be explicitly included in the free energy change of each elementary step (ΔG). This simplified model has been widely used in simulating various electrochemical reactions and, in most cases, allows reliable alignment of theoretical potentials to those measured in experiment. Next, we will focus on the implementations of this model in HER.

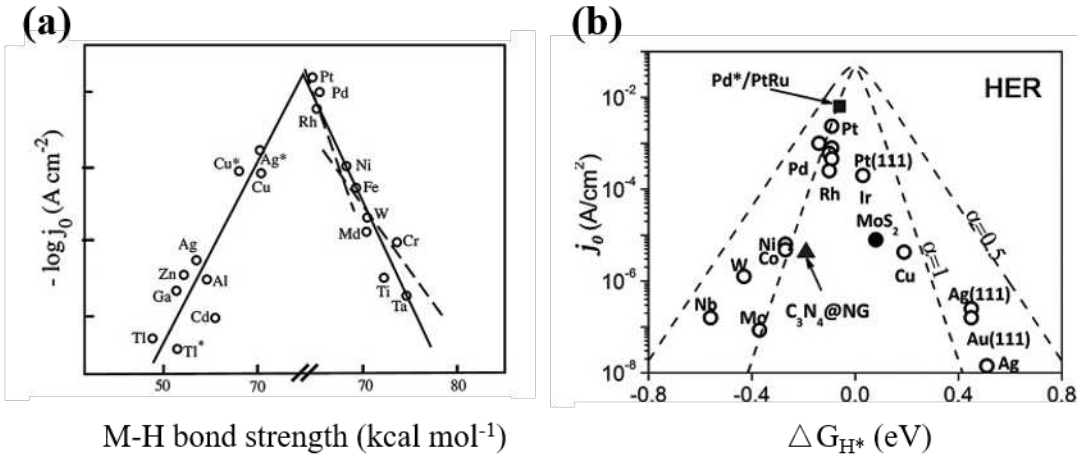

Figure 4. (a) Relationship between measured j_0 and the strength of M-H bond derived from the heat of hydride formation. (b) Dependence of j_0 on calculated ΔG_{H^*} for the wide range of catalyst surfaces. Adapted with permission from ref [2]. Copyright 2015 Wiley.

3.2. Calculating ΔG_{H^*}. As shown in Sec. 2.4, ΔG_{H^*} is an important factor for describing the HER activity. To compute ΔG_{H^*}, we first calculate the hydrogen adsorption energy (ΔE_{H^*}) using the gas-phase H_2 as reference states based on the CHE model,[14]

$$\Delta E_{H*} = E_{(cat.+H*)} - E_{cat.} - \frac{1}{2}E_{H2} \quad (2),$$

where $\Delta E_{(cat.+H*)}$, $\Delta E_{cat.}$, and E_{H2} refer to the total energy of catalyst with adsorbed H, the catalyst itself, and the free H_2 gas, respectively. Next, ΔG_{H*} is computed as follows:[9]

$$\Delta G_{H*} = \Delta E_{H*} + \Delta E_{zpe} - T\Delta S_H \quad (3),$$

where ΔE_{ZPE} is the difference of zero-point energy between adsorbed H* and the gas phase H_2.[65] ΔS_H is the change of entropy from the gas phase H_2 to the adsorbed H*.[66] Under standard condition, ΔS_H is approximately half the entropy of gas-phase H_2. Thanks to its simplicity, ΔG_{H*} from the CHE model has enjoyed wide adoptions.[3] **Figure 4b** shows the volcano curve of j_0 vs calculated ΔG_{H*} for a wide range of catalyst surfaces, demonstrating the power of the CHE.[2]

The CHE model has been very successful in predicting the activities and intermediates of various electrochemical reactions. Although this model is simple and widely used for HER, it oversimplifies several important factors:[67] (1) the free energy of surface configurations is linear with potential, neglecting change in capacitive contributions to the energy;[68, 69] (2) the CHE model neglects the effect from solvent environment, such as the H-bond network in water; (3) the CHE considers only the thermodynamics, while kinetics is equally important.[17] Next we will describe some theoretical advances beyond CHE.

3.3. Applying the potential. ΔG_{H*} from the CHE provides a convenient thermodynamic reference. Further mechanistic insights, especially reaction barriers, can be obtained as a function of the applied potential. Filhol and Neurock proposed charging the surface by adding (subtracting) electrons to a metal slab, using the homogeneous neutralizing background to maintain charge neutrality.[70] To account for the counter-ion, Neurock et al. reported another method by introducing solvated ions in solution or vacuum (**Figure 5a**).[18] Otani[20] and Sugino[21] et al. introduced the effective screening medium by placing the counter charge in a layer outside of the water about 15-20 Å from the electrode. Nørskov et al. used the electrochemical double layer model by adding solvated protons in the water layer, while electrons are distributed on the metal slab (**Figure 5b**).[71] The electrode potential can be tuned by varying the proton/electron concentration.

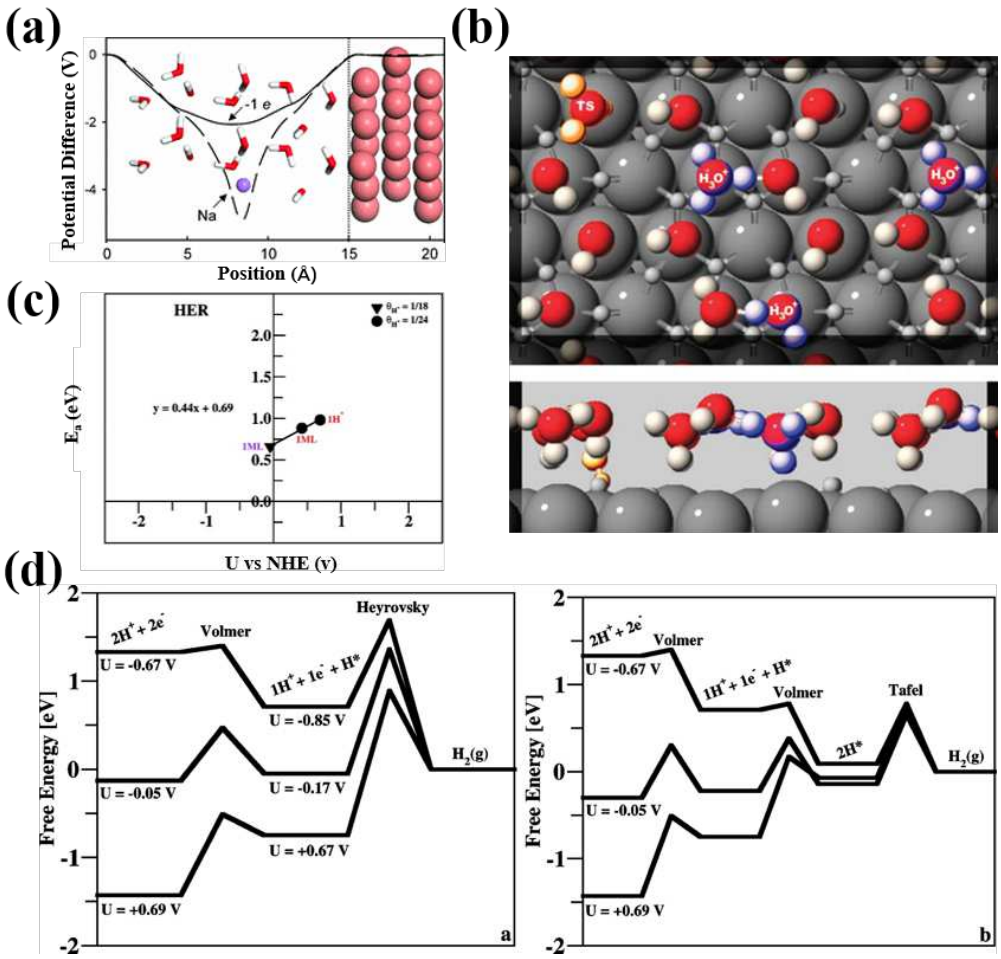

Figure 5. (a) Introducing background charge to the system by solvated ions for simulating electrode potential. Adapted with permission from ref [18]. Copyright 2006 American Physical Society. (b) Top and side view of the model system for electrochemical double layer above Pt(111) electrode. Reproduced with permission from ref [71]. Copyright 2007 Royal Society of Chemistry. (c) Activation barrier (E_a) for the Volmer step as a function of electrode potential (U vs NHE) and (d) standard free energy diagram for the elementary HER steps on Pt(111). Adapted with permission from ref [8]. Copyright 2010 American Chemical Society.

In the Volmer and Heyrovsky steps, the change of the activation energy with the applied potential is more complicated for traditional DFT calculations, due to the great variation of the interfacial polarization between the initial and final states. To address this issue, Nørskov et al.[8] proposed a two-step extrapolation scheme to derive the barrier under different U, such as the

association of E_a for the Volmer step and U in **Figure 5c**: (1) simulate the surface under different U through the tailored number of protons in the first water layer; (2) calculate the barrier under a series of selected unit cell sizes, and then extrapolate these results to the limit where the change in potential, ΔU, approaches zero. Afterwards, the thermodynamics and reaction barriers of the elementary HER steps were used to establish the standard free energy diagrams at different electrode potentials (**Figure 5d**). The calculated HER exchange current using kinetic model that takes the free energy landscape as input shows good agreement with experimental data.[8] Under this scheme, Nørskov et al. later proposed a much simpler way to determine the potential dependence of activation energy that use only (1) one single barrier calculation in an electrochemical environment and (2) the corresponding surface charge at each state (initial state, transition state, and final state).[72, 73] The essence of the idea is that the potential-dependent activation energy can be mathematically expressed by the partial charge transferred in the transition state, which greatly reduces the computational effort for further DFT-based kinetic analysis of the electrochemical reactions beyond HER.

To go beyond the constant-charge method (cnm) discussed above, Liu et al. proposed a constant-potential method (cpm) by using the grand canonical DFT as implemented in the JDFTx code to study the charge effect on the Volmer reaction for 2D materials.[74] They found that cpm and cnm give significantly different values of ΔG_{H^*} for 2D materials, especially at higher U (**Figure 6**). Hence, the surface-charge effect on HER is substantial in 2D materials. Recently, Goddard et al. developed the Grand Canonical Potential Kinetics method (GCP-K) (**Figure 7**), beyond the conventional Butler-Volmer Kinetics, to understand the electrochemical kinetics, which allows for the charge to change continuously to keep the applied voltage (U) constant during the electrochemical process.[75, 76] The GCP-K method enables the U to be fixed by tuning the charges of the system to hold fractional occupations. In fact, the BV scheme can be regarded as a special case of GCP-K in which the electron transfer takes place instantly. The onset potentials predicted by the GCP-K method agree qualitatively with experimental findings. The GCP-K method

provides a theoretical foundation for a new understanding of heterogeneous electrochemistry. Particularly, this method combines fixed charge and fixed potential to allow the reaction barriers to change continuously with the potential, which leads directly to current density versus potential via micro-kinetic calculations and can describe the kinetics for direct comparison with experiment.

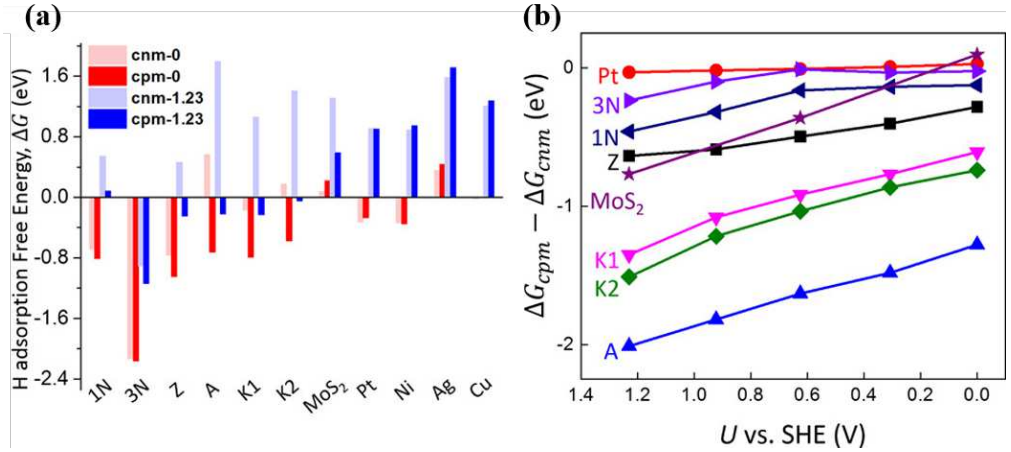

Figure 6. (a) Calculated ΔG_{H^*} on selected 2D electrocatalysts and common 3D metals at $pH = 0$ and U=0/1.23V, using the cnm and cpm method. (b) $|\Delta G_{cpm}H^*-\Delta G_{cnm}H^*|$ as the function of U for various materials. Adapted with permission from ref [74]. Copyright 2018 American Chemical Society.

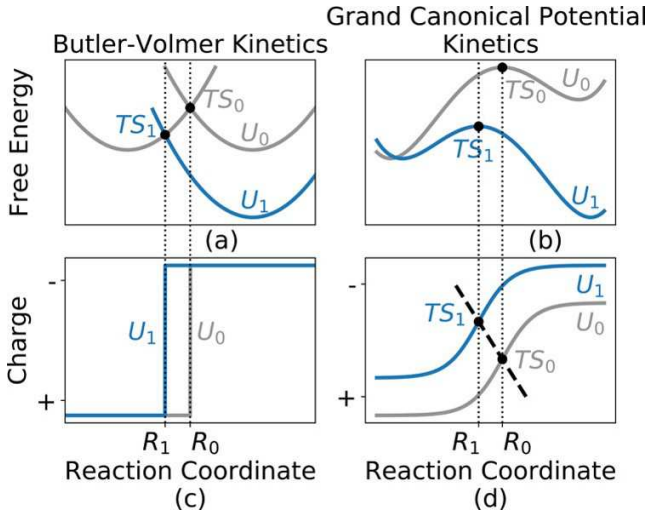

Figure 7. The schematic showing the description of voltage-dependent electrochemical reactions based on BV-K (a, c) and GCP-K (b, d). Adapted with permission from ref [76]. Copyright 2018 American Chemical Society.

3.4. Solvation. The chemical interactions between reaction intermediates and the surrounding solvent play an important role in HER.[8] An important feature of water solvent is that the H-bond network changes dynamically during the reaction, and the commonly used barrier evaluation methods cannot capture this change due to their reliance on the static configuration. There are mainly two methods to add solvation into DFT: explicit solvation and implicit solvation. The explicit method treats water molecules,[23] one or two water bilayers,[77] or complete solvation with several water bilayers explicitly in their DFT model.[17, 78] A great deal of effort has been devoted to water adsorption on the surface of various catalysts, especially Pt(111).[8, 79] The bilayer water was demonstrated in experiment at the solid/liquid interface of Pt (111),[80] which was widely used in the theoretical studies of HER.[8, 71, 78, 81, 82] To obtain an accurate statistical representation of the solvation effect, ab initio molecular dynamics (AIMD) and/or quantum mechanics/molecular mechanics simulations have been used as well.[83-86]

The polarized continuum model (PCM) is the most commonly used implicit solvation model.[87] In this model, the quantum-mechanical solute is embedded in a dielectric cavity surrounded by a continuum dielectric description of the solvent. Hennig et al.[88] implemented the Poisson-Boltzmann implicit solvation in the framework of the plane-wave DFT code VASP to describe the effects of electrostatics, cavitation, and dispersion on the interaction between the solute and the solvent. This approach was used to investigate the H adsorption on the defected MXene surface:[89] compared with the gas-phase model; the inclusion of the Poisson-Boltzmann implicit solvation (permittivity of $\varepsilon = 80$ for water) increases the H adsorption strength by 0.17~0.18 eV, indicating that the solvation contributes to the stability of H* species.

More advanced implicit solvation models treat the fluid distribution as an independent variable and optimizes it based on the interaction of the fluid with the solute. This approach captures the characteristics of the fluid distribution, such as the shell structure and the oscillation of the fluid density on the molecular size scale of the solvent.[25] In practice, integral equation theory usually yields more accurate density distributions, and classical DFT usually yields more accurate

free energy, both of which can be combined with electronic DFT calculations of solutes or electrodes to achieve structured or cavity-free techniques of implicit solvation. For example, the integral equation theory in the reference interaction-site model (RISM) is combined with the electrostatic screening medium (ESM) technique to perform DFT solvation in the ESM-RISM method.[90] Three-dimensional RISM (3D-RISM) is a molecular theory closely related to classical DFT.[91] It describes the local solvent density around a solute using 3D spatial solute-solvent distribution functions, which are obtained via iterative solution of a system of integral equations. Using 3D-RISM, a series of thermodynamic properties and structural information of solvents can be calculated in a relatively short time. In principle, it can be applied to arbitrary solvent compositions and temperatures.

Classical DFT of the solvents and the electronic DFT of the solutes can be combined in joint density functional theory (JDFT) of solvated system.[92, 93] Unlike solvation of integral equations based on approximate coupling of interaction potentials (e.g., pair potentials) between solute and solvent atoms, JDFT directly approximate the free energy of the liquid and coupling terms as functional of the density. Note that the continuum charge-asymmetric nonlocally determined local-electric (CANDLE) solvation model in JDFT adequately describes the basic features of the ideal electrochemical interface (the Gouy–Chapman–Stern model), but misses the nonlinear capacitance effects due to ion adsorption.[94] This requires the inclusion of explicit ions into the quantum-mechanical calculation.

The challenges for implicit solvation are to accurately describe the interfacial region and define the near-surface region boundaries. In explicit DFT solvation, challenges include reducing computational overhead and designing computations in the grand canonical ensemble. For practical simulations, the inclusion of both implicit and localized explicit solvation might achieve a good compromise such that the chemical reactions around the electrochemical interface can be precisely described by QM calculations.

3.5. *pH* Effect. The rate of electrochemical reaction is strongly dependent on solution *pH*. In 2013,

Rossmeisl et al. developed a novel generalization of the CHE to explicitly capture the respective *pH* and potential effects on the electrochemical interface.[95] They determined the ground state interface structure as a function of *pH* and potential based on simple thermodynamic parameters. The basic principle is that for a given metal/solution interface, if the work functions of e^- in metal (ϕ_{e^-}) and the electrochemical potential of protons and electrons ($\mu_{H^+ + e^-}$) are known, the corresponding *pH* can be determined by the following relation:

$$\mu_{H^+ + e^-} = \phi_{e^-}(SHE) - 2.3kT \times pH - \phi_{e^-} \quad (4).$$

At electrochemical equilibrium ($\mu_{H^+ + e^-} = 0$), the free energy of each surface metal atom can be expressed as:

$$G^{int}(\mu_{H^+ + e^-} = 0, \phi_{e^-}) = \frac{G_{N,n} - G_{N,0}}{N} - \frac{1}{2}\frac{n}{N}G_{H_2} \quad (5),$$

where *n* and *N* represent the number of hydrogen and surface metal atoms, respectively. $G_{N,n}$, $G_{N,0}$, and G_{H2} represent the free energy of the metal|solution system, a reference metal system with no ions or adsorbates, and gas-phase H_2 under standard conditions, respectively. G^{int} at another *pH*, i.e., $\mu_{H^+ + e^-} \neq 0$, can be given by a linear extrapolation scheme, as illustrated the blue arrows in **Figure 8a**. It follows from Eq.(6),

$$G^{int}(\mu_{H^+ + e^-}, \phi_{e^-}) = G^{int}(\mu_{H^+ + e^-} = 0, \phi_{e^-}) - \frac{n}{N}\mu_{H^+ + e^-} \quad (6),$$

that under constant ϕ_{e^-}, the change of $\mu_{H^+ + e^-}$ is due to the change of *pH* (red lines in **Figure 8a**). In the original CHE mode (**Figure 8b**), the influence of potential is only considered a posteriori by $\mu_{H^+ + e^-} = -eU_{RHE}$. Rossmeisl's scheme provides a computational approach to include the *pH* effect on electrochemical interface and electrocatalytic activity.

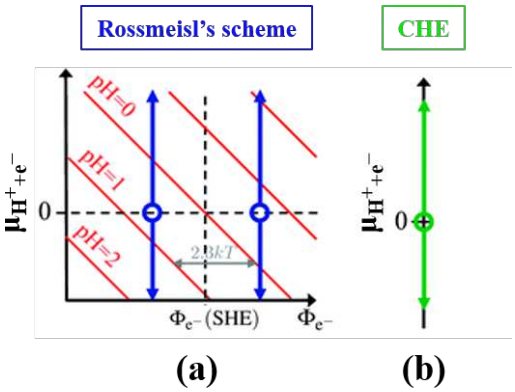

Figure 8. (a) Rossmeisl's scheme vs. (b) the CHE. Adapted with permission from ref [95]. Copyright 2013 the Owner Societies.

HER proceeds several orders of magnitude slower in alkaline media than in acidic solutions.[62, 96-98] Several hypotheses attempt to explain this strong *pH*-dependent activity. First, the H-binding energy varies with the *pH*, resulting in *pH*-effect.[51, 99, 100] Cheng et al. applied AIMD with explicit considerations of solvent and potential (*U*) to study the *pH*-dependent hydrogen binding on Pt(100).[101] They found that water reorientates from parallel position to vertical position as *pH* increases or the potential decreases (**Figure 9a**), which decreases the surface hydrophilicity and enhances the surface binding for H. The predicted increase in hydrogen binding as a function of *pH* well reproduces the experimental observation (**Figure 9b**).[101] The second hypothesis is that the proton donor is *pH* dependent. Rossmeisl et al. suggested that changes in proton configurational entropy cause *pH* dependence.[95] A recent theoretical study by Chan and workers.[102] clearly demonstrated the *pH* effect on the PCET barrier from H_3O^+ and H_2O (**Figure 9c**). Their simulation found that as the *pH* increases, the proton donor shifts from H_3O^+ to H_2O (**Figure 9d**). The resulting theoretical polarization curves and Tafel slopes were qualitatively consistent with the experimental observations. From microkinetic modelling, they proposed that the inherently larger barrier of water splitting compared to H_3O^+ is the cause of the slower HER kinetics in alkaline media than in acidic one.

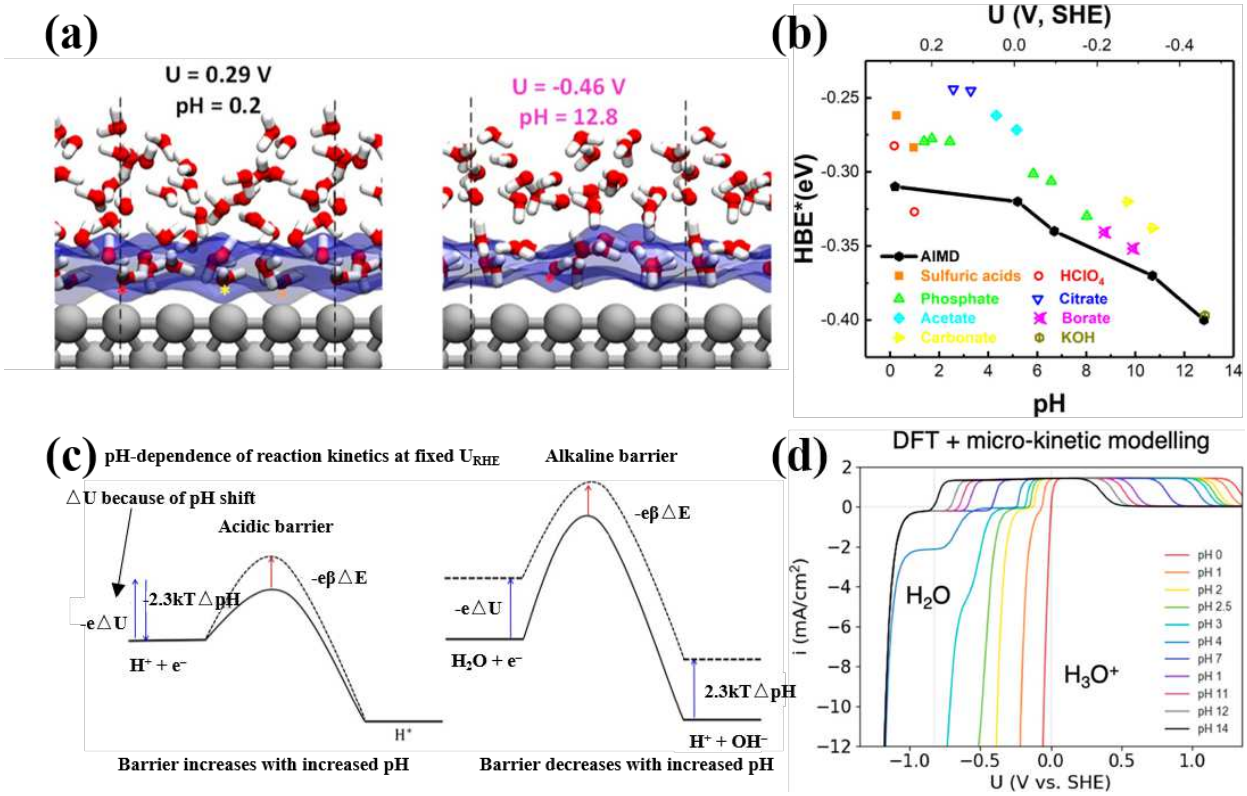

Figure 9. (a) The snapshots with atomic details of the interfaces, and (b) comparison of apparent HBE between QMMD predictions vs. experiment at *pH* ranging from 0.2 to 12.8 or *U* ranging from +0.29 to -0.46 V. Adapted with permission from ref [101]. Copyright 2018 American Chemical Society. (c) The effect of *pH* increases on the PET barrier from H_3O^+ and H_2O, and (d) simulated HER polarization curves at different *pH* using DFT activation energies & micro-kinetic modeling. Adapted with permission from ref [102]. Copyright 2019 American Chemical Society.

The third hypothesis is the *pH*-dependence of water reorganization energy at the electrode/electrolyte interface. This hypothesis stems from a contradictory fact that the H_{upd} peak on Pt (111) shows no significant shift with the *pH*, but there is a significant *pH* dependence of the HER kinetics.[103] The electrochemical measurements by Koper et al. identified that the alkaline H_{upd} peak and HER occur at potentials far from the potential of zero free charge (PZFC), making the interfacial water interact strongly with the interfacial electric field and therefore resulting in higher barrier for water reorganization and proton−electron transfer.[104] They further showed that

modification of the Pt(111) surface with nickel shifts the PZFC by 25 meV, which decreases the interfacial field, lowers the barrier for water reorganization and leads to improved HER kinetics. This hypothesis also implies that the hydrogen binding may not be the only descriptor for HER, and the interfacial electric field could also be important in HER kinetics by influencing the mobility and barrier of interfacial water reorganization.

3.6. H Coverage. Direct experimental determination of hydrogen coverage on a catalyst surface is challenging, so this effect mostly relies on theoretical modeling.[105, 106] Pickering et al. proposed the calculation of hydrogen coverage and the rate constants of HER on metal surfaces from polarization data analysis and showed that the hydrogen coverage (θ_H) increases as the electrode potential becomes more negative (**Figure 10a**).[107] Morikawa et al. investigated the coverage effect on the energetic and vibrational properties of H on Pt (111) surface (**Figure 10b**).[82] They found that at $\theta_H \leq 1$ ML (H prefers the fcc hollow site), the adsorption energy, the Pt-H stretching frequency ($\nu_{Pt\text{-}H}$) and the Pt-H bond length ($d_{Pt\text{-}H}$) show small changes with the coverage. While at $\theta_H > 1$ ML (the fcc hollow sites are fully occupied, and H will appear at the atop site), the adsorption energy and $\nu_{Pt\text{-}H}$ decrease rapidly as θ_H increases, and the corresponding Pt-H bond length is elongated, indicating the repulsive interaction between the absorbed H. The repulsion interaction of terminal H is also reflected in the Frumkin isotherm experiment performed by Kunimatsu et al.[108, 109]

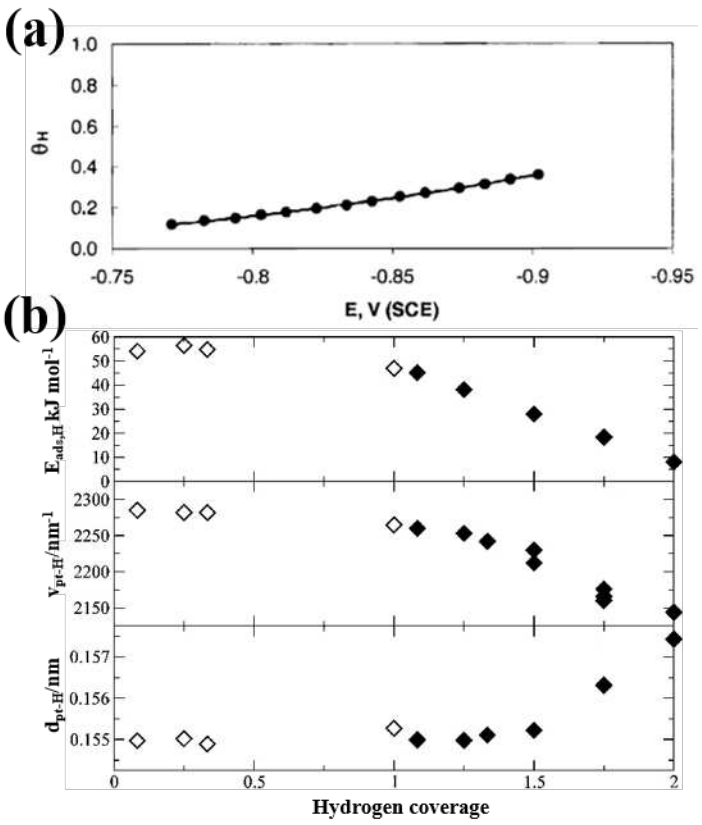

Figure 10. (a) The relation between H-coverage and electrode potential obtained on copper in 0.1 N H_2SO_4 + 0.9 N Na_2SO_4. Adapted with permission from ref [107]. Copyright 2000 the Electrochemical Society. (b) Adsorption energy of hydrogen ($E_{ads,H}$), Pt-H stretching frequency ($\nu_{Pt\text{-}H}$), and Pt-H bond length ($d_{Pt\text{-}H}$) as a function of hydrogen coverage. Adapted with permission from ref [82]. Copyright 2008 American Chemical Society.

3.7. Electric field effect. Physical properties of low-dimensional semiconductor electrocatalysts are sensitive to external electric field which can be used to tune the HER activity. For example, Wang and coworkers conducted an in-depth study on the effect of a gate electric field on electrocatalytic HER based on a backgated 2D MoS_2 working electrode.[110] They found that as the gate voltage increased from 0 to 5 V, both the overpotential and the Tafel slope gradually decreased, which was related to the increased conductivity of MoS_2. This explanation is supported by a recent first-principles computational study.[111] In addition, ΔG_{H^*} has also been found to be sensitive to the electric field: a positive electric field induces electron transfer from H to MoS_2, resulting in

stronger H-MoS_2 bonds, while a negative electric field suppresses electron transfer and weakens H* adsorption.[111] A subsequent study predicted that an external electric field could tailor H* adsorption on MoS_2 defects and edges.[112] In addition, theoretical simulations unveiled that gate-induced injection of excess electrons can stabilize H* bonding on pristine and S-deficient MoS_2.[113-114] The electric field can also adjust the carrier type of the catalyst. For example, theoretical calculations manifested that ΔG_{H^*} of electron-dominated WSe_2 is significantly lower than that of hole-dominated WSe_2, due to charge redistribution induced by electrostatic doping.[115] After hole doping, the adsorption is weakened because the H* will be surrounded by the depletion layer. Conversely, when electrons are doped, the adsorption is enhanced due to the accumulation of electrons around H*.

The electric field can also affect the distribution of reactants in the electrolyte at the interface.[116-118] For example, it was found that as gate voltage changes from 0 to −1 V, overpotential first decreases and then slightly increases, which was attributed to a back gate electric field-induced ion redistribution at VSe_2–electrolyte interface:[119] a negative gate voltage accumulates H_3O^+ on the outer surface of VSe_2. Moreover, the position of the Fermi level of the electrode can be tuned with respect to redox couples in the electrolyte for electrostatic doping.[120] For instance, Zhang et al. observed that as gate voltage increases from 0 to 3 V, the HER overpotential on 2H MoS_2 decreases markedly from 228 to 74 mV.[121] This is because the higher positive gate voltage caused electrons in 2H MoS_2 to occupy a higher energy state through electrostatic coupling, reducing the potential barrier for electrons to traverse from catalyst to reactive species in the electrolyte.

3.8. Descriptors beyond ΔG_{H^*}. As discussed extensively above, ΔG_{H^*} is the key descriptor and widely used to predict the HER performance of many materials. Besides ΔG_{H^*}, some other descriptors have been proposed, which will be discussed below.

3.8.1. d-band Center. The d-band center (ε_d) defined as the central position of the d-orbitals has been widely used to understand and predict the catalytic behavior of transition metals.[122] Taking

the H* adsorption as an example (**Figure 11a**), the localized metal d-electrons are participated in the formation of M-H bonds.[122] The hybridization of H* s-state and the metal d-state will give rise to a low-energy, deep-lying filled bonding state (σ) and a high-energy, partially filled antibonding state (σ*), where the M-H bond strength is determined by the σ* occupancy (the higher the occupancy, the weaker the bonding). Since the energy of the metal d states varies significantly from one metal to the other, the energy level of the anti-bonding states will depend on the specific metal of interest. It is found that ε_d, as a single parameter, is linearly correlated with ΔG_{H^*} on transition metal surface (**Figure 11b**).[5] As a general rule, the closer ε_d to the Fermi level, the higher the anti-bonding level, and thus the stronger the H* adsorption. An optimal HER catalyst should have a moderate ε_d with suitable affinity for H*, as evidenced by the volcano-shaped activity curve.[123, 124]

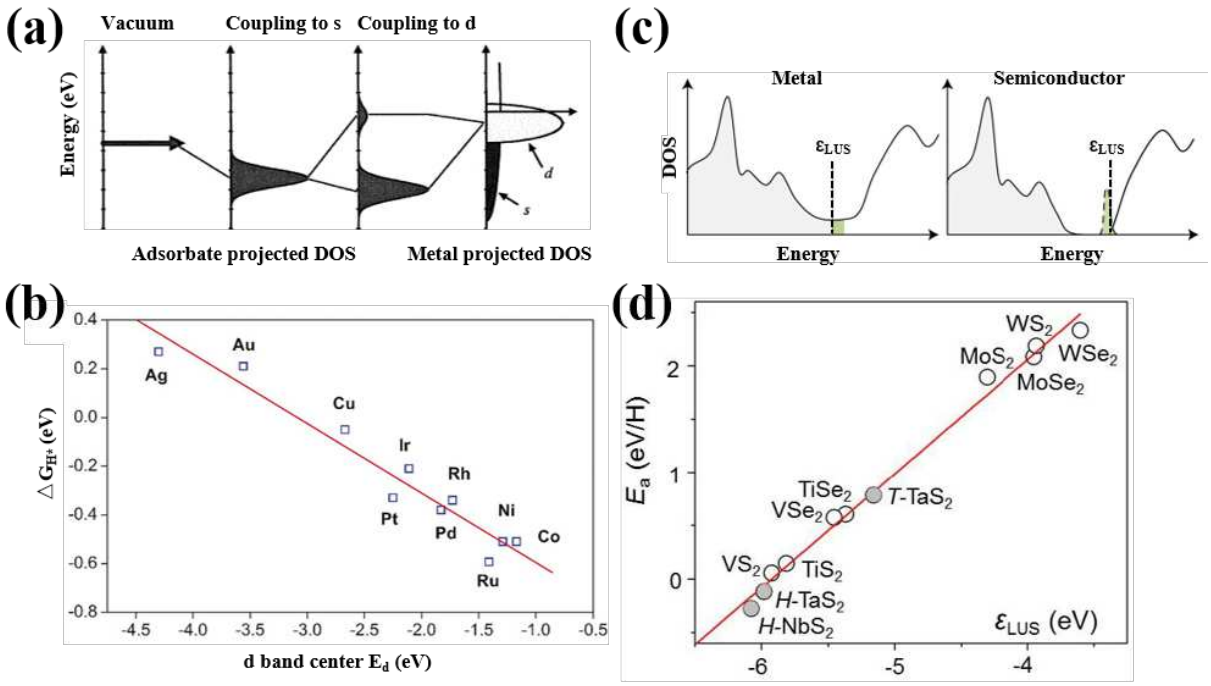

Figure 11. (a) Schematic illustration of the formation of metal-H bond. Adapted with permission from ref [122]. Copyright 2005 Springer. (b) Relations between ε_d with hydrogen binding strength ΔG_{H^*} on transition metals. Adapted with permission from ref [5]. Copyright 2015 Royal Society of Chemistry. (c) Schematic of MX_2 DOS, highlighting initial filled states in grey and newly filled states following H adsorption in green; (d) correlation

between ε_{LUS} and H adsorption energy E_a. Reproduced with permission from ref [125]. Copyright 2017 Macmillan Publishers Limited.

3.8.2. Levels of lowest unoccupied state and valence-band orbital. For transition metal compounds where the adsorption center is not a metal, Liu et al. identified the lowest unoccupied state (ε_{LUS}) as a key descriptor of surface activity of transition metal dichalcogenides (MX_2, X = S, Se, Te; **Figure 11c**). They found that ε_{LUS} is directly correlated with the H adsorption energy (E_H) on all MX_2 surfaces (**Figure 11d**).[125] The metallic MX_2 compounds have lower ε_{LUS} and hence stronger E_a than the semiconducting ones, which led to the discovery of basal-plane-active group-5 MX_2 (*H*-TaS_2 and *H*-NbS_2).

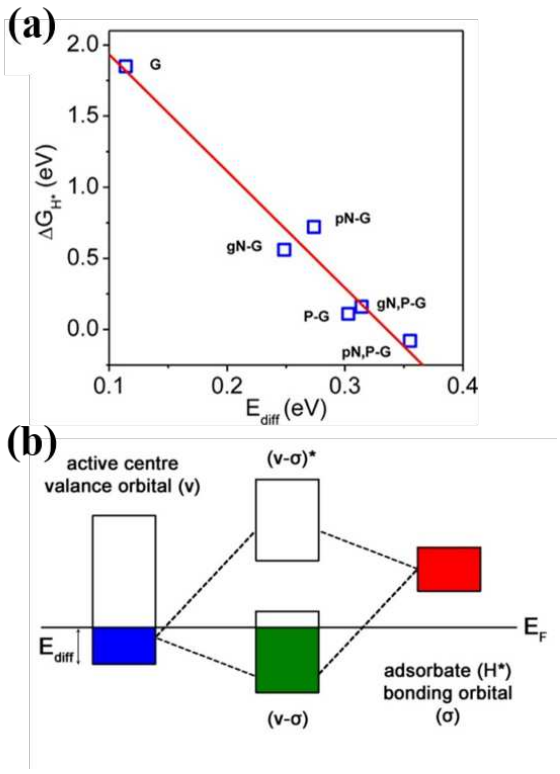

Figure 12. (a) Correlation between ΔG_{H^*} and E_{diff} for various N- and/or P-doped graphene models; (b) Schematic illustration of orbital hybridization between the valence band of active C atom and the bonding σ orbital of adsorbed H*. Adapted with permission from ref [126]. Copyright 2014 American Chemical Society.

Many metal-free catalysts such as carbon-based materials have shown promising HER activity.[2, 127] Using a cluster model and DFT calculations, Qiao et al. investigated the H adsorption on a series of heteroatom-doped graphene and discovered that N/P co-doping can synergistically activate adjacent C atoms to an optimal $|\Delta G_{H^*}|$ of 0.08 eV.[126] They came up with the E_{diff} descriptor, defined as the difference between the lowest valence orbital energy of the C active center and the highest valence orbital energy of the graphene matrix. E_{diff} displays apparent linear correlation with ΔG_{H^*} (**Figure 12a**), and can thus be used to characterize the adsorption behavior. The hybridization between the valence band of the active C atom and the bonding orbital of adsorbed H* leads to the formation of bonding (ν-σ) and anti-bonding (ν-σ)* (**Figure 12b**). Compared to the pristine graphene (inert with highly positive ΔG_{H^*} of 1.85 eV), N and/or P doping leads to the lowering of the C valence orbital, which induces an increase in the filling of the (ν-σ) state and strengthens the C-H interaction to optimize ΔG_{H^*}.

3.8.3. Other descriptors. In 2020, Gao et al. successfully introduced an electronic descriptor (ψ) based on the valence electron numbers and electronegativity of transition metals, the coordination of active sites, and the valence of adsorbates for describing adsorption properties.[128] Soon after, they demonstrated that the ψ descriptor can well explain the adsorption energy of hydrogen as well as HER activity on a variety of catalysts including transition metals, alloys, and single-atom catalysts.[129] Beyond the traditional descriptor determined by the physical or chemical quantities, machine learning (ML), as a critical technique for data mining, is playing a more and more important role in accelerating the discovery of materials via big data. In addition to serving as a powerful means for discovery of electrocatalysts, these data-driven techniques also establish a deeper understanding for the relationships between intrinsic properties of materials and their electrocatalytic performance.[130] For example, Rappe and coworkers used the regularized random forest ML algorithm to discover the relative importance of structure and charge descriptors in determining the HER activity of $Ni_2P(0001)$ under different doping concentrations.[131] They found

that the intuitive Ni−Ni bond length is quite descriptive of HER activity, suggesting that the nonmetallic dopants induce a chemical pressure-like effect on the Ni_3-hollow site. Recently, with the analysis of ML and DFT methods, Wang and coworkers found that various electronic structural properties of metal atoms and the p-band center of surface atoms are the key to governing the HER activity of 2D MA_2Z_4 materials.[132] The rank of the five most important features by the random forest method showed that H adsorption is predominately affected by the electron affinity of the surface atom (ε_Z).

4. Zoom-in on the Active Sites.

Because it is experimentally challenging to locate active sites in catalysis,[133] DFT-based first-principles calculations prove to be an indispensable tool for identifying active sites on the catalyst surface that can be verified by the increasing development of advanced spectroscopy techniques and in situ/operando electrochemical methods.[134] Below we highlight the theoretical insights on the identification of HER active sites in several different types of nanocatalysts.

4.1. On surfaces of bulk materials. Pt is at the top of many volcano curves, so it is not surprising that Pt is one of the most active HER electrocatalysts. In the past few decades, research on the effects of surface structure and particle size of Pt has gradually emerged. DFT calculations by Nørskov[8] and Chen[135] et al. confirmed that the HER reaction on Pt is structurally sensitive, and its activity has a strong correlation with θ_H on different facets. To simulate the effects of low coordination defect sites, Nørskov et al. calculated the H adsorption energy at different θ_H on a number of stepped metal (211) surfaces (**Figure 13a,** in which the number indicates the order of H adsorption).[8] In general, the overall adsorption trend is similar on metal surfaces: the steps are initially occupied; then the terrace will be filled with H at U = 0 V (**Figure 13b-c**). Based on microkinetic modeling and DFT calculations of H adsorption from CHE model, Chen et al. studied the HER kinetics and predicted that the exchange current density (j_0) increased in the order of Pt (111) < Pt (100) ≈ Pt (110).[135] They found that the H atom prefers to occupy the 3-fold fcc hollow

sites on Pt (111), the 2-fold bridge sites on Pt (100), and the short-bridge sites between the adjacent top atom rows on Pt (110). After those preferred sites are filled, H atoms will bind to the on-top sites above 1 ML on Pt (111) and the long-bridge sites between two adjacent Pt atoms next to the rim on Pt (110). In particular, when all surface atoms on the Pt (110) are covered (1ML), the next H* is more likely to bind to the bridge in the valley. On Pt (100), H atoms can occupy all the bridge sites up to 2 ML as each surface atom possesses two bridge sites.

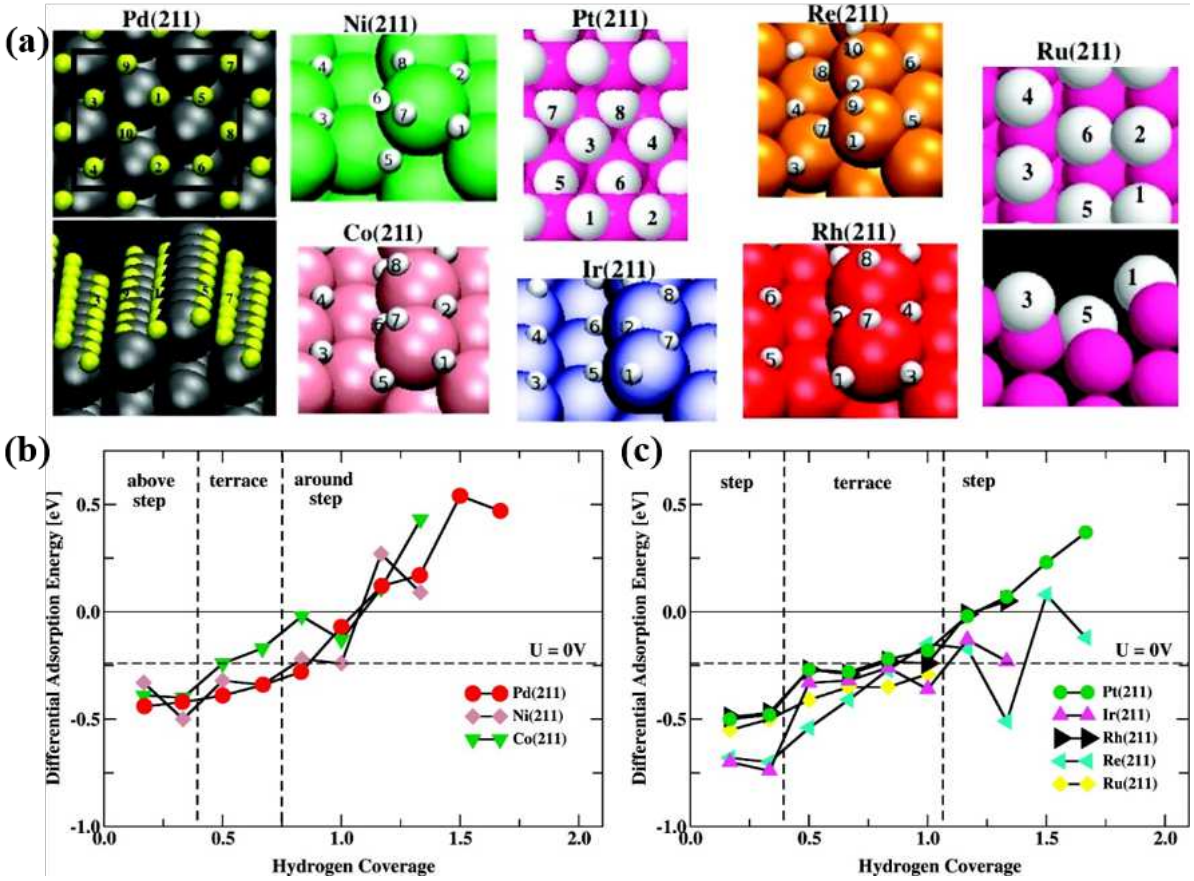

Figure 13. (a) The atomic structures above show the order of H adsorption. (b) and (c) Calculated different H* adsorption energy on a number of stepped surfaces. Adapted with permission from ref [8]. Copyright 2010 American Chemical Society.

Transition metal phosphides (TMPs), nickel phosphides and cobalt phosphides in particular, have emerged as one of the most promising earth-abundant alternatives to noble metals for

HER.[136-138] They also have high acid-stability. In 2005, Liu et al.[139] predicted from DFT that the $Ni_2P(001)$ surface displays potentially higher HER activity than Pt(111) and Ni(111), and the Ni-P bridge site is the preferential site for H adsorption after 1/3 surface coverage of H at the Ni_3 hollow sites. Their prediction was then confirmed by experiments as highly efficient electrocatalyst for HER and water splitting.[138, 140] CoP is another widely studied HER electrocatalyst that exhibits high HER activities in diverse form of morphologies and grain sizes.[141-143] Using DFT and first principles thermodynamics, Hu et al. studied the activity and stability of different crystalline facets of CoP.[144] Among the investigated low-index surfaces, the (111) surface is predicted to be the most promising facet for HER. There are four types of stable H* sites on CoP(111) (**Figure 14a**): the Co-Co bridge sites for the first 25% H coverage; the Co-Co bridge sites and P top sites for 25% to 75% θ_H; and the Co top sites for 75% to 100% θ_H. Their calculations estimated close-to-zero ΔG_{H^*} during 25% ~ 75% θ_H (**Figure 14b**), and suggested H in cobalt bridge sites and P top sites as likely active sites for HER on (111) surface. The synergy between Co and P is important in enhancing the adsorption of H over P site at medium coverage after H pre-occupying the Co site. In another work, the (011) surface of CoP is predicted to have lower surface energy than (111) and is also highly active where the thermo-neutral hydrogen binding is on the P sites rather than the Co sites.[145] By correlating the experimental exchange current density with the DFT calculated ΔG_{H^*}, Jaramillo et al. showed that the TMPs follow the HER volcano relationship and the (101) surface of $Fe_{0.5}Co_{0.5}P$ has more thermo-neutral ΔG_{H^*} and higher activity than pure FeP and CoP.[146] The above works undoubtedly provide important theoretical insights for the demystification of the active sites and the understanding of the mechanism on the surface of bulk materials for HER.

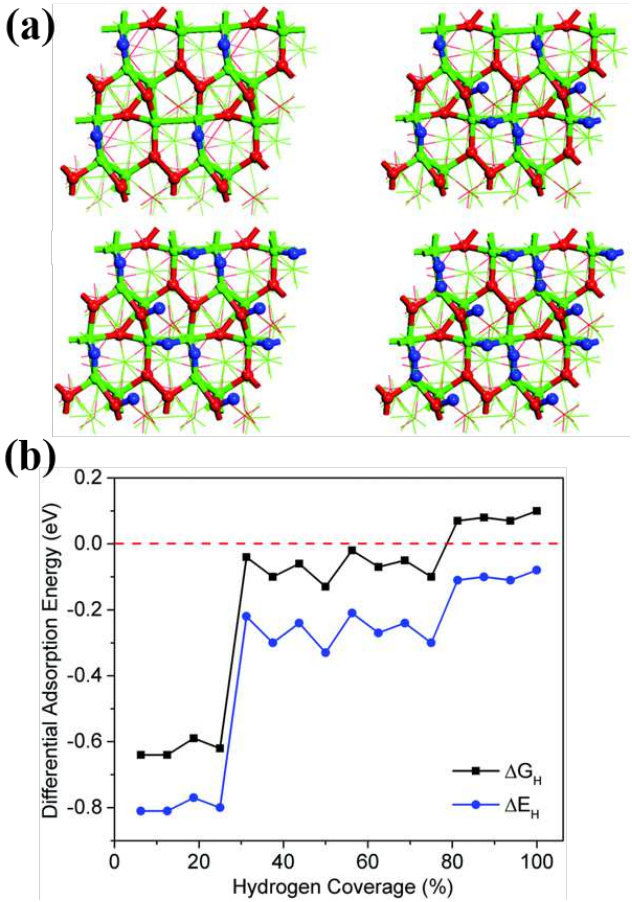

Figure 14. (a) Optimized adsorption configuration on CoP (111) at 25%, 50%, 75% and 100% H coverage, respectively, and (b) the calculations estimated differential energy as a function of hydrogen coverage on CoP(111). Color legend: H, blue; Co, green; P, red. Adapted with permission from ref [144]. Copyright 2016 the Owner Societies.

4.2. 2D materials. Because of their unique physicochemical properties and atomically thin geometry, the 2D materials exhibit many fascinating properties differ from their bulk counterparts and have garnered widespread interest in catalytic energy conversion.[147] Particularly, their ultra-thin thickness enables great design flexibility to tune their catalytic properties via many techniques such as mechanical strain, doping, substrate effects, defect engineering, and ion intercalation.

4.2.1. Transition metal dichalcogenides. The family of transition metal dichalcogenides (TMDs) have aroused particular interest as economical alternatives to accelerate the reaction kinetics in

HER, especially MoS_2.[148-151] The metastable 1T-MoS_2 phase is not found in nature, but can be obtained via phase change induced by chemical or electrochemical Li-intercalation of the more stable hexagonal 2H phase.[152-154] Experiments and theories have reached a consensus that the HER active site of the 2H-MoS_2 polymorph is mainly contributed by its sulfided Mo edge.[155-157] The basal plane of 2H-MoS_2 is inert for HER due to the hindered charge transfer kinetics by its poor conductivity, thereby rendering the basal plane catalytically useless.[156, 157]

Theoretical investigations suggested that the catalytic activity of 2H-MoS_2 can be triggered by heteroatom doping, defect site generation (e.g., S vacancies), strain engineering and heterostructure construction.[156, 158-160] For example, the substitutional doping of 2H MoS_2 with hetero-metal can effectively tune the adsorption behavior of H at the in-plane S atom neighboring the metal dopant and lead to a volcano-shaped activity (**Figure 15a**).[161] Metal dopants such as Pt and Ag bond with only four S atoms, leaving the other two S atoms unsaturated and causing stronger H adsorption; they are the top of the volcano plot with comparable activity to the MoS_2 edge. The high HER stability and activity of single Pt-doped MoS_2 was confirmed experimentally.[161] ΔG_{H^*} of doped MoS_2 can be further optimized by applying compressive strain (**Figure 15b-c**),[162] which weakens the hydrogen binding on the surface S atom next to the doping atom.

Defect engineering is also effective in activating the inert basal plane. Wang et al. evaluated about sixteen types of structural defects, including point defects and grain boundaries (GBs) (**Figure 15d**, defect regions are framed by the dashed line, and the H atom is colored by cyan).[163] Their calculations showed that, in addition to the single S vacancies, other designated defects such as V_{MoS3} and Mo_{S2} point defects, as well as 4|8a, S bridge, and Mo−Mo bond GBs can also greatly improve the in-plane HER activities (**Figure 15e**). In these defects, the Mo atoms around the defect region act as the main active site for hydrogen adsorption. The Mo-H bond strength is mainly determined by the localized d-states of Mo atom under and near the Fermi level. The defect concentration is an important tuning parameter. In the case of S vacancies, the coupling between

S-vacancies leads to the decreased band gap and enhanced H adsorption at the unsaturated Mo site with the increasing number of S vacancies, and the optimal S-vacancy concentration is found to be below 12.5 % for HER.[164] Goddard et al. predicted the potential and pH dependent chemistry for HER at S vacancy of MoS_2 using GCP-K based method. They found that under acidic and alkaline conditions, RDS of reaction is the Volmer step in which the second hydrogen atom is adsorbed at the S vacancy.[76]

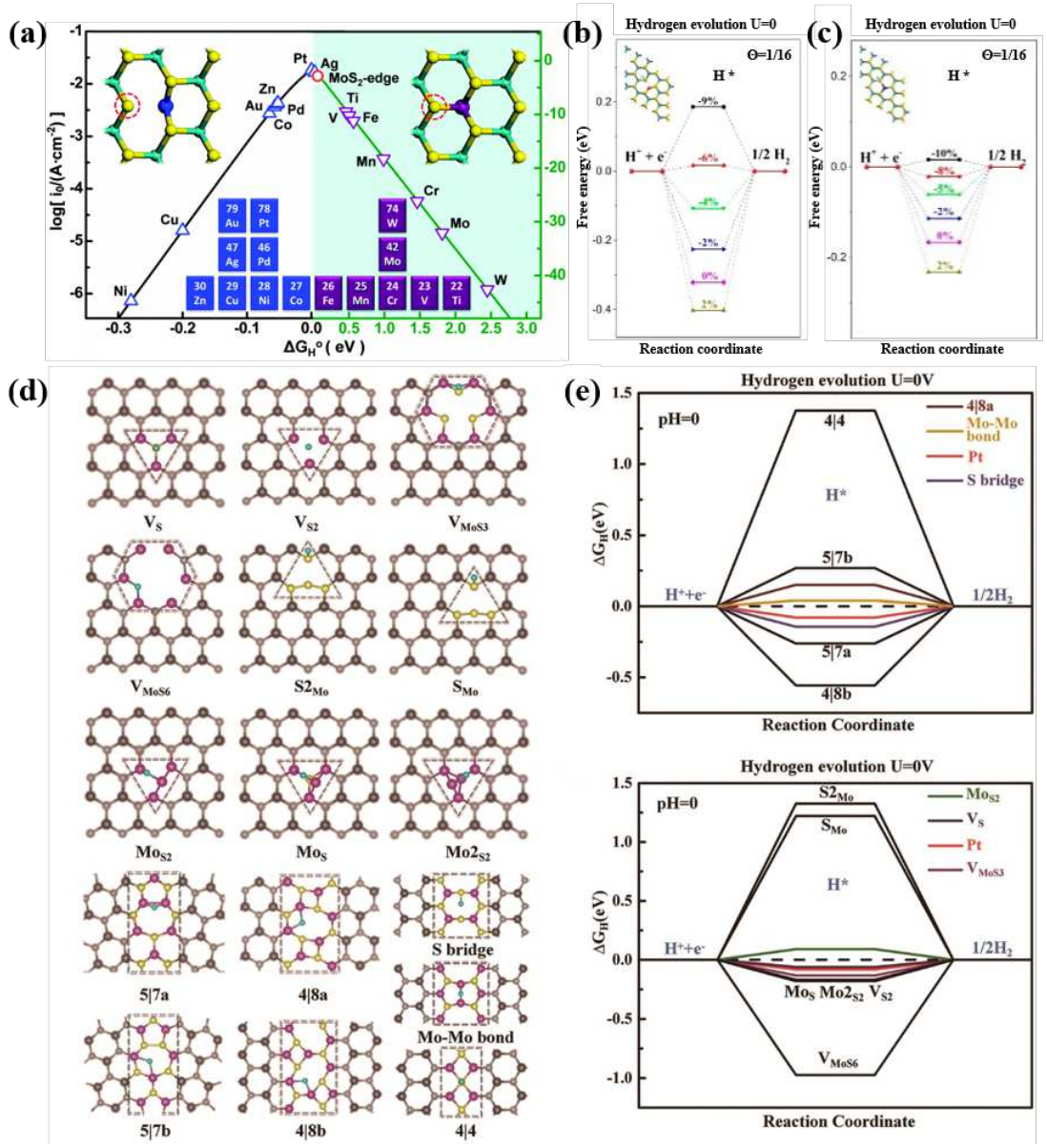

Figure 15. (a) The volcano-shaped relationship of MoS_2 doped with a number of transition metals. Adapted with permission from ref [161]. Copyright 2015 Royal Society of Chemistry. Energetics of HER on Rh (b) and Ag (c)-

doped MoS_2 at different strains. Adapted with permission from ref [162]. Copyright 2016 American Chemical Society. (d) Examples of different structural defects of MoS_2 with one adsorbed H atom (cyan balls) and (e) their corresponding free energy diagram for HER. Adapted with permission from ref [163]. Copyright 2016 American Chemical Society.

The conducting 1T MoS_2 has been demonstrated by many experimental studies to possess appealing activity for HER on both the edge sites and the basal plane, and the much greater active surface area with respect to the metallic edges can thus guarantee its higher performance than 2H MoS_2.[152, 165-172] To elucidate the origin underlying the activity, Tang et al. studied the mechanism of 1T-MoS_2 monolayer with the consideration of explicit solvation with water layer and different proton concentrations,[155] allowing the study of PCET reactions. They showed that the basal plane activity arises from the facile affinity of the surface S atoms for H binding, and predicted an optimal 25% surface H coverage to balance the stability and activity of the 1T structure. Under this θ_H coverage, they examined the barriers of the three elementary reactions (Volmer, Heyrovsky and Tafel steps) at the water/1T-MoS_2 interface and indicated that Volmer-Heyrovsky is the preferred mechanism (**Figure 16a**), in which the Heyrovsky process is the rate-limiting step. The H coverage and aqueous proton concentration are poised to impact on the reaction kinetics. Chen et al. predicted that 1T-MoS_2 would go through the Volmer-Tafel route at a high surface H coverage of 37% and low H_3O^+ concentration.[173] The activity of the surface S sites of 1T-MoS_2 can be tuned and promoted by many approaches, such as substitutional hetero-metal doping (e.g., Mn, Cr, Cu, Ni, Fe) (**Figure 16b-c**), covalent functionalization,[174] and metal intercalation.[175] The insights above into the HER sites of MoS_2 serves as a window on understanding HER on other 2D TMDs.

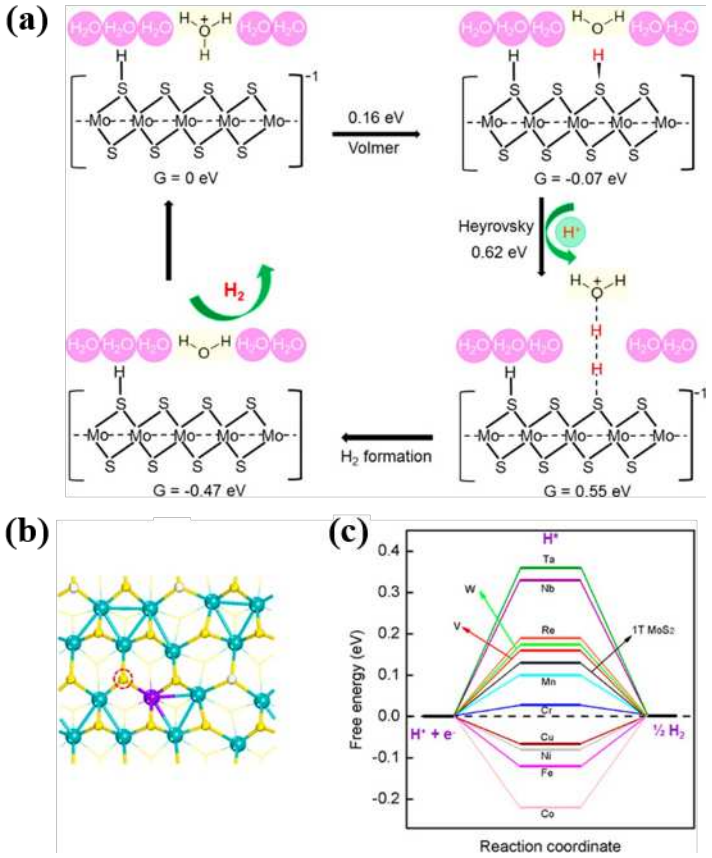

Figure 16. (a) The overall V-H mechanism on the surface of 1T-MoS_2. (b) The monatomic doped 1T-MoS_2 (the dashed circle indicates the surface S site for H adsorption), and (c) corresponding free energy diagram for HER. Adapted with permission from ref [155]. Copyright 2016 American Chemical Society.

4.2.2. MXenes. Discovered in 2011, MXenes are another fast-growing family of 2D materials with a general formula of $M_{n+1}X_nT_x$ (n = 1 to 3), where M stands for early transition metals, X is C and/or N, and T_x is the surface functional groups such as O, OH, or F.[176, 177] They are attractive for catalysis because of their high electrical conductivity, tunable surface terminations and high surface activity. In 2016, Seh et al. reported the first experimental study of MXenes as HER electrocatalyst.[178] Since then, the HER activity of MXenes has been explored substantially by both theory and experiment; the basal-plane O atoms are suggested to be the main active site for HER.[179] Hence, the key to designing high-efficiency MXenes for HER is to tailor the strength of the O-H

bond.

Wang et al. predicted the O-terminated surfaces of monometal carbides/nitrides (Ti_2CO_2, W_2CO_2, Ti_2NO_2, Nb_2NO_2) and bimetallic carbide ($TiVCO_2$) have relatively high HER activity.[180, 181] They proposed a Fermi-abundance model that the occupied p electronic states of surface O atoms play a crucial role in the activity. Pandey et al. screened a large number of O-functionalized M_2X, M_3X_2, and M_4X_3 compositions, and identified several promising candidates (e.g., Sc_2CO_2, $Sc_4C_3O_2$, $V_3C_2O_2$, Cr_2CO_2, $Cr_4C_3O_2$, $Mn_4C_3O_2$, Nb_2NO_2).[182] For chemical modifications, the metal modification has been proposed to be very effective. Wang et al.[183] and Song et al.[184] reported that the HER performance of V_2CO_2 and Cr_2CO_2 MXene can be improved by decorating single atom metal (e.g., Fe, Co, Ni), where the transition metal functions as the promoter. Gan et al. examined the effect of metal decoration on the H adsorption over the surface O active centers that are not directly bonded to the TM atom (the possible active sites under different TM concentration are given in **Figure 17a-c**), and showed that the charge transfer from the decorated metal to surface O would result in the weakened adsorption of H on Mo_2CO_2.[185] A Mn and Fe decoration at 12.5% ML coverage is found to be promising to tune the H adsorption to the optimal value (**Figure 17d-e**). Differently, applying the tensile strain would enhance the O-H binding caused by the up-shifted p electronic states of surface O atoms. They proposed the synergistic effect between TM modification and strain engineering to realize efficient HER on MXene. For defect regulation, Gan et al. studied the intrinsic vacancy defects in M_2CO_2 MXene.[89] Their DFT results showed that single C vacancy would weaken the H adsorption, while M vacancy and M + C vacancy tend to enhance the adsorption. Under this design principle, the single Ta vacancy is good enough to make Ta_2CO_2 an excellent HER electrocatalyst. The combined C vacancy and Zr/Hf vacancy is well suitable for activity optimization of Zr_2CO_2 and Hf_2CO_2. For V_2CO_2 and Cr_2CO_2 with intrinsic very strong H adsorption, double C vacancies modifications are more effective. In addition, the catalytic properties of MXene can be modified by changing the functional groups. Recent studies calculated the catalytic properties of S- and P-functionalized MXenes, and several promising

candidates with HER activities were identified, e.g., S-terminated $Sc_{n+1}N_n$, M_2CP_2 (M = Cr, Mo, W).[186, 187]

We should note that most of the current theoretical predictions and catalyst screening are conducted based on the assumption that the MXenes are functionalized entirely by one uniform functional groups. However, in the synthesis process, the MXene surfaces have very complicated functionalities, which are known to contain mixed functional groups, e.g., the fluorine group is always present in most synthetic procedure. Yet the influence of mixed termination on the basal plane has been largely unexplored in theory, which is important in the modulation of surface stability and reactivity. A recent case study by Zhang et al. showed that the H adsorption free energy on the surface O site of Ti_2CT_x can be largely influenced by the surface F/O ratios.[188] To shed light on the design of truly reliable and robust HER catalyst for practical use, there is an urgent need to develop advanced simulations to capture the plausible surface structures and explore the coverage effect of different functional groups on the HER activity.

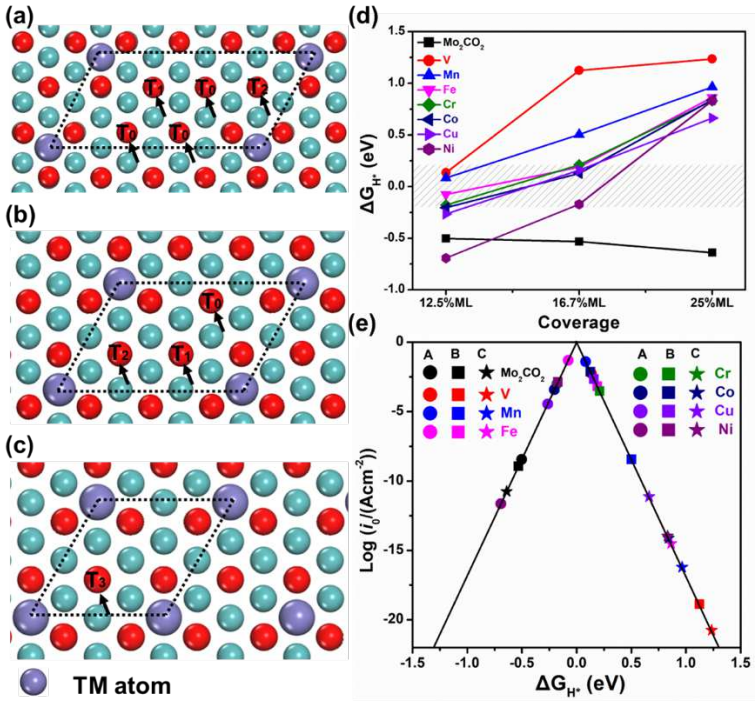

Figure 17. The computational models of 12.5% (a), 16.7% (b), and 25% (c) TM-modified Mo_2CO_2. T_0, T_1, T_2 and T_3 are the active sites, where T represents the O top site, the subscripts (0, 1, 2, 3) represent the number of

surrounding Mo atoms that connected to both the TM atom and the active O atom. The calculated ΔG_{H^*} (d) and volcano curve (e), where A, B and C represent 12.5%, 16.7% and 25% TM coverage. Adapted with permission from ref [185]. Copyright 2020 Wiley-VCH GmbH.

4.2.3. 2D MA_2Z_4. Recently, novel 2D layered $MoSi_2N_4$ and WSi_2N_4 materials were sysnthesized.[189] The 2D $MoSi_2N_4$ has 7 atomic layer thicknesses and the structure can be viewed as a 2H-MoS_2-type MoN_2 layer sandwiched between two InSe-type Si-N bilayers. Unlike the traditional 2D materials, the 2D $MoSi_2N_4$ has no known 3D layered parents and was realized by introducing Si during CVD growth of molybdenum nitride. Its successful synthesis opens up a new synthetic paradigm of realizing 2D vdW materials without existing 3D layered allotropes. This emerging 2D MA_2Z_4 structures are predicted to have intriguing electrocatalytic properties. Chen et al. explored the surface reactivity of MA_2Z_4 monolayers from 42 dynamically stable candidates, and predicted that IVB and VB MA_2Z_4 with N or P termination are promising catalysts for HER.[190] Moreover, by varying the alignment mode of MZ_2 and AZ layers, Liu et al.[191] proposed four types of structural derivatives of MA_2Z_4 (2H-α, 2H-β, 1T-α, 1T-β, **Figure 18a**). Among the constructed 144 MA_2Z_4 materials from the combination of M (Ti, V, Cr, Zr, Nb, Mo, Hf, Ta, W), A (Si, Ge) and Z (N, P), they screened out seven metallic MA_2Z_4 that are highly active for HER (**Figure 18b**), where the outmost N or P layers have optimal $|\Delta G_{H^*}|$ (< 0.1 eV) at a low H coverage <25%. The 2H-α-VGe_2N_4 is the closest to the volcano peak with ΔG_{H^*} of 0.01eV. They found that the electrocatalytic activity is closely correlated to the lowest unoccupied state energy (E_{LUS}) of MA_2Z_4 (**Figure 18c**), which influence the electron filling and eventually determine the binding strength of H. The range of E_{LUS} from −6.0 to −5.6 eV is suggested as a good descriptor for activity screening of 2D MA_2Z_4 materials. Thus far, the development of the 2D MA_2Z_4 family is still in their early infancy, the intriguing properties are mainly predicted from theory. Future efforts are highly expected to synthesize these novel MA_2Z_4 and apply them to HER and other catalytic reactions.

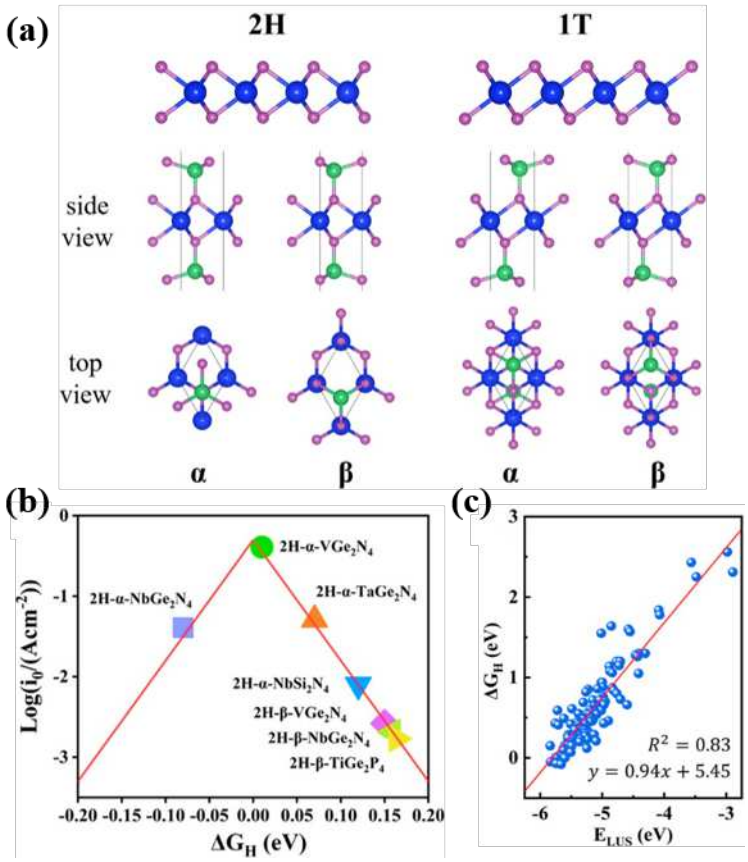

Figure 18. (a) Four types of structural configurations of MA_2Z_4. (b) Dependence of the exchange current density on calculated ΔG_{H^*} for the seven promising screened catalysts. (c) ΔG_{H^*} versus the E_{LUS} for a 2 × 2 supercell of MA_2Z_4. Adapted with permission from ref [191]. Copyright 2021 American Chemical Society.

4.2.4. Metal-free 2D catalysts. Another type of eye-attracting 2D electrocatalysts for HER is the metal-free catalysts. The graphitic carbon nitride (g-C_3N_4) has received great attention due to its abundance and high stability. The pure g-C_3N_4 is a semiconductor and shows negligible activity for HER. In this regard, Qiao et al.[13] reported the enhanced HER performance of g-C_3N_4 by chemical coupling of g-C_3N_4 with nitrogen-doped graphene (C_3N_4@NG). According to the predicted volcano curve, the C_3N_4@NG hybrid (ΔG_{H^*} of -0.19 eV) demonstrated a comparable electrocatalytic activity to the existing metallic catalysts (**Figure 19a**). In the preferred adsorption configuration, each H* bonds with two pyridinic-N in one tri-s-triazine periodic unit to form a C_2N_3H heteroring (**Figure 19b-d**). At low o4verpotential, a C_3N_4@NG unit cell prefers to adsorb

only one H* in view of its smallest $|\Delta G_{H^*}|$, yielding a mediated adsorption-desorption behavior at θ_H of 0.33 (**Figure 19b**). A followed up theoretical study by Du et al. further pointed that the improved hydrogen binding on the hybrid C_3N_4@NG is attributed to the interlayer charge-transfer induced strain in g-C_3N_4 monolayer.[192] Such an atomic-level HER insight on the C_3N_4@NG surface clearly reveals the reason for its amazing electrocatalytic activity.

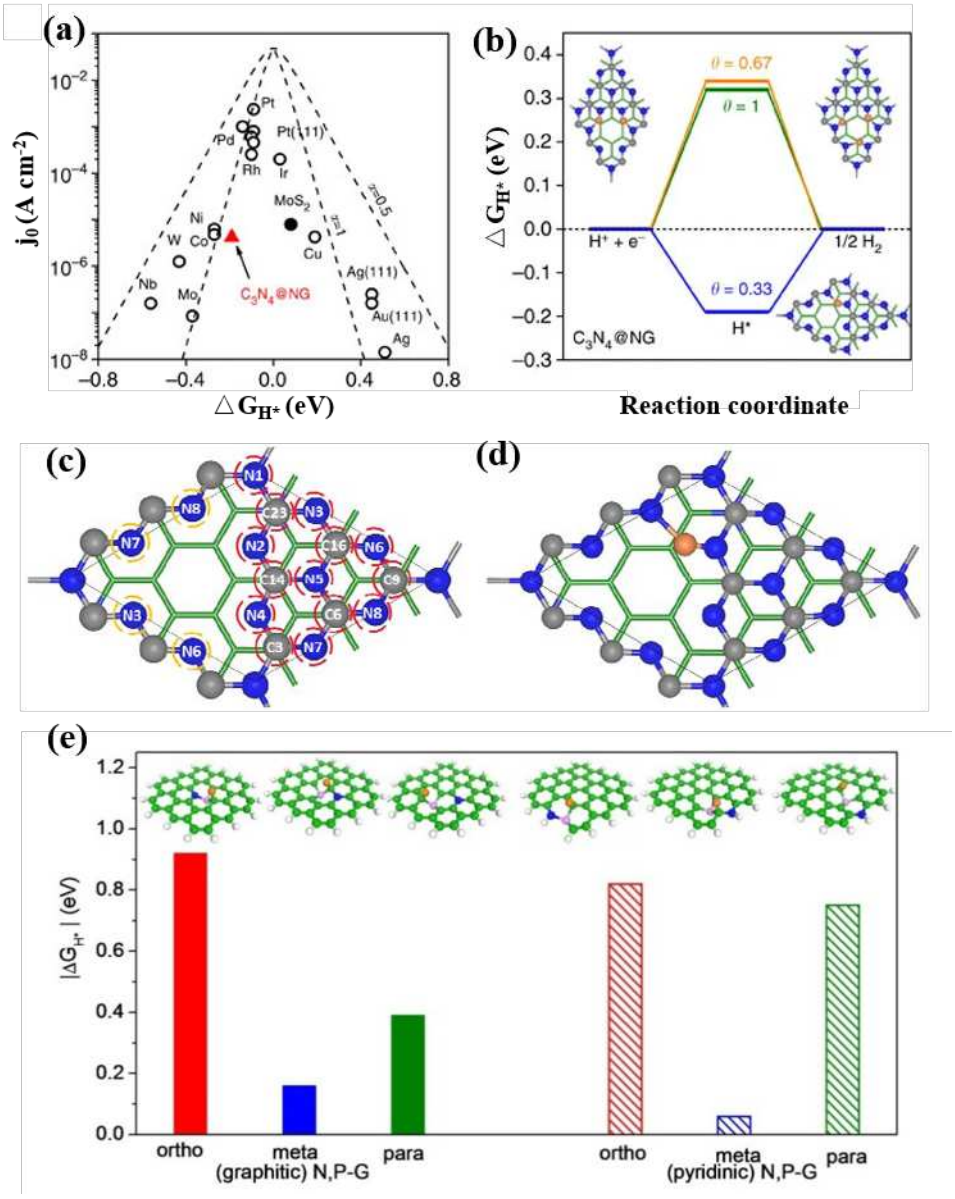

Figure 19. (a) The volcano plot for C_3N_4@NG (red triangle) and other common catalysts. (b) Calculated HER diagrams on C_3N_4@NG under different H* coverage. (c) Possible H* adsorption sites (red circles) and (d) the most stable H* adsorption pattern on C_3N_4@NG. Adapted with permission from ref [13]. Copyright 2014

Macmillan Publishers Limited. (e) ΔG_{H^*} and active sites (inset) on different graphitic/pyridinic-N,P dual-doped graphene. Ortho, Meta, and Para represents the relative positions of heteroatoms (N, blue; P, pink) in one benzene heteroring. Adapted with permission from ref [126]. Copyright 2014 American Chemical Society.

Graphene is a more well-known 2D material. However, the pristine graphene surface reveals little electrochemical activity, and the activity of the basal plane C atom can be initiated by heteroatom doping. Based on theoretical predictions, Qiao et al. discussed the trend of H* adsorption on different N,P co-doped graphene configurations with pyridinic or graphitic N groups as nonmetallic electrocatalysts for H_2 production.[126] In these models, the C atom between meta-type N and P dual-doped in the heteroring acts as the most active site for H* binding (**Figure 19e**). The N and P heteroatoms can co-activate the adjacent C atom in the graphene matrix by tuning its valence orbital energy levels and inducing a synergistic enhancement. Their predictions are successfully verified by their experimental results.

Furthermore, the monolayer phosphorene derived from layered black phosphorous (BP) is another fascinating metal-free catalyst for hydrogen evolution.[193, 194] Like graphene, the perfect phosphorene is also catalytically inert in its basal plane. The unfavorable H binding results from the electron-rich surfaces linked to the lone-pair states of sp^3 hybridized P atoms. There has been much effort in recent studies to improve hydrogen adsorption to boost the HER activity. Cai et al.[195] and Lu et al.[196] found that phosphorene can serve as a superior HER catalyst via the creation of atomic vacancy defects and exposed edges. However, a significant drawback that places restriction on the practical applications of phosphorene is its poor stability, which can be easily degraded upon exposure to air, water and light. To make phosphorene a truly realistic catalyst, not only the surface activity but also the structural stability need to be improved. Covalent functionalization has been demonstrated to be effective in improving the stability and protecting exfoliated BP from degradation.[197] Cheng et al. showed that NH_2-functionalized BP outperforms the un-functionalized bulk BP for electrocatalytic hydrogen evolution at a low overpotential.[193]

Zhou et al. performed DFT calculations to reveal the activity origin of functionalized phosphorene.[198] They explored three types of aryl groups, 4-nitrophenyl (4NP), 4-methoxyphenyl (4MP) and 4-aminophenyl (4AP), and found that the formation of a new P-C bond via covalent functionalization is accompanied by the breaking of an intralayer P-P bond (**Figure 20**). The under-coordinated sublayer P atom with unsaturated dangling bonds becomes active and greatly enhances the H adsorption (H is colored by green in **Figure 20a**). The HER activity of modified BP is mainly affected by the coverage of functional groups. The optimal coverage is found to be 8.33%, such that a small ΔG_{H^*} close to thermo-neutral can be achieved (**Figure 20b**). These understanding indicate that surface modification could be a promising strategy in enhancing both the stability and activity of phosphorene, which can be applied to other 2D cousins of phosphorene, such as arsenene, antimonene and bismuthene.

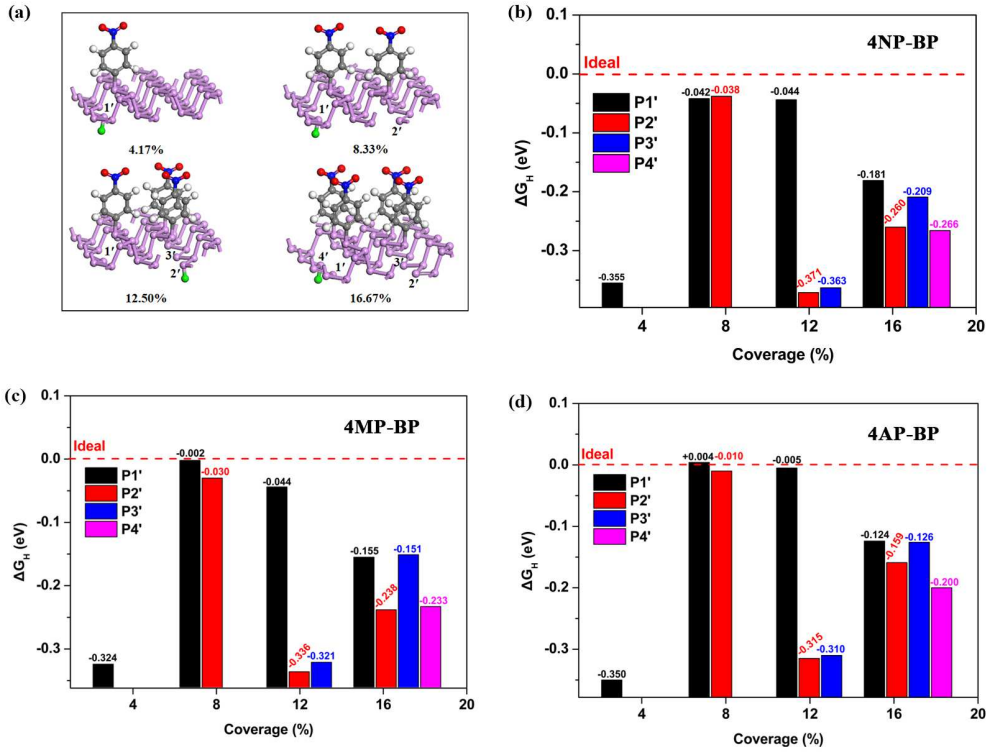

Figure 20. (a) The H adsorption sites on the functionalized BP at different coverage (only the lowest energy H adsorption sites are given), the green balls represent H atoms. (b) to (d) corresponds to the calculated ΔG_{H^*} at different sublayer P sites of functionalized BP by 4-nitrophenyl (4NP), 4-methoxyphenyl (4MP) and 4-

aminophenyl (4AP) groups at different coverage. Adapted with permission from ref [198]. Copyright 2021 American Chemical Society.

4.3. 0D materials or nanoclusters. As compared to the conventional metal nanoparticles (NPs), atomically precise ligand-protected metal nanoclusters (NCs), also known as ultra-small NCs, can provide unprecedented opportunities to elucidate the structure-property relationships and active-sites at the atomic level derived from their well-defined structures of both the core and the surface with atomic precision.[199] Additionally, its ultrasmall size about 1 nm allows computational simulation of realistic NCs-adsorbate systems.[200-202] Recently, a bimetallic $[PtAu_{24}(SR)_{18}]$ NC (1.1 nm) was first explored by Kwak et al. as an HER electrocatalyst, exhibiting an exceptionally higher catalytic activity than state-of-the-art Pt/C catalysts.[203] The Pt dopant is at the central location, which can significantly modulate the electronic properties of this NC system from 8e in un-doped $[Au_{25}(SR)_{18}]^{-1}$ to 6e in $[PtAu_{24}(SR)_{18}]^{0}$ and finely tune the redox potentials and binding affinity during the catalytic process. The implicit solvation DFT calculation was employed to investigate the origin of the extraordinary catalytic activity of $PtAu_{24}$. The combined experimental and theoretical analysis revealed that the Volmer-Heyrovsky route is the thermodynamically preferred path for H_2 generation on $PtAu_{24}$ (**Figure 21**): the reduced $[PtAu_{24}]^{2-}$ species firstly reacts with one proton to form an $[H\text{-}PtAu_{24}]^{-}$ intermediate with a ΔE_1 of -0.059 eV, and then the hydrogen adsorbed on $[H\text{-}PtAu_{24}]^{-}$ is coupled with another proton from the solution to generate H_2 with a ΔE_{2b} of -0.155 eV. The H prefers to occupy the surface hollow site of the $PtAu_{12}$ core, which will spontaneously migrate from subsurface to interact directly with the central Pt atom via breaking some surface Au-Au bonds, rendering a significantly shorter H-Pt bond (1.788 Å) than surface H-Au bond (2.031 Å). This result underlines that $H\text{-}Pt_{center}$ bond formation is a facile process, and the stronger affinity of Pt_{center} with H is a crucial factor in the favored HER activity observed in experiment.

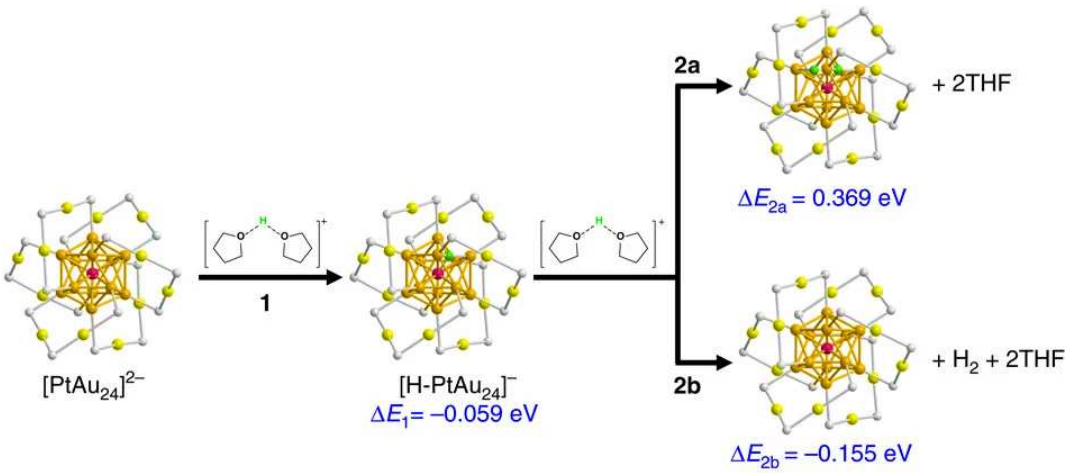

Figure 21. DFT computed results of H_2 evolution via Volmer-Heyrovsky (1-2b) and Volmer-Tafel (1-2a) route on $PtAu_{24}$ NC catalyst. Adapted with permission from ref [203]. Copyright 2017 Springer Nature Limited.

Motivated by this seminal experimental work, the Jiang's group then computationally studied how exactly H interacts with different charge states $[Au_{25}(SR)_{18}]^q$ (q = -1, 0, 1) and mono-atom-doped bimetallic $[M_1Au_{24}(SR)_{18}]^q$ clusters (M = Pt, Pd, Ag, Cu, Hg or Cd; q = -2, -1, 0, +1).[204] For the $[Au_{25}(SR)_{18}]^q$ system, H prefers to absorb onto the bridge site associated with two core-coated Au atoms on the $[Au_{25}(SR)_{18}]^-$ surface, while the hollow site of the surface of the Au_{13} nucleus is energetically more favored for H on $[Au_{25}(SR)_{18}]^0$ and $[Au_{25}(SR)_{18}]^+$ (**Figure 22a**). The H bonding strength of $[Au_{25}(SR)_{18}]^q$ followed an order of 0> +1 > -1, with optimized H-Au_{center} distances of 1.979, 1.967, and 3.049 Å, respectively. For the central-doped Pt/Pd atom in NC, they found that 6e $[PtAu_{24}(SR)_{18}]^0$ and $[PdAu_{24}(SR)_{18}]^0$ readily adsorb two H atoms to become an 8e superatom, being isoelectronic to $[PtAu_{24}(SR)_{18}]^{2-}$ and $[PdAu_{24}(SR)_{18}]^{2-}$. **Figure 22b** shows the optimized H* adsorption configuration on $[PtAu_{24}(SR)_{18}]^0$, where two H atoms prefer to occupy the opposite sides of the Pt center. The Pt-H interaction will cause geometrical distortion of the metal core. The Cu or Ag dopant can replace three different positions (center-doped, surface-doped, and staple-doped). The calculations predict three different H* binding sites for the three isomers of $[CuAu_{24}(SR)_{18}]^0$ (**Figure 22c**), similar to the $[AgAu_{24}H(SR)_{18}]^0$. The energetics of H adsorption indicate that $PtAu_{24}(SR)_{18}$ is the best candidate for HER with the lowest ΔG_{H^*}, followed by

$PdAu_{24}(SR)_{18}$ and center-doped $CuAu_{24}(SR)_{18}$. The experimental studies by Lee et al.[205] observed a higher HER rate in $PtAu_{24}$ than $PdAu_{24}$ NC, which is in good agreement with Jiang's predictions. They also observed the same trend in HER for a larger Au_{36} NCs.[205] The electrocatalytic potential of $CuAu_{24}(SR)_{18}$ needs to be tested experimentally in future. Particularly, another interesting finding from their calculations is that H behaves as a metal and contributes its 1s electron to the superatomic free-electron count of the Au_{25} NCs, which differs from the case of H in Cu or Ag NCs acting only as a hydride ligand. This is because the electronegativity of H is smaller than Au but larger than Ag and Cu.

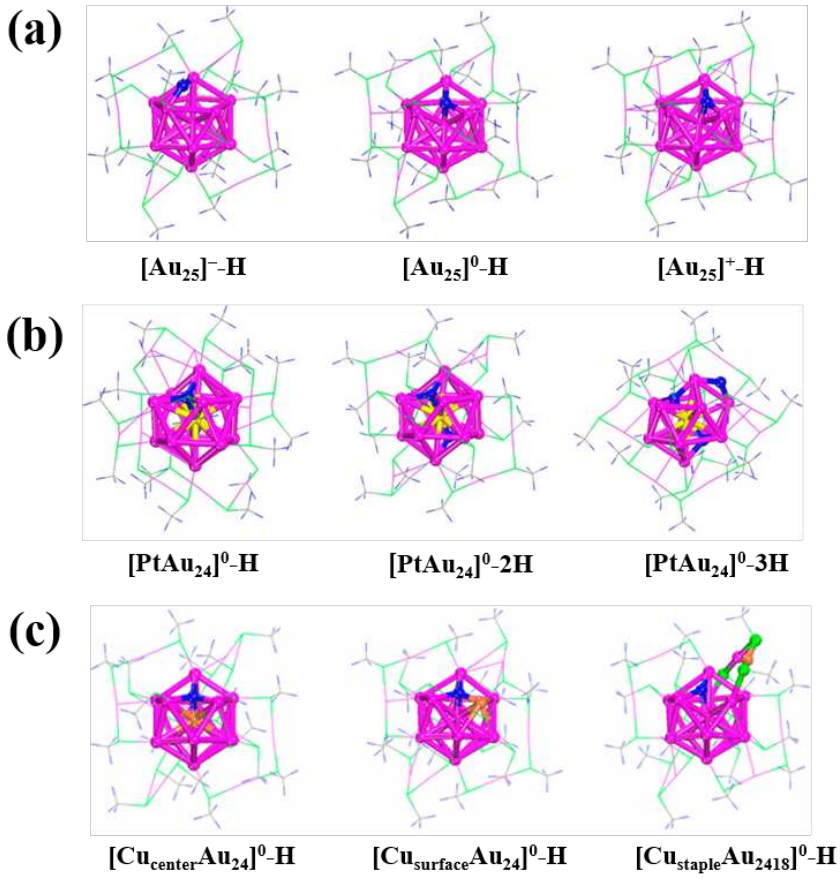

Figure 22. Optimized structures of different charge states $[Au_{25}(SCH_3)_{18}]^q$ (a) and Pt/Cu-doped bimetallic $[M_1Au_{24}(SCH_3)_{18}]^0$ (b, c) with adsorbed H atom. Protecting motifs are showed in line mode. Color legend: Au, colored magenta; Pt, yellow; Cu, orange; C, grey; S, green; H, blue. Adapted with permission from ref [204]. Copyright 2017 American Chemical Society.

Unlike the fully protected Au NCs discussed above, the diphosphine-capped Au_{22} NC is structurally unique in that this cluster is partially protected with the exposure of eight coordination unsaturated (cus) Au sites, also known as in situ non-coordinated sites, at the interface of two Au_{11} units.[206] These cus sites have been identified as the catalytic active sites for CO and O_2 adsorption.[207-209] Jiang et al. found that these unsaturated sites also offer unique opportunities for H adsorption.[210] Their DFT results (**Figure 23**) indicated that Au_{22} can adsorb up to six H atoms with favorable energetics for HER. The first four H atoms prefer to occupy the long-bridge sites of the cus Au atoms, showing a moderate barrier to activate and dissociate H_2 and favorable energetics of H adsorption (ΔG_{H^*} ~ -0.40 to 0.10 eV). After the eight cus Au atoms are fully passivated by H, the fifth and the sixth H atoms would adsorb at the bridge Au atoms at the opposite ends of this cluster protected by phosphine ligands. The charge analysis indicates that the adsorbed H in Au_{22} NC behaves as a negatively charged hydride, which is different from the near-neutral metallic H in thiolate-passivated Au NCs. This suggests that the behavior of H in gold NCs may depend on the type of ligand used. The Tsukuda's group[211] and Wang's group[212] subsequently made great progress in experimentally detecting the presence of negative H in several hydride-doped gold nanoclusters by various spectrometry techniques. Recently, a dramatic advance in synthesis has led to the successful isolation and characterization of a $[Au_{22}H_4(dppo)_6]^{2+}$ nanohydride cluster.[213] The four H atoms are found to be located in the bridging positions, which is exactly the same as the prediction by Jiang et al.[210]

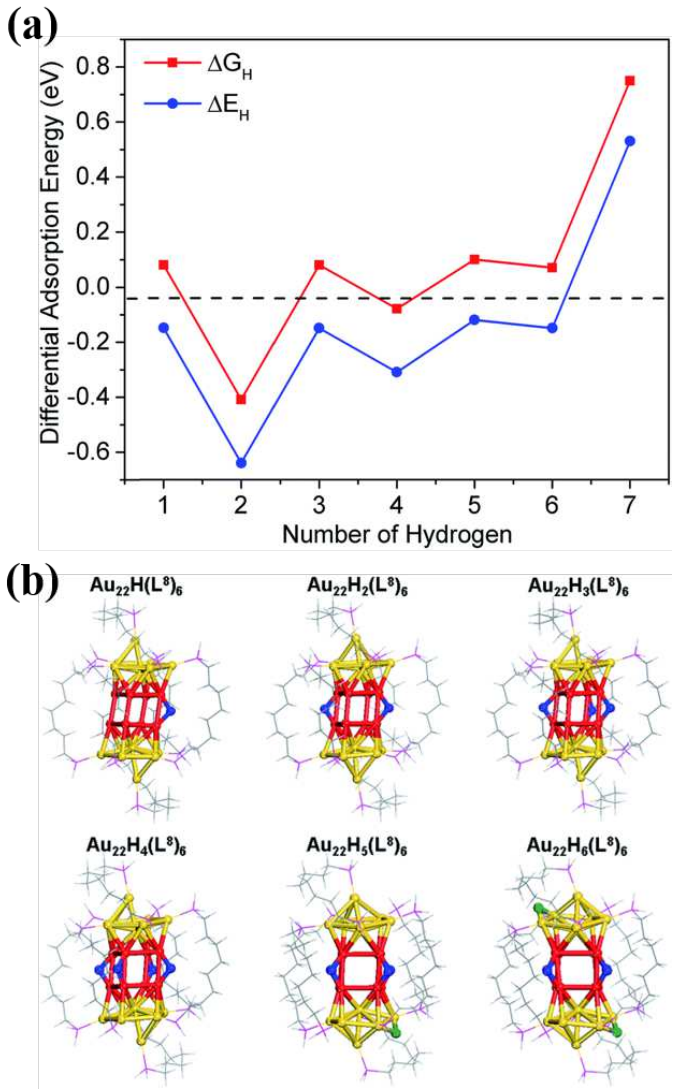

Figure 23. (a) ΔG_{H^*} (red) and ΔE_{H^*} (blue) as a function of the number of H atoms adsorbed on Au_{22} cluster, and their corresponding structures with adsorbed H atom (b). Cus Au, red; other Au, yellow; H at the cus Au sites, blue; H at the non-cus Au sites, green; other H, light grey; P, magenta; C, grey. Adapted with permission from ref [210]. Copyright 2018 Royal Society of Chemistry.

Just recently, Jin et al.[214] reported a trimeric $Au_{36}Ag_2(SR)_{18}$ NC with low ligand coverage for catalyzing HER efficiently where three icosahedral (I_h) units are face-fused together in a cyclic manner. This NC exhibits higher HER catalytic performance and lower overpotential than the monomeric $Au_{25}(SR)_{18}^-$ and dimeric $Au_{38}(SR)_{24}$ NC (**Figure 24a-b)**. Its higher activity is found to

be related to the low ligand-to-metal ratio, the lower-coordinated Au atoms and unfilled 20e superatomic orbitals. DFT calculations reveal that the trimeric NC exhibits thermodynamically favorable hydrogen binding for the rate-determining Volmer step (ΔG_{H^*} = 0.83 eV vs 1.29 eV in $Au_{25}(SR)_{18}^-$ and 1.35 eV in $Au_{38}(SR)_{24}$, **Figure 24c**). The greater negative electron affinity of $Au_{36}Ag_2(SR)_{18}$ (EA = −2.65 eV vs 0.41 eV for $Au_{25}(SR)_{18}^-$ and -2.31 eV for $Au_{38}(SR)_{24}$) could also be a reason for its higher activity, which is crucial for the enhanced proton coupled electron transfer. The most feasible active site for H* formation on this NC is the exposed Au atom on each I_h unit of the fused $Au_{27}Ag_2$ shell (**Figure 24d-e**). This work suggests a design prospect to tune the HER activity of metal NCs by tailoring the geometrical and electronic structures. Note that the atomically precise metal NCs are a unique type of model catalysts. The promising examples we showed here are only the beginning of their electrocatalytic applications in HER. The available large number of NCs provide many opportunities to establish the structure-activity correlation and find the active site descriptor in NC-based HER, which need much more future efforts from the interplay of both theory and experiment.

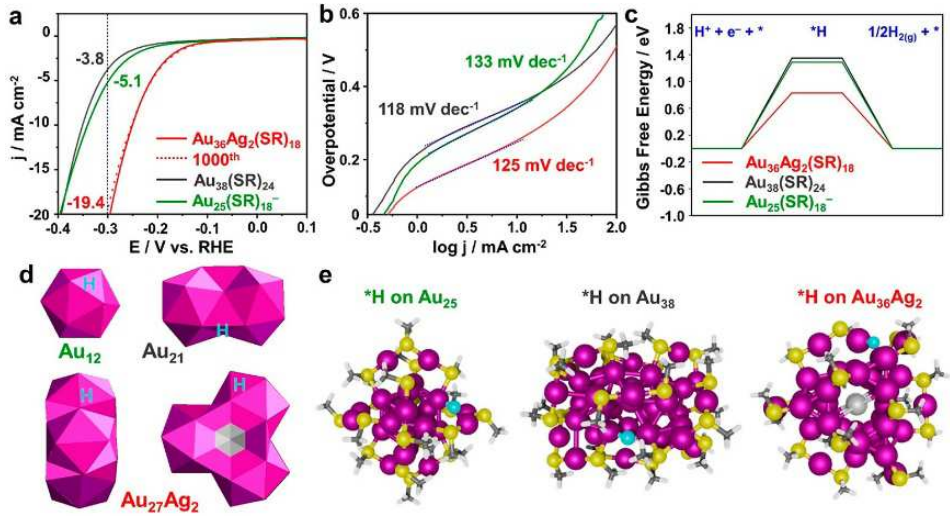

Figure 24. (a) HER voltammograms, (b) Tafel plots, (c) calculated ΔG_{H^*}, (d) illustrated kernel surfaces for H* adsorption, and (e) relaxed structures with adsorbed H on the NC catalysts. Au, magenta; Ag, light gray; S, yellow; adsorbed H, cyan; C, gray; other H, white. Adapted with permission from ref [214]. Copyright 2021 American Chemical Society.

Larger ligand-free nanoparticles (NPs) have been studied for HER as well, with size, shape, and facet being three key factors.[215,216,217] Core-shell construction is another strategy, as shown by a high-throughput screening study.[218] The reader is referred to a recent review[215] on this topic. In the same spirit of the atomically precise nanoclusters discussed above, the ideal system for coupling theory and experiment here involves the realization of well-defined NPs up to a few nanometers in size.[219]

4.4. Single atom catalysts. Single-atom catalysts (SACs) are regarded as the smallest size-limit of metal nanoparticles/nanoclusters, which are a new research frontier in heterogeneous electrocatalysis.[220-223] They have been explosively studied due to their 100% atom utilization, excellent catalytic performance and convenient separation.[224-226] The individual and uniformly dispersed atom on SACs acts as the active catalytic center, which provides ideal models for accurately monitoring the HER kinetics at an atomic level.[227] So far, M-N_X and M-C_X have been developed as appropriate active sites for HER, and are expected to become promising alternatives to the commercial Pt/C catalysts.[228-230] Recently, the synthesis and applications of SACs have been summarized in several excellent reviews.[223, 231-233] For example, Li et al. reviewed the up-to-date atomic active centers and the existing synthetic strategies, focusing on the influence of diverse active centers (e.g., one metal atom, hetero dual-atom and non-metal atom) and coordination configurations on the HER activity at the atomic scale.[231] Gong et al.[232] and Li et al.[223] summarized the theoretical understanding of the stability, electronic structures, metal-support interaction and their intrinsic connection to the catalytic performances of SACs for various chemical reactions. The coordination environment is found to be important in the regulation of active center electronic structure and adsorption of reaction intermediate and thereby tuning the catalytic properties.[234] Given that these reviews provide detailed summaries of the nature of the active sites, we will not dwell on the details of such materials here. Below we will select several typical studies to illustrate the applications of SACs for HER, namely noble Pt-based SAC, non-precious Co- based SAC, N-doped graphene supported metal SACs, and non-metal single-iodine-atom electrocatalysts.

Compared with the conventional Pt-based catalysts, Pt-based SACs anchored in a conductive matrix have attracted intense interest due to the low precious metal loading.[235-239] In 2019, Song et al. demonstrate that the atomically dispersed Pt immobilized on an nanosized onion-like carbon (OLC) matrix, i.e. curved supports, can be used as a highly active electrocatalyst for HER.[240] Their simulations with the PtO_2C_{295} model extracted from the experimental characterization suggested that H atoms show strong bonding to the unsaturated Pt. When three H atoms are adsorbed, the calculated ΔG_H is adjusted to -0.01 eV (**Figure 25a**). Based on this, they argued that the active body on the catalyst formed in situ may be H_2Pt_1/OLC. The enhanced activity can be understood by a tip-enhancement effect at the Pt site that induces strong localized electric field from the curved OLC surface (**Figure 25b**) and a high local proton concentration near the surface (**Figure 25c**).

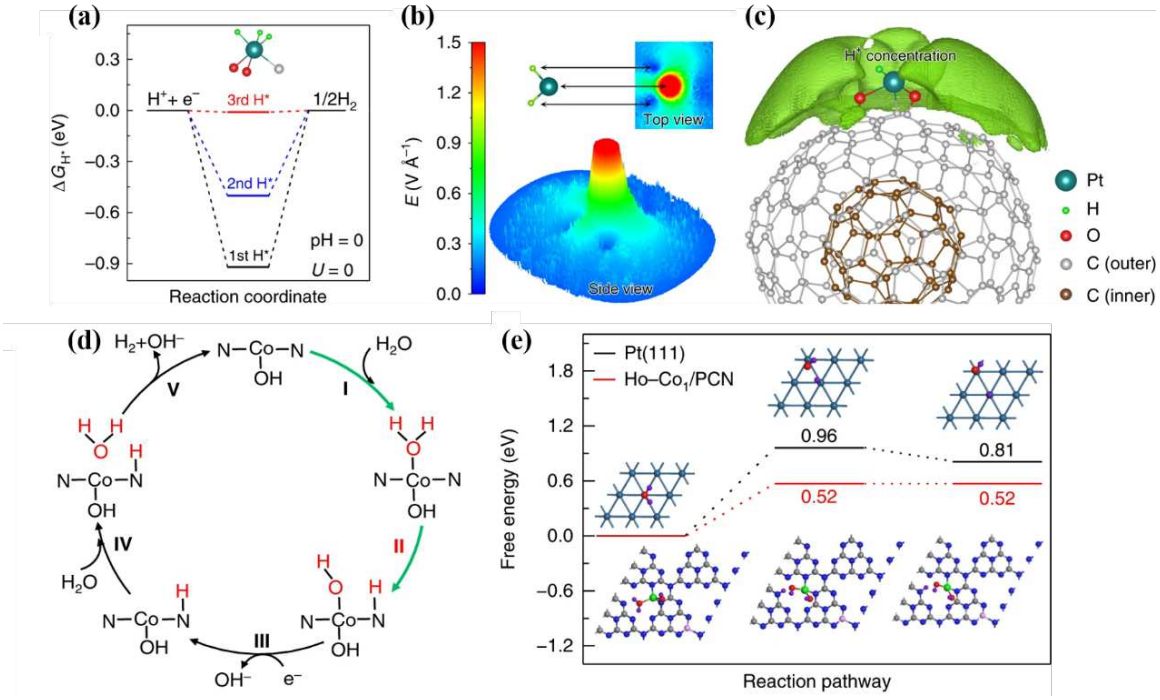

Figure 25. (a) Calculated ΔG_{H^*}, (b) the map of the localized electric field, and (c) the high concentration distribution of protons on the Pt_1/OLC catalyst. Adapted with permission from ref [240]. Copyright 2019 Springer Nature. (d) Alkaline HER mechanism and (e) calculated energy diagram for H_2O dissociation on HO-Co_1/PCN. Adapted with permission from ref [241]. Copyright 2018 Springer Nature.

Despite the fabulous performance of Pt-based SACs in HER electrocatalysis, their extensive applications are hindered for the fancy price and scarcity of Pt. As a consequence, the research of non-precious SACs is more imperative.[242] Transition metals, especially nickel[1, 243-245], cobalt[246-249] and iron[49, 250, 251], are expected to be potential substitutes for Pt due to their abundant reserves and outstanding catalytic performance. For example, Wei et al. discovered that the isolated Co_1-N_4 sites can link with electrolyte hydroxide to form a high-valence HO-Co_1-N_2 active moiety that can induce strong charge transfer under alkaline HER.[241] Theoretical simulations rationalize a catalytic cycle over HO-Co_1/PCN (alkaline Volmer-Heyrovsky, **Figure 25d**): the reaction is triggered by adsorption of a water molecule on Co (step I); then the adsorbed H_2O is dissociated into adsorbed OH* and H* which are bonded to Co and N, respectively (step II); afterwards, another proton from the adjacent water molecule will interact with the first H* to generate H_2 (step III-V). The energetics of the Volmer step (**Figure 25e**) show a much lower barrier for water dissociation on HO-Co_1/PCN than that on Pt (111). This suggests a faster supply of protons on HO-Co_1/PCN that helps to overcome the efficiency loss of the Volmer process. The Wei's research highlights the electrochemical susceptibility of active sites on SACs, opening up a coordination engineering strategy for the development of single-site catalysis.

We should note that the HER activity on SACs is not solely governed by the metal center and the coordination environment, the size effect of the substrate should not be ignored, as indicated by Jiang et al. from their recent theoretical studies.[252] Using N-doped graphene (NG) as the substrate, they made an interesting analogy between nanographene and 2D graphene supported metal SACs (**Figure 26**). The nanographene is sampled by hydrogen-saturated graphene clusters with three different sizes (small, medium and large). The H is found to preferentially adsorb at the top site of the TM atoms. The adsorption strength of H on the large and medium sized nanographenes is comparable to that on the extended 2D graphene, but a significantly weakened H binding by 0.1 ~ 0.3 eV is observed for the small ones. This insight can be used to improve the M-H interaction on the strongly interacted SACs by decreasing the substrate size. Among the

screened 3d, 4d, and 5d TM SACs, the V center embedded in the small N-doped nanographene is the best HER candidate.

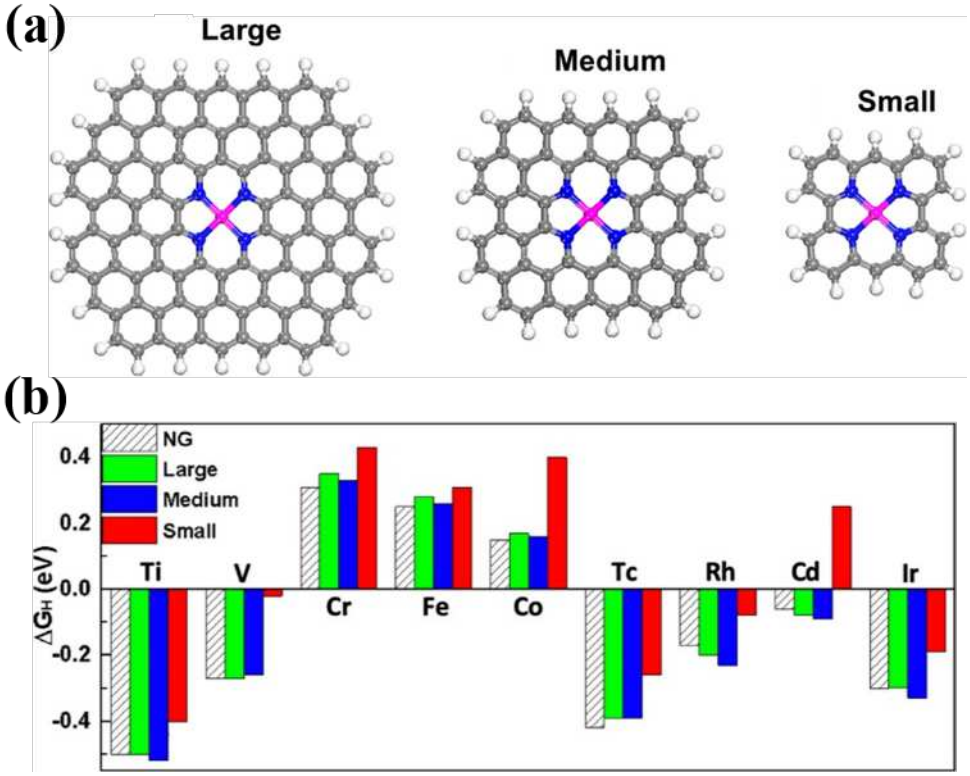

Figure 26. (a) SACs embedded in N-doped nanographenes of different sizes. (b) Comparison of ΔG_H for SACs embedded in N-doped graphene (NG) and N-doped nanographenes. Adapted with permission from ref [252]. Copyright 2020 American Chemical Society.

In addition to the commonly studied metal-based SACs, the non-metal SACs have caught the recent research attention. In this context, Qiao et al. made a ground-breaking progress in the realization of atomically dispersed iodide (I) coordinated with O and Ni (SANi-I) on a Ni foam.[253] The SANi-I catalyst gives rise to good activity and stability for alkaline HER. The in situ Raman spectrum observed the formation of I-H vibrational band. They speculated that the single I atom is the active center to accelerate H_2O dissociation and form I-H_{ads} intermediate, which facilitates the HER kinetics. Building upon this experimental progress, it would be desirable for future study to develop a fundamental understanding of the catalytic mechanism, and guide the design of more

promising non-metal-based SACs.

4.5. MOF−based Catalysts. Metal organic framework (MOFs) materials are a new class of crystalline porous materials, which are composed of metal ions/cluster centers and organic ligands.[254] In recent years, MOFs and their derivatives have drawn great attention for possible use in the hydrogen production technologies.[255] The MOF-based material can be either used in its pristine forms or as a support to disperse, stabilize, and separate extrinsic catalytically active species. MOFs can also be used as the precursor for the synthesis of various metal compounds or metal/carbon composites with deliberately designed elemental composition and structure.[256, 257] At present, a lot of publications have reviewed the recent progress on the design, characteristics, synthesis and HER applications of MOFs.[255, 258-260] These works are mainly overviewed from an experimental perspective.

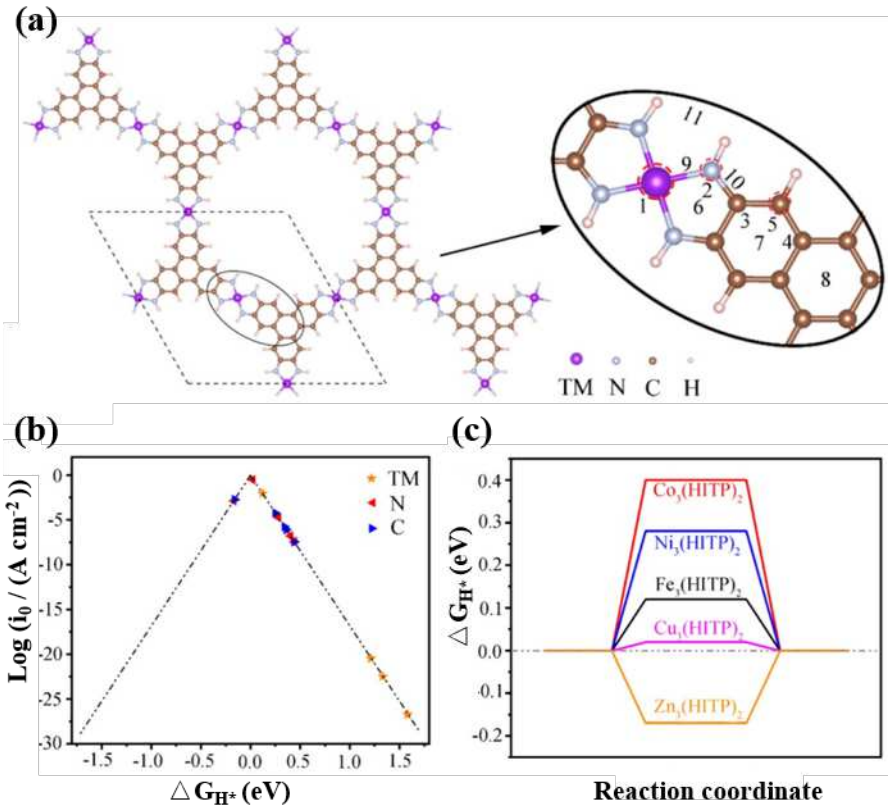

Figure 27. (a) Atomic structure of 2D $TM_3(HITP)_2$ monolayer. The different adsorption sites are labeled in the inset. (b) Volcano curve on $TM_3(HITP)_2$. (c) Calculated free-energy diagram of HER at the equilibrium potential

for $TM_3(HITP)_2$. Adapted with permission from ref [261]. Copyright 2020 American Chemical Society.

Particularly, the 2D MOFs nanosheets are gaining increasing attention for HER. They can be considered as a unique type of single-atom catalysts immobilized by organic linker in a highly robust and well-arranged form. Compared with the 3D counterparts, the 2D MOFs have many favorable features such as the higher accessibility of the active sites without diffusion limitations and the exchangeable coordination positions at the metal or linker nodes.[262] This enables a flexible design of the coordination structure around the nodes to tune the electronic and catalytic properties. For example, based on the synthesized 2D cobalt dithiolene nanosheets,[263] Li et al. theoretically designed a series of 2D π-conjugated MOFs by changing the metal atoms and the linker ligands, and discovered several promising catalysts (Rh–N, Ir–N, Ru–O, Rh–O, and Pd–S linkage) with metallic conductivity and high HER activity comparable to the experimental cobalt dithiolene catalysts.[264] They found the coordinated metal center is the main active center for hydrogen adsorption. In another example, Zhao et al. explored the electrocatalytic activity of various 2D $TM_3(HITP)_2$ nanosheets (HITP = 2,3,6,7,10,11-hexaiminotriphenylene group, **Figure 27**), which are built upon the experimental $Ni_3(HITP)_2$ structure by altering the TM from Fe to Zn.[261] They tested different adsorption sites, and found that the optimal active sites of 2D $TM_3(HITP)_2$ for hydrogen adsorption are on the top of the N atom, expect for $Fe_3(HITP)_2$ where the top of TM is more active. They attributed the high HER activity of the N atom to the p−d hybridization between N and TM atoms which tunes the interaction with adsorbed H. Finally, they predicted $Cu_3(HITP)_2$ to be an active bifunctional catalyst for both HER and OER. In their another work, they showed that the TM embedded in the 2D polymeric phthalocyanine (PC) nanosheets exhibit multifunctional electrocatalytic activity and the pyridine N site is the preferred active center for HER.[265] Although 2D MOFs show potential good activity and efficiency, their developments are still in an early stage, and the number of theoretical studies at the moment is quite low. The limited examples shown here are expected to trigger further research and theoretical understanding of 2D

MOFs in HER electrocatalysis.

5. Summary and Perspectives

In this review, the basic aspects of the HER have been introduced, including the proton–coupled electron transfer, its reaction mechanisms, kinetic analysis and key activity descriptors. Moreover, some developments of DFT-based calculation toward HER are also emphasized systematically such as the CHE model introduced by Nørskov et al., ΔG_{H^*} calculation, Free-Energy Diagram, some local environment considerations in model system, electronic structure (d-band center, valence-band orbital levels), and some theoretical development beyond CHE, aiming to sort out a clear context for theoretical simulation of HER electrocatalysis. The essence of exploring the catalytic mechanism is to reach a reasonable understanding of the active sites of the catalyst, and theoretical simulations and related calculation algorithms can provide great opportunities for carrying out a series of basic research and comprehensively exploring the inherent active sites. The theoretical understanding and insights on the identification of active sites towards the HER process in some typical case examples are specially summarized, which is crucially important for theoretically exploring the structure-activity relationship and catalytic mechanism of HER electrocatalyst, thereby providing essential guidelines for the activity screening and design of such electrocatalysts at the atomic level. Therefore, the design of HER electrocatalysts under the guidance of theoretical calculations is expected to achieve efficient atomic utilization and large-scale applications.

Combining the existing calculation and experimental methods, it can be seen that great progress has been made in the design of high-efficiency HER electrocatalysts, but there are still some problems to be solved. Among them, the research of high-performance alkaline HER electrocatalysts has made significant progress, but the origin of its activity still needs the fundamental basis, especially there are still many controversies about the descriptors of alkaline HER. In addition, although the correlation between j_0 and ΔG_{H^*} in DFT-derived volcano plots is

attractive, the model is still too simplistic, ignoring some important effects, such as double-layer effects and solvation. In general, the main process of theoretical simulation is carried out under ideal conditions such as ultra-high vacuum. At present, calculating ΔG_{H^*} in vacuum can fundamentally meet the requirements for efficient screening of HER electrocatalysts, but it will be of scientific significance to fully consider all experimental parameters and variables in a calculation scheme. In practice, the actual reaction atmosphere is complex, including reactants, environmental molecules, *pH* and solvation issues. The interaction between environment and reaction intermediates is of paramount importance to explore the accurate catalytic mechanisms. The current theoretical simulations are mainly focused on simple reactions involving only key intermediates and electronic structures. To address these challenges, from the perspective of atomic scale simulation, DFT methodology for accurately describing relatively complex surface and interface under real HER conditions is urgently needed to explore the essence of catalytic activity. Among them, the combination of various physical and chemical methods, such as ab initio constrained thermodynamics and micro-kinetic models, may be a promising simulation direction for the development of multi-scale computational modeling methodologies. However, extending this scheme to more complex reactions and systems will likely be computationally extremely expensive, so the exploitation for more readily developed and time-efficient DFT methods will also be an arduous challenge, which requires the close cooperation of various scientists, e.g. materials scientists, computational chemists and electrochemists. At the same time, it is also a promising method to establish a database combining theory and experiment to provide a data platform for systematic and comprehensive exploration of electrocatalysts. Then, use high-throughput calculations, screening and other related methods to quickly and truly predict their structure-property relationships. In this regard, recent developments in artificial intelligence algorithms, such as the convolutional neural network based machine learning model, in lieu of DFT, has begun to show its ability to reveal complex heterogeneous reaction mechanisms, which may also become a trend of vigorous development in the future.

Acknowledgments

D.J. is sponsored by National Science Foundation (CBET-1924545). Q. T. acknowledges the support from National Natural Science Foundation of China (No.21903008), the Chongqing Science and Technology Commission (cstc2020jcyj-msxmX0382), and the Fundamental Research Funds for the Central Universities (2020CDJQY-A031, 2020CDJ-LHZZ-063).

References

(1) Subbaraman, R.; Tripkovic, D.; Strmcnik, D.; Chang, K.-C.; Uchimura, M.; Paulikas, A. P.; Stamenkovic, V.; Markovic, N. M. Enhancing Hydrogen Evolution Activity in Water Splitting by Tailoring Li^+-$Ni(OH)_2$-Pt Interfaces. *Science* **2011,** *334*, 1256-1260.

(2) Zheng, Y.; Jiao, Y.; Jaroniec, M.; Qiao, S. Z. Advancing the Electrochemistry of the Hydrogen-Evolution Reaction through Combining Experiment and Theory. *Angew. Chem. Int. Ed.* **2015,** *54*, 52-65.

(3) Nørskov, J. K.; Bligaard, T.; Rossmeisl, J.; Christensen, C. H. Towards the computational design of solid catalysts. *Nat. Chem.* **2009,** *1*, 37-46.

(4) Greeley, J.; Markovic, N. M. The road from animal electricity to green energy: combining experiment and theory in electrocatalysis. *Energy Environ. Sci.* **2012,** *5*, 9246-9256.

(5) Jiao, Y.; Zheng, Y.; Jaroniec, M.; Qiao, S. Z. Design of electrocatalysts for oxygen- and hydrogen-involving energy conversion reactions. *Chem. Soc. Rev.* **2015,** *44*, 2060-2086.

(6) Jiao, Y.; Zheng, Y.; Davey, K.; Qiao, S.-Z. Activity origin and catalyst design principles for electrocatalytic hydrogen evolution on heteroatom-doped graphene. *Nat. Energy* **2016,** *1*, 16130.

(7) Stamenkovic, V. R.; Mun, B. S.; Arenz, M.; Mayrhofer, K. J. J.; Lucas, C. A.; Wang, G.; Ross, P. N.; Markovic, N. M. Trends in electrocatalysis on extended and nanoscale Pt-bimetallic alloy surfaces. *Nat. Mater.* **2007,** *6*, 241-247.

(8) Skúlason, E.; Tripkovic, V.; Björketun, M. E.; Gudmundsdottir, S.; Karlberg, G.; Rossmeisl, J.; Bligaard, T.; Jónsson, H.; Nørskov, J. K. Modeling the Electrochemical Hydrogen Oxidation and Evolution Reactions on the Basis of Density Functional Theory Calculations. *J. Phys. Chem. C* **2010,** *114*, 18182-18197.

(9) Nørskov, J. K.; Bligaard, T.; Logadottir, A.; Kitchin, J. R.; Chen, J. G.; Pandelov, S.; Norskov, J. K. Trends in the exchange current for hydrogen evolution. *J. Electrochem. Soc.* **2005,** *152*, J23-J26.

(10) Trasatti, S. Work function, electronegativity, and electrochemical behaviour of metals: III. Electrolytic hydrogen evolution in acid solutions. *J. Electroanal. Chem. Interfacial Electrochem.*

1972, *39*, 163-184.

(11) Greeley, J.; Jaramillo, T. F.; Bonde, J.; Chorkendorff, I. B.; Norskov, J. K. Computational high-throughput screening of electrocatalytic materials for hydrogen evolution. *Nat. Mater.* **2006,** *5*, 909-913.

(12) Hinnemann, B.; Moses, P. G.; Bonde, J.; Jorgensen, K. P.; Nielsen, J. H.; Horch, S.; Chorkendorff, I.; Norskov, J. K. Biornimetic hydrogen evolution: MoS_2 nanoparticles as catalyst for hydrogen evolution. *J. Am. Chem. Soc.* **2005,** *127*, 5308-5309.

(13) Zheng, Y.; Jiao, Y.; Zhu, Y.; Li, L. H.; Han, Y.; Chen, Y.; Du, A.; Jaroniec, M.; Qiao, S. Z. Hydrogen evolution by a metal-free electrocatalyst. *Nat. Commun.* **2014,** *5*, 3783.

(14) Nørskov, J. K.; Rossmeisl, J.; Logadottir, A.; Lindqvist, L.; Kitchin, J. R.; Bligaard, T.; Jónsson, H. Origin of the Overpotential for Oxygen Reduction at a Fuel-Cell Cathode. *J. Phys. Chem. B* **2004,** *108*, 17886-17892.

(15) Peterson, A. A.; Abild-Pedersen, F.; Studt, F.; Rossmeisl, J.; Norskov, J. K. How copper catalyzes the electroreduction of carbon dioxide into hydrocarbon fuels. *Energy Environ. Sci.* **2010,** *3*, 1311-1315.

(16) Calle-Vallejo, F.; Koper, M. T. M. Theoretical Considerations on the Electroreduction of CO to C_2 Species on Cu(100) Electrodes. *Angew. Chem., Int. Ed.* **2013,** *52*, 7282-7285.

(17) Yeh, K.-Y.; Janik, M. J. Density Functional Theory-Based Electrochemical Models for the Oxygen Reduction Reaction: Comparison of Modeling Approaches for Electric Field and Solvent Effects. *J. Comput. Chem.* **2011,** *32*, 3399-3408.

(18) Taylor, C. D.; Wasileski, S. A.; Filhol, J. S.; Neurock, M. First principles reaction modeling of the electrochemical interface: Consideration and calculation of a tunable surface potential from atomic and electronic structure. *Phys. Rev. B* **2006,** *73*, 165402.

(19) Dabo, I., Li, Y., Bonnet, N., Marzari, N. In Fuel Cell Science; Wieckowski, A., Nørskov, J. K., Eds.;. *John Wiley & Sons, Inc.: Hoboken, NJ* **2010,** *108*, pp 415-431.

(20) Otani, M.; Sugino, O. First-principles calculations of charged surfaces and interfaces: A plane-wave nonrepeated slab approach. *Phys. Rev. B* **2006,** *73*, 115407.

(21) Sugino, O.; Hamada, I.; Otani, M.; Morikawa, Y.; Ikeshoji, T.; Okamoto, Y. First-principles molecular dynamics simulation of biased electrode/solution interface. *Surf. Sci.* **2007,** *601*, 5237-5240.

(22) Schnur, S.; Gross, A. Challenges in the first-principles description of reactions in electrocatalysis. *Catal. Today* **2011,** *165*, 129-137.

(23) Nie, X.; Esopi, M. R.; Janik, M. J.; Asthagiri, A. Selectivity of CO_2 Reduction on Copper Electrodes: The Role of the Kinetics of Elementary Steps. *Angew. Chem., Int. Ed.* **2013,** *52*, 2459-2462.

(24) Melander, M. M. Grand canonical ensemble approach to electrochemical thermodynamics, kinetics, and model Hamiltonians. *Curr. Opin. Electrochem.* **2021,** *29*, 100749.

(25) Schwarz, K.; Sundararaman, R. The electrochemical interface in first-principles calculations. *Surf. Sci. Rep.* **2020,** *75*, 100492.

(26) Zheng, Y.; Jiao, Y.; Vasileff, A.; Qiao, S.-Z. The Hydrogen Evolution Reaction in Alkaline Solution: From Theory, Single Crystal Models, to Practical Electrocatalysts. *Angew. Chem. Int. Ed.* **2018,** *57*, 7568-7579.

(27) Tian, X.; Zhao, P.; Sheng, W. Hydrogen Evolution and Oxidation: Mechanistic Studies and Material Advances. *Adv. Mater.* **2019,** *31*, 1808066.

(28) Costentin, C.; Saveant, J.-M. Theoretical and mechanistic aspects of proton-coupled electron transfer in electrochemistry. *Curr. Opin. Electrochem.* **2017,** *1*, 104-109.

(29) Warburton, R. E.; Soudackov, A. V.; Hammes-Schiffer, S. Theoretical Modeling of Electrochemical Proton-Coupled Electron Transfer. *Chem. Rev.* **2022**, doi.org/10.1021/acs.chemrev.1c00929.

(30) McCarthy, B. D.; Donley, C. L.; Dempsey, J. L. Electrode initiated proton-coupled electron transfer to promote degradation of a nickel(II) coordination complex. *Chem. Sci.* **2015,** *6*, 2827-2834.

(31) Costentin, C.; Robert, M.; Savéant, J.-M. Electrochemical and Homogeneous Proton-Coupled Electron Transfers: Concerted Pathways in the One-Electron Oxidation of a Phenol Coupled with an Intramolecular Amine-Driven Proton Transfer. *J. Am. Chem. Soc.* **2006,** *128*, 4552-4553.

(32) Costentin, C.; Louault, C.; Robert, M.; Savéant, J.-M. Evidence for Concerted Proton−Electron Transfer in the Electrochemical Oxidation of Phenols with Water As Proton Acceptor. Tri-tert-butylphenol. *J. Am. Chem. Soc.* **2008,** *130*, 15817-15819.

(33) Costentin, C.; Robert, M.; Saveant, J.-M.; Tard, C. Inserting a Hydrogen-Bond Relay between Proton Exchanging Sites in Proton-Coupled Electron Transfers. *Angew. Chem., Int. Ed.* **2010,** *49*, 3803-3806.

(34) Costentin, C.; Drouet, S.; Robert, M.; Saveant, J.-M. A Local Proton Source Enhances CO_2 Electroreduction to CO by a Molecular Fe Catalyst. *Science* **2012,** *338*, 90-94.

(35) Savéant, J.-M.; Tard, C. Proton-Coupled Electron Transfer in Azobenzene/Hydrazobenzene Couples with Pendant Acid–Base Functions. Hydrogen-Bonding and Structural Effects. *J. Am. Chem. Soc.* **2014,** *136*, 8907-8910.

(36) Rountree, E. S.; Dempsey, J. L. Potential-Dependent Electrocatalytic Pathways: Controlling Reactivity with pKa for Mechanistic Investigation of a Nickel-Based Hydrogen Evolution Catalyst. *J. Am. Chem. Soc.* **2015,** *137*, 13371-13380.

(37) Jackson, M. N.; Surendranath, Y. Donor-Dependent Kinetics of Interfacial Proton-Coupled Electron Transfer. *J. Am. Chem. Soc.* **2016,** *138*, 3228-3234.

(38) Elgrishi, N.; McCarthy, B. D.; Rountree, E. S.; Dempsey, J. L. Reaction Pathways of Hydrogen-Evolving Electrocatalysts: Electrochemical and Spectroscopic Studies of Proton-Coupled Electron Transfer Processes. *ACS Catal.* **2016,** *6*, 3644-3659.

(39) Bonin, J.; Costentin, C.; Robert, M.; Routier, M.; Savéant, J.-M. Proton-Coupled Electron Transfers: pH-Dependent Driving Forces? Fundamentals and Artifacts. *J. Am. Chem. Soc.* **2013,** *135*, 14359-14366.

(40) Costentin, C.; Drouet, S.; Robert, M.; Savéant, J.-M. Turnover Numbers, Turnover Frequencies, and Overpotential in Molecular Catalysis of Electrochemical Reactions. Cyclic Voltammetry and Preparative-Scale Electrolysis. *J. Am. Chem. Soc.* **2012,** *134*, 11235-11242.

(41) Costentin, C.; Dridi, H.; Savéant, J.-M. Molecular Catalysis of H2 Evolution: Diagnosing Heterolytic versus Homolytic Pathways. *J. Am. Chem. Soc.* **2014,** *136*, 13727-13734.

(42) Savéant, J.-M. Molecular Catalysis of Electrochemical Reactions. Mechanistic Aspects. *Chem. Rev.* **2008,** *108*, 2348-2378.

(43) Roubelakis, M. M.; Bediako, D. K.; Dogutan, D. K.; Nocera, D. G. Proton-coupled electron transfer kinetics for the hydrogen evolution reaction of hangman porphyrins. *Energy Environ. Sci.* **2012,** *5*, 7737-7740.

(44) Rountree, E. S.; McCarthy, B. D.; Eisenhart, T. T.; Dempsey, J. L. Evaluation of Homogeneous Electrocatalysts by Cyclic Voltammetry. *Inorg. Chem.* **2014,** *53*, 9983-10002.

(45) Venkataraman, C.; Soudackov, A. V.; Hammes-Schiffer, S. Theoretical Formulation of Nonadiabatic Electrochemical Proton-Coupled Electron Transfer at Metal−Solution Interfaces. *J. Phys. Chem. C* **2008,** *112*, 12386-12397.

(46) Ludlow, M. K.; Soudackov, A. V.; Hammes-Schiffer, S. Electrochemical Proton-Coupled Electron Transfer of an Osmium Aquo Complex: Theoretical Analysis of Asymmetric Tafel Plots and Transfer Coefficients. *J. Am. Chem. Soc.* **2010,** *132*, 1234-1235.

(47) Horvath, S.; Fernandez, L. E.; Soudackov, A. V.; Hammes-Schiffer, S. Insights into proton-coupled electron transfer mechanisms of electrocatalytic H_2 oxidation and production. *Proc. Natl. Acad. Sci. U. S. A.* **2012,** *109*, 15663-15668.

(48) Shi, Y.; Zhang, B. Recent advances in transition metal phosphide nanomaterials: synthesis and applications in hydrogen evolution reaction. *Chem. Soc. Rev.* **2016,** *45*, 1529-1541.

(49) Zou, X.; Zhang, Y. Noble metal-free hydrogen evolution catalysts for water splitting. *Chem. Soc. Rev.* **2015,** *44*, 5148-5180.

(50) Subbaraman, R.; Tripkovic, D.; Chang, K.-C.; Strmcnik, D.; Paulikas, A. P.; Hirunsit, P.; Chan, M.; Greeley, J.; Stamenkovic, V.; Markovic, N. M. Trends in activity for the water electrolyser reactions on 3d M(Ni,Co,Fe,Mn) hydr(oxy)oxide catalysts. *Nat. Mater.* **2012,** *11*, 550-557.

(51) Sheng, W.; Zhuang, Z.; Gao, M.; Zheng, J.; Chen, J. G.; Yan, Y. Correlating hydrogen oxidation and evolution activity on platinum at different pH with measured hydrogen binding energy. *Nat. Commun.* **2015,** *6*, 5848.

(52) Shinagawa, T.; Garcia-Esparza, A. T.; Takanabe, K. Mechanistic Switching by Hydronium Ion Activity for Hydrogen Evolution and Oxidation over Polycrystalline Platinum Disk and Platinum/Carbon Electrodes. *ChemElectroChem* **2014,** *1*, 1497-1507.

(53) Shinagawa, T.; Takanabe, K. Identification of intrinsic catalytic activity for electrochemical reduction of water molecules to generate hydrogen. *Phys. Chem. Chem. Phys.* **2015,** *17*, 15111-15114.

(54) Shinagawa, T.; Takanabe, K. Electrocatalytic Hydrogen Evolution under Densely Buffered

Neutral pH Conditions. *J. Phys. Chem. C* **2015,** *119*, 20453-20458.

(55) Shinagawa, T.; Takanabe, K. New Insight into the Hydrogen Evolution Reaction under Buffered Near-Neutral pH Conditions: Enthalpy and Entropy of Activation. *J. Phys. Chem. C* **2016,** *120*, 24187-24196.

(56) Murthy, A. P.; Govindarajan, D.; Theerthagiri, J.; Madhavan, J.; Parasuraman, K. Metal-doped molybdenum nitride films for enhanced hydrogen evolution in near-neutral strongly buffered aerobic media. *Electrochim. Acta* **2018,** *283*, 1525-1533.

(57) Son, D.-Y.; Bae, K.-H.; Kim, H.-S.; Park, N.-G. Effects of Seed Layer on Growth of ZnO Nanorod and Performance of Perovskite Solar Cell. *J. Phys. Chem. C* **2015,** *119*, 10321-10328.

(58) Strmcnik, D.; Uchimura, M.; Wang, C.; Subbaraman, R.; Danilovic, N.; van der Vliet, D.; Paulikas, A. P.; Stamenkovic, V. R.; Markovic, N. M. Improving the hydrogen oxidation reaction rate by promotion of hydroxyl adsorption. *Nat. Chem.* **2013,** *5*, 300-306.

(59) Zhou, Z.; Pei, Z.; Wei, L.; Zhao, S.; Jian, X.; Chen, Y. Electrocatalytic hydrogen evolution under neutral pH conditions: current understandings, recent advances, and future prospects. *Energy Environ. Sci.* **2020,** *13*, 3185-3206.

(60) Conway, B. E.; Tilak, B. V. Interfacial processes involving electrocatalytic evolution and oxidation of H2, and the role of chemisorbed H. *Electrochim. Acta* **2002,** *47*, 3571-3594.

(61) Katsounaros, I.; Meier, J. C.; Klemm, S. O.; Topalov, A. A.; Biedermann, P. U.; Auinger, M.; Mayrhofer, K. J. J. The effective surface pH during reactions at the solid–liquid interface. *Electrochem. Commun* **2011,** *13*, 634-637.

(62) Durst, J.; Siebel, A.; Simon, C.; Hasché, F.; Herranz, J.; Gasteiger, H. A. New insights into the electrochemical hydrogen oxidation and evolution reaction mechanism. *Energy Environ. Sci.* **2014,** *7*, 2255-2260.

(63) Sabatier, P. *La catalyse en chimie organique*; Librairie Polytechnique, Paris et Liège, 1920.

(64) Parsons, R. The rate of electrolytic hydrogen evolution and the heat of adsorption of hydrogen. *Trans. Faraday Soc.* **1958,** *54*, 1053-1063.

(65) Sholl, D. S.; Steckel, J. A. *Density functional theory: A practical introduction*; Wiley, 2009.

(66) Bendavid, L. I.; Carter, E. A. CO_2 adsorption on Cu_2O (111): a DFT+ U and DFT-D study. *J. Phys. Chem. C* **2013,** *117*, 26048-26059.

(67) Zhao, X.; Liu, Y. Unveiling the Active Structure of Single Nickel Atom Catalysis: Critical Roles of Charge Capacity and Hydrogen Bonding. *J. Am. Chem. Soc.* **2020,** *142*, 5773-5777.

(68) Sundararaman, R.; Vigil-Fowler, D.; Schwarz, K. Improving the Accuracy of Atomistic Simulations of the Electrochemical Interface. *Chem. Rev.* **2022**, doi.org/10.1021/acs.chemrev.1c00800.

(69) Hörmann, N. G.; Marzari, N.; Reuter, K. Electrosorption at metal surfaces from first principles. *npj Comput. Mater.* **2020,** *6*, 136.

(70) Filhol, J. S.; Neurock, M. Elucidation of the electrochemical activation of water over Pd by first principles. *Angew. Chem. Int. Ed.* **2006,** *118*, 416-420.

(71) Skúlason, E.; Karlberg, G. S.; Rossmeisl, J.; Bligaard, T.; Greeley, J.; Jónsson, H.; Nørskov,

J. K. Density functional theory calculations for the hydrogen evolution reaction in an electrochemical double layer on the Pt(111) electrode. *Phys. Chem. Chem. Phys.* **2007,** *9*, 3241-3250.

(72) Chan, K.; Nørskov, J. K. Electrochemical Barriers Made Simple. *J. Phys. Chem. Lett.* **2015,** *6*, 2663-2668.

(73) Chan, K.; Nørskov, J. K. Potential Dependence of Electrochemical Barriers from ab Initio Calculations. *J. Phys. Chem. Lett.* **2016,** *7*, 1686-1690.

(74) Kim, D.; Shi, J.; Liu, Y. Substantial Impact of Charge on Electrochemical Reactions of Two-Dimensional Materials. *J. Am. Chem. Soc.* **2018,** *140*, 9127-9131.

(75) Sundararaman, R.; Goddard III, W. A.; Arias, T. A. Grand canonical electronic density-functional theory: Algorithms and applications to electrochemistry. *J. Chem. Phys.* **2017,** *146*, 114104.

(76) Huang, Y.; Nielsen, R. J.; Goddard, W. A. Reaction Mechanism for the Hydrogen Evolution Reaction on the Basal Plane Sulfur Vacancy Site of MoS_2 Using Grand Canonical Potential Kinetics. *J. Am. Chem. Soc.* **2018,** *140*, 16773-16782.

(77) Roudgar, A.; Groß, A. Water bilayer on the Pd/Au(111) overlayer system: Coadsorption and electric field effects. *Chem. Phys. Lett.* **2005,** *409*, 157-162.

(78) Rossmeisl, J.; Skúlason, E.; Björketun, M. E.; Tripkovic, V.; Nørskov, J. K. Modeling the electrified solid-liquid interface. *Chem. Phys. Lett.* **2008,** *466*, 68-71.

(79) Feibelman, P. J.; Bartelt, N. C.; Nie, S.; Thürmer, K. Interpretation of high-resolution images of the best-bound wetting layers on Pt (111). *J. Chem. Phys.* **2010,** *133*, 154703.

(80) Ogasawara, H.; Brena, B.; Nordlund, D.; Nyberg, M.; Pelmenschikov, A.; Pettersson, L. G. M.; Nilsson, A. Structure and bonding of water on Pt (111). *Phys. Rev. Lett.* **2002,** *89*, 276102.

(81) Taylor, C.; Kelly, R. G.; Neurock, M. Theoretical analysis of the nature of hydrogen at the electrochemical interface between water and a Ni (111) single-crystal electrode. *J. Electrochem. Soc.* **2007,** *154*, 55-64.

(82) Hamada, I.; Morikawa, Y. Density-functional analysis of hydrogen on Pt (111): Electric field, solvent, and coverage effects. *J. Phys. Chem. C* **2008,** *112*, 10889-10898.

(83) Saleheen, M.; Heyden, A. Liquid-Phase Modeling in Heterogeneous Catalysis. *ACS Catal.* **2018,** *8*, 2188-2194.

(84) Steinmann, S. N.; Sautet, P.; Michel, C. Solvation free energies for periodic surfaces: comparison of implicit and explicit solvation models. *Phys. Chem. Chem. Phys.* **2016,** *18*, 31850-31861.

(85) Zhang, X.; Sewell, T. E.; Glatz, B.; Sarupria, S.; Getman, R. B. On the water structure at hydrophobic interfaces and the roles of water on transition-metal catalyzed reactions: A short review. *Catal. Today* **2017,** *285*, 57-64.

(86) He, Z.-D.; Hanselman, S.; Chen, Y.-X.; Koper, M. T.; Calle-Vallejo, F. Importance of solvation for the accurate prediction of oxygen reduction activities of Pt-based electrocatalysts. *J. Phys. Chem. Lett.* **2017,** *8*, 2243-2246.

(87) Tomasi, J.; Mennucci, B.; Cammi, R. Quantum mechanical continuum solvation models. *Chem. Rev.* **2005,** *105*, 2999-3094.

(88) Mathew, K.; Sundararaman, R.; Letchworth-Weaver, K.; Arias, T.; Hennig, R. G. Implicit solvation model for density-functional study of nanocrystal surfaces and reaction pathways. *J. Chem. Phys.* **2014,** *140*, 084106.

(89) Gan, J.; Li, F.; Tang, Q. Vacancies-Engineered M_2CO_2 MXene as an Efficient Hydrogen Evolution Reaction Electrocatalyst. *J. Phys. Chem. Lett.* **2021,** *12*, 4805-4813.

(90) Nishihara, S.; Otani, M. Hybrid solvation models for bulk, interface, and membrane: Reference interaction site methods coupled with density functional theory. *Phys. Rev. B* **2017,** *96*, 115429.

(91) Misin, M.; Fedorov, M. V.; Palmer, D. S. Communication: Accurate hydration free energies at a wide range of temperatures from 3D-RISM. *J. Chem. Phys.* **2015,** *142*, 091105.

(92) Plaza, M.; Huang, X.; Ko, J. Y. P.; Shen, M.; Simpson, B. H.; Rodriguez-Lopez, J.; Ritzert, N. L.; Letchworth-Weaver, K.; Gunceler, D.; Schlom, D. G.; Arias, T. A.; Brock, J. D.; Abruna, H. D. Structure of the Photo-catalytically Active Surface of $SrTiO_3$. *J. Am. Chem. Soc.* **2016,** *138*, 7816-7819.

(93) Sundararaman, R.; Letchworth-Weaver, K.; Schwarz, K. A.; Gunceler, D.; Ozhabes, Y.; Arias, T. A. JDFTx: Software for joint density-functional theory. *SoftwareX* **2017,** *6*, 278-284.

(94) Sundararaman, R.; Goddard, W. A., III The charge-asymmetric nonlocally determined local-electric (CANDLE) solvation model. *J. Chem. Phys.* **2015,** *142*, 064107.

(95) Rossmeisl, J.; Chan, K.; Ahmed, R.; Tripković, V.; Björketun, M. E. pH in atomic scale simulations of electrochemical interfaces. *Phys. Chem. Chem. Phys.* **2013,** *15*, 10321-10325.

(96) Durst, J.; Simon, C.; Hasché, F.; Gasteiger, H. A. Hydrogen oxidation and evolution reaction kinetics on carbon supported Pt, Ir, Rh, and Pd electrocatalysts in acidic media. *J. Electrochem. Soc.* **2014,** *162*, F190-F203.

(97) Marković, N. M.; Schmidt, T. J.; Grgur, B. N.; Gasteiger, H. A.; Behm, R. J.; Ross, P. N. Effect of temperature on surface processes at the Pt (111)−liquid interface: hydrogen adsorption, oxide Formation, and CO oxidation. *J. Phys. Chem. B* **1999,** *103*, 8568-8577.

(98) Govindarajan, N.; Xu, A.; Chan, K. How pH affects electrochemical processes. *Science* **2022,** *375*, 379-380.

(99) Sheng, W.; Myint, M.; Chen, J. G.; Yan, Y. Correlating the hydrogen evolution reaction activity in alkaline electrolytes with the hydrogen binding energy on monometallic surfaces. *Energy Environ. Sci.* **2013,** *6*, 1509-1512.

(100) Zheng, J.; Sheng, W.; Zhuang, Z.; Xu, B.; Yan, Y. Universal dependence of hydrogen oxidation and evolution reaction activity of platinum-group metals on pH and hydrogen binding energy. *Sci. Adv.* **2016,** *2*, e1501602.

(101) Cheng, T.; Wang, L.; Merinov, B. V.; Goddard III, W. A. Explanation of dramatic pH-dependence of hydrogen binding on noble metal electrode: Greatly weakened water adsorption at high pH. *J. Am. Chem. Soc.* **2018,** *140*, 7787-7790.

(102) Lamoureux, P. S.; Singh, A. R.; Chan, K. pH Effects on Hydrogen Evolution and Oxidation over Pt(111): Insights from First-Principles. *ACS Catal.* **2019,** *9*, 6194-6201.

(103) Schouten, K. J. P.; Van Der Niet, M. J. T. C.; Koper, M. T. M. Impedance spectroscopy of H and OH adsorption on stepped single-crystal platinum electrodes in alkaline and acidic media. *Phys. Chem. Chem. Phys.* **2010,** *12*, 15217-15224.

(104) Ledezma-Yanez, I.; Wallace, W. D. Z.; Sebastián-Pascual, P.; Climent, V.; Feliu, J. M.; Koper, M. T. M. Interfacial water reorganization as a pH-dependent descriptor of the hydrogen evolution rate on platinum electrodes. *Nat. Energy* **2017,** *2*, 17031.

(105) Lasia, A. Studies of the mechanism and kinetics of hydrogen adsorption and absorption. *Pol. J. Chem.* **1995,** *69*, 639-650.

(106) Bockris, J. O. M.; Carbajal, J. L.; Scharifker, B. R.; Chandrasekaran, K. Adsorbed hydrogen on iron in the electrochemical reduction of protons: an FTIR study. *J. Electrochem. Soc* **1987,** *134*, 1957.

(107) Abd Elhamid, M. H.; Ateya, B. G.; Weil, K. G.; Pickering, H. W. Calculation of the hydrogen surface coverage and rate constants of the hydrogen evolution reaction from polarization data. *J. Electrochem. Soc.* **2000,** *147*, 2148-2150.

(108) Kunimatsu, K.; Uchida, H.; Osawa, M.; Watanabe, M. In situ infrared spectroscopic and electrochemical study of hydrogen electro-oxidation on Pt electrode in sulfuric acid. *J. Electroanal. Chem.* **2006,** *587*, 299-307.

(109) Kunimatsu, K.; Senzaki, T.; Samjeské, G.; Tsushima, M.; Osawa, M. Hydrogen adsorption and hydrogen evolution reaction on a polycrystalline Pt electrode studied by surface-enhanced infrared absorption spectroscopy. *Electrochim. Acta* **2007,** *52*, 5715-5724.

(110) Wang, J.; Yan, M.; Zhao, K.; Liao, X.; Wang, P.; Pan, X.; Yang, W.; Mai, L. Field effect enhanced hydrogen evolution reaction of MoS_2 nanosheets. *Adv. Mater.* **2017,** *29*, 1604464.

(111) Ling, F.; Zhou, T.; Liu, X.; Kang, W.; Zeng, W.; Zhang, Y.; Fang, L.; Lu, Y.; Zhou, M. Electric field tuned MoS_2/metal interface for hydrogen evolution catalyst from first-principles investigations. *Nanotechnology* **2017,** *29*, 03LT01.

(112) Ling, F.; Liu, X.; Jing, H.; Chen, Y.; Zeng, W.; Zhang, Y.; Kang, W.; Liu, J.; Fang, L.; Zhou, M. Optimizing edges and defects of supported MoS_2 catalysts for hydrogen evolution via an external electric field. *Phys. Chem. Chem. Phys.* **2018,** *20*, 26083-26090.

(113) Wu, Y.; Ringe, S.; Wu, C.-L.; Chen, W.; Yang, A.; Chen, H.; Tang, M.; Zhou, G.; Hwang, H. Y.; Chan, K. A two-dimensional MoS_2 catalysis transistor by solid-state ion gating manipulation and adjustment (SIGMA). *Nano Lett.* **2019,** *19*, 7293-7300.

(114) Wang, Y.; Udyavara, S.; Neurock, M.; Frisbie, C. D. Field effect modulation of electrocatalytic hydrogen evolution at back-gated two-dimensional MoS_2 electrodes. *Nano Lett.* **2019,** *19*, 6118-6123.

(115) Wang, Z.; Wu, H. H.; Li, Q.; Besenbacher, F.; Li, Y.; Zeng, X. C.; Dong, M. Reversing interfacial catalysis of ambipolar WSe_2 single crystal. *Adv. Sci.* **2020,** *7*, 1901382.

(116) Braga, D.; Gutiérrez Lezama, I.; Berger, H.; Morpurgo, A. F. Quantitative determination

of the band gap of WS_2 with ambipolar ionic liquid-gated transistors. *Nano lett.* **2012,** *12*, 5218-5223.

(117) Lieb, J.; Demontis, V.; Prete, D.; Ercolani, D.; Zannier, V.; Sorba, L.; Ono, S.; Beltram, F.; Sacépé, B.; Rossella, F. Ionic-Liquid Gating of InAs Nanowire-Based Field-Effect Transistors. *Adv. Funct. Mater.* **2019,** *29*, 1804378.

(118) Zakhidov, D.; Rehn, D. A.; Reed, E. J.; Salleo, A. Reversible electrochemical phase change in monolayer to bulk-like $MoTe_2$ by ionic liquid gating. *ACS nano* **2020,** *14*, 2894-2903.

(119) Yan, M.; Pan, X.; Wang, P.; Chen, F.; He, L.; Jiang, G.; Wang, J.; Liu, J. Z.; Xu, X.; Liao, X. Field-effect tuned adsorption dynamics of VSe_2 nanosheets for enhanced hydrogen evolution reaction. *Nano Lett.* **2017,** *17*, 4109-4115.

(120) Shi, Y.; Zhou, Y.; Yang, D.-R.; Xu, W.-X.; Wang, C.; Wang, F.-B.; Xu, J.-J.; Xia, X.-H.; Chen, H.-Y. Energy level engineering of MoS_2 by transition-metal doping for accelerating hydrogen evolution reaction. *J. Am. Chem. Soc.* **2017,** *139*, 15479-15485.

(121) Zhang, W.; Liao, X.; Pan, X.; Yan, M.; Li, Y.; Tian, X.; Zhao, Y.; Xu, L.; Mai, L. Superior Hydrogen Evolution Reaction Performance in 2H-MoS_2 to that of 1T Phase. *Small* **2019,** *15*, 1900964.

(122) Nilsson, A.; Pettersson, L. G. M.; Hammer, B.; Bligaard, T.; Christensen, C. H.; Nørskov, J. K. The electronic structure effect in heterogeneous catalysis. *Catal. Lett.* **2005,** *100*, 111-114.

(123) Greeley, J.; Stephens, I. E. L.; Bondarenko, A. S.; Johansson, T. P.; Hansen, H. A.; Jaramillo, T. F.; Rossmeisl, J.; Chorkendorff, I.; Nørskov, J. K. Alloys of platinum and early transition metals as oxygen reduction electrocatalysts. *Nat. Chem.* **2009,** *1*, 552-556.

(124) Shao, M.; Liu, P.; Zhang, J.; Adzic, R. Origin of enhanced activity in palladium alloy electrocatalysts for oxygen reduction reaction. *J. Phys. Chem. B* **2007,** *111*, 6772-6775.

(125) Liu, Y.; Wu, J.; Hackenberg, K. P.; Zhang, J.; Wang, Y. M.; Yang, Y.; Keyshar, K.; Gu, J.; Ogitsu, T.; Vajtai, R. Self-optimizing, highly surface-active layered metal dichalcogenide catalysts for hydrogen evolution. *Nat. Energy* **2017,** *2*, 17127.

(126) Zheng, Y.; Jiao, Y.; Li, L. H.; Xing, T.; Chen, Y.; Jaroniec, M.; Qiao, S. Z. Toward design of synergistically active carbon-based catalysts for electrocatalytic hydrogen evolution. *ACS nano* **2014,** *8*, 5290-5296.

(127) Su, D. S.; Zhang, J.; Frank, B.; Thomas, A.; Wang, X.; Paraknowitsch, J.; Schlögl, R. Metal-free heterogeneous catalysis for sustainable chemistry. *ChemSusChem* **2010,** *3*, 169-180.

(128) Gao, W.; Chen, Y.; Li, B.; Liu, S.-P.; Liu, X.; Jiang, Q. Determining the adsorption energies of small molecules with the intrinsic properties of adsorbates and substrates. *Nat. Commun.* **2020,** *11*, 1196.

(129) Qi, L.; Gao, W.; Jiang, Q. Effective Descriptor for Designing High-Performance Catalysts for the Hydrogen Evolution Reaction. *J. Phys. Chem. C* **2020,** *124*, 23134-23142.

(130) Wang, M.; Zhu, H. Machine Learning for Transition-Metal-Based Hydrogen Generation Electrocatalysts. *ACS Catal.* **2021,** *11*, 3930-3937.

(131) Wexler, R. B.; Martirez, J. M. P.; Rappe, A. M. Chemical Pressure-Driven Enhancement

of the Hydrogen Evolving Activity of Ni_2P from Nonmetal Surface Doping Interpreted via Machine Learning. *J. Am. Chem. Soc.* **2018,** *140*, 4678-4683.

(132) Zheng, J.; Sun, X.; Hu, J.; Wang, S.; Yao, Z.; Deng, S.; Pan, X.; Pan, Z.; Wang, J. Symbolic Transformer Accelerating Machine Learning Screening of Hydrogen and Deuterium Evolution Reaction Catalysts in MA_2Z_4 Materials. *ACS Appl. Mater. Interfaces* **2021,** *13*, 50878-50891.

(133) Jiao, Y.; Zheng, Y.; Jaroniec, M.; Qiao, S. Z. Origin of the electrocatalytic oxygen reduction activity of graphene-based catalysts: a roadmap to achieve the best performance. *J. Am. Chem. Soc.* **2014,** *136*, 4394-4403.

(134) Marković, N. M.; Ross Jr, P. N. Surface science studies of model fuel cell electrocatalysts. *Surf. Sci. Rep.* **2002,** *45*, 117-229.

(135) Yang, F.; Zhang, Q.; Liu, Y.; Chen, S. A theoretical consideration on the surface structure and nanoparticle size effects of Pt in hydrogen electrocatalysis. *J. Phys. Chem. C* **2011,** *115*, 19311-19319.

(136) Sun, F.; Wang, Y.; Fang, L.; Yang, X.; Fu, W.; Tian, D.; Huang, Z.; Li, J.; Zhang, H.; Wang, Y. New vesicular carbon-based rhenium phosphides with all-pH range electrocatalytic hydrogen evolution activity. *Appl. Catal. B: Environmental* **2019,** *256*, 117851.

(137) Shi, Y.; Zhang, B. Correction: Recent advances in transition metal phosphide nanomaterials: synthesis and applications in hydrogen evolution reaction. *Chem. Soc. Rev.* **2016,** *45*, 1781-1781.

(138) Popczun, E. J.; McKone, J. R.; Read, C. G.; Biacchi, A. J.; Wiltrout, A. M.; Lewis, N. S.; Schaak, R. E. Nanostructured nickel phosphide as an electrocatalyst for the hydrogen evolution reaction. *J. Am. Chem. Soc.* **2013,** *135*, 9267-9270.

(139) Liu, P.; Rodriguez, J. A. Catalysts for hydrogen evolution from the [NiFe] hydrogenase to the Ni_2P (001) surface: the importance of ensemble effect. *J. Am. Chem. Soc.* **2005,** *127*, 14871-14878.

(140) Li, S. H.; Zhang, N.; Xie, X.; Luque, R.; Xu, Y. J. Stress-Transfer-Induced In Situ Formation of Ultrathin Nickel Phosphide Nanosheets for Efficient Hydrogen Evolution. *Angew. Chem.* **2018,** *130*, 13266-13269.

(141) Popczun, E. J.; Read, C. G.; Roske, C. W.; Lewis, N. S.; Schaak, R. E. Highly active electrocatalysis of the hydrogen evolution reaction by cobalt phosphide nanoparticles. *Angew. Chem. Int. Ed.* **2014,** *53*, 5427-5430.

(142) Jiang, N.; You, B.; Sheng, M.; Sun, Y. Electrodeposited cobalt-phosphorous-derived films as competent bifunctional catalysts for overall water splitting. *Angew. Chem. Int. Ed.* **2015,** *54*, 6251-6254.

(143) Wang, J.; Liu, Z.; Zheng, Y.; Cui, L.; Yang, W.; Liu, J. Recent advances in cobalt phosphide based materials for energy-related applications. *J. Mater. Chem. A* **2017,** *5*, 22913-22932.

(144) Hu, G.; Tang, Q.; Jiang, D.-E. CoP for hydrogen evolution: implications from hydrogen adsorption. *Phys.Chem.Chem.Phys.* **2016,** *18*, 23864-23871.

(145) Ha, D.-H.; Han, B.; Risch, M.; Giordano, L.; Yao, K. P.; Karayaylali, P.; Shao-Horn, Y. Activity and stability of cobalt phosphides for hydrogen evolution upon water splitting. *Nano Energy* **2016,** *29*, 37-45.

(146) Kibsgaard, J.; Tsai, C.; Chan, K.; Benck, J. D.; Nørskov, J. K.; Abild-Pedersen, F.; Jaramillo, T. F. Designing an improved transition metal phosphide catalyst for hydrogen evolution using experimental and theoretical trends. *Energy Environ. Sci.* **2015,** *8*, 3022-3029.

(147) Zhang, X.; Chen, A.; Chen, L.; Zhou, Z. 2D materials bridging experiments and computations for electro/photocatalysis. *Adv. Energy Mater.* **2021**, 2003841.

(148) Merki, D.; Hu, X. Recent developments of molybdenum and tungsten sulfides as hydrogen evolution catalysts. *Energy Environ. Sci.* **2011,** *4*, 3878-3888.

(149) Yan, Y.; Xia, B.; Xu, Z.; Wang, X. Recent Development of Molybdenum Sulfides as Advanced Electrocatalysts for Hydrogen Evolution Reaction. *ACS Catal.* **2014,** *4*, 1693-1705.

(150) Lv, R.; Robinson, J. A.; Schaak, R. E.; Sun, D.; Sun, Y.; Mallouk, T. E.; Terrones, M. Transition Metal Dichalcogenides and Beyond: Synthesis, Properties, and Applications of Single- and Few-Layer Nanosheets. *Acc. Chem. Res.* **2015,** *48*, 56-64.

(151) Cao, Y. Roadmap and Direction toward High-Performance MoS_2 Hydrogen Evolution Catalysts. *ACS Nano* **2021,** *15*, 11014-11039.

(152) Voiry, D.; Salehi, M.; Silva, R.; Fujita, T.; Chen, M.; Asefa, T.; Shenoy, V. B.; Eda, G.; Chhowalla, M. Conducting MoS_2 Nanosheets as Catalysts for Hydrogen Evolution Reaction. *Nano Lett.* **2013,** *13*, 6222-6227.

(153) Eda, G.; Yamaguchi, H.; Voiry, D.; Fujita, T.; Chen, M.; Chhowalla, M. Photoluminescence from Chemically Exfoliated MoS_2. *Nano Lett.* **2011,** *11*, 5111-5116.

(154) Sokolikova, M. S.; Mattevi, C. Direct synthesis of metastable phases of 2D transition metal dichalcogenides. *Chem. Soc. Rev.* **2020,** *49*, 3952-3980.

(155) Tang, Q.; Jiang, D.-E. Mechanism of Hydrogen Evolution Reaction on 1T-MoS_2 from First Principles. *ACS Catal.* **2016,** *6*, 4953-4961.

(156) Seo, B.; Joo, S. H. Recent advances in unveiling active sites in molybdenum sulfide-based electrocatalysts for the hydrogen evolution reaction. *Nano Converg.* **2017,** *4*, 19.

(157) Zhang, X.; Jia, F.; Song, S. Recent advances in structural engineering of molybdenum disulfide for electrocatalytic hydrogen evolution reaction. *Chem. Eng. J.* **2021,** *405*, 127013.

(158) Li, F.; Tang, Q. Modulating the electronic structure and in-plane activity of two-dimensional transition metal dichalcogenide (MoS_2, TaS_2, NbS_2) monolayers by interfacial engineering. *J. Phys. Chem.* **2020,** *124*, 8822-8833.

(159) Ling, F.; Kang, W.; Jing, H.; Zeng, W.; Chen, Y.; Liu, X.; Zhang, Y.; Qi, L.; Fang, L.; Zhou, M. Enhancing hydrogen evolution on the basal plane of transition metal dichacolgenide van der Waals heterostructures. *NPJ Comput. Mater.* **2019,** *5*, 1-7.

(160) Xu, J.; Zhao, Z.; Wei, W.; Chang, G.; Xie, Z.; Guo, W.; Liu, D.; Qu, D.; Tang, H.; Li, J. Tuning the Intrinsic Activity and Electrochemical Surface Area of MoS_2 via Tiny Zn Doping: Toward an Efficient Hydrogen Evolution Reaction (HER) Catalyst. *Chem. Eur. J.* **2021,** *27*, 15992-

15999.

(161) Deng, J.; Li, H.; Xiao, J.; Tu, Y.; Deng, D.; Yang, H.; Tian, H.; Li, J.; Ren, P.; Bao, X. Triggering the electrocatalytic hydrogen evolution activity of the inert two-dimensional MoS 2 surface via single-atom metal doping. *Energy Environ. Sci.* **2015,** *8*, 1594-1601.

(162) Gao, G.; Sun, Q.; Du, A. Activating Catalytic Inert Basal Plane of Molybdenum Disulfide to Optimize Hydrogen Evolution Activity via Defect Doping and Strain Engineering. *J. Phys. Chem. C* **2016,** *120*, 16761-16766.

(163) Ouyang, Y.; Ling, C.; Chen, Q.; Wang, Z.; Shi, L.; Wang, J. Activating Inert Basal Planes of MoS_2 for Hydrogen Evolution Reaction through the Formation of Different Intrinsic Defects. *Chem. Mater.* **2016,** *28*, 4390-4396.

(164) Zhou, W.; Dong, L.; Tan, L.; Tang, Q. First-principles study of sulfur vacancy concentration effect on the electronic structures and hydrogen evolution reaction of MoS_2. *Nanotechnology* **2021,** *32*, 145718.

(165) Fan, X.; Wang, S.; An, Y.; Lau, W. Catalytic Activity of MS_2 Monolayer for Electrochemical Hydrogen Evolution. *J. Phys. Chem. C* **2016,** *120*, 1623-1632.

(166) Tsai, C.; Chan, K.; Norskov, J. K.; Abild-Pedersen, F. Theoretical insights into the hydrogen evolution activity of layered transition metal dichalcogenides. *Surf. Sci.* **2015,** *640*, 133-140.

(167) Putungan, D. B.; Lin, S.-H.; Kuo, J.-L. A first-principles examination of conducting monolayer 1T ˈ-MX_2 (M = Mo, W; X = S, Se, Te): promising catalysts for hydrogen evolution reaction and its enhancement by strain. *Phys. Chem. Chem. Phys.* **2015,** *17*, 21702-21708.

(168) Pandey, M.; Vojvodic, A.; Thygesen, K. S.; Jacobsen, K. W. Two-Dimensional Metal Dichalcogenides and Oxides for Hydrogen Evolution: A Computational Screening Approach. *J. Phys. Chem. Lett.* **2015,** *6*, 2669-2670.

(169) Lin, S.-H.; Kuo, J.-L. Activating and tuning basal planes of MoO_2, MoS_2, and $MoSe_2$ for hydrogen evolution reaction. *Phys. Chem. Chem. Phys.* **2015,** *17*, 29305-29310.

(170) Gao, G.; Jiao, Y.; Ma, F.; Jiao, Y.; Waclawik, E.; Du, A. Charge Mediated Semiconducting-to-Metallic Phase Transition in Molybdenum Disulfide Monolayer and Hydrogen Evolution Reaction in New 1T' Phase. *J. Phys. Chem. C* **2015,** *119*, 13124-13128.

(171) Chen, X.; Gu, Y.; Tao, G.; Pei, Y.; Wang, G.; Cui, N. Origin of hydrogen evolution activity on MS_2 (M = Mo or Nb) monolayers. *J. Mater. Chem. A* **2015,** *3*, 18898-18905.

(172) Fan, X.-L.; Yang, Y.; Xiao, P.; Lau, W.-M. Site-specific catalytic activity in exfoliated MoS_2 single-layer polytypes for hydrogen evolution: basal plane and edges. *J. Mater. Chem. A* **2014,** *2*, 20545-20551.

(173) Chen, S.; Chen, X.; Wang, G.; Liu, L.; He, Q.; Li, X.-B.; Cui, N. Reaction mechanism with thermodynamic structural screening for electrochemical hydrogen evolution on monolayer 1T′ phase MoS_2. *Chem. Mater.* **2018,** *30*, 5404-5411.

(174) Chen, J.; Li, F.; Tang, Y.; Tang, Q. Tuning the phase stability and surface HER activity of 1T′-MoS_2 by covalent chemical functionalization. *J. Mater. Chem. C* **2020,** *8*, 15852-15859.

(175) Attanayake, N. H.; Thenuwara, A. C.; Patra, A.; Aulin, Y. V.; Tran, T. M.; Chakraborty, H.; Borguet, E.; Klein, M. L.; Perdew, J. P.; Strongin, D. R. Effect of intercalated metals on the electrocatalytic activity of 1T-MoS_2 for the hydrogen evolution reaction. *ACS Energy Lett.* **2017,** *3*, 7-13.

(176) Naguib, M.; Kurtoglu, M.; Presser, V.; Lu, J.; Niu, J.; Heon, M.; Hultman, L.; Gogotsi, Y.; Barsoum, M. W. Two-dimensional nanocrystals produced by exfoliation of Ti_3AlC_2. *Adv. Mater.* **2011,** *23*, 4248-4253.

(177) Nam, H.; Sim, E. S.; Je, M.; Choi, H.; Chung, Y.-C. Theoretical Approach toward Optimum Anion-Doping on MXene Catalysts for Hydrogen Evolution Reaction: an Ab Initio Thermodynamics Study. *ACS Appl. Mater. Inter.* **2021,** *13*, 37035-37043.

(178) Seh, Z. W.; Fredrickson, K. D.; Anasori, B.; Kibsgaard, J.; Strickler, A. L.; Lukatskaya, M. R.; Gogotsi, Y.; Jaramillo, T. F.; Vojvodic, A. Two-dimensional molybdenum carbide (MXene) as an efficient electrocatalyst for hydrogen evolution. *ACS Energy Lett.* **2016,** *1*, 589-594.

(179) Gao, G.; O'Mullane, A. P.; Du, A. 2D MXenes: a new family of promising catalysts for the hydrogen evolution reaction. *ACS Catal.* **2017,** *7*, 494-500.

(180) Ling, C.; Shi, L.; Ouyang, Y.; Wang, J. Searching for Highly Active Catalysts for Hydrogen Evolution Reaction Based on O-Terminated MXenes through a Simple Descriptor. *Chem. Mater.* **2016,** *28*, 9026-9032.

(181) Bai, X.; Ling, C.; Shi, L.; Ouyang, Y.; Li, Q.; Wang, J. Insight into the catalytic activity of MXenes for hydrogen evolution reaction. *Sci. Bull.* **2018,** *63*, 1397-1403.

(182) Pandey, M.; Thygesen, K. S. Two-dimensional MXenes as catalysts for electrochemical hydrogen evolution: A computational screening study. *J. Phys. Chem. C* **2017,** *121*, 13593-13598.

(183) Ling, C.; Shi, L.; Ouyang, Y.; Chen, Q.; Wang, J. Transition metal-promoted V_2CO_2 (MXenes): a new and highly active catalyst for hydrogen evolution reaction. *Adv. Sci.* **2016,** *3*, 1600180.

(184) Cheng, Y.-W.; Dai, J.-H.; Zhang, Y.-M.; Song, Y. Transition metal modification and carbon vacancy promoted Cr_2CO_2 (MXenes): a new opportunity for a highly active catalyst for the hydrogen evolution reaction. *J. Mater. Chem. A* **2018,** *6*, 20956-20965.

(185) Gan, J.; Li, F.; Tang, Y.; Tang, Q. Theoretical Study of Transition-Metal-Modified Mo_2CO_2 MXene as a Catalyst for the Hydrogen Evolution Reaction. *ChemSusChem* **2020,** *13*, 6005-6015.

(186) Kong, Y.; Yan, S.; Feng, J.; Wang, S.; Pan, H. Design of phosphorus-functionalized MXenes for highly efficient hydrogen evolution reaction. *J. Mater. Chem. A* **2021,** *9*, 597-606.

(187) Zheng, J.; Sun, X.; Qiu, C.; Yan, Y.; Yao, Z.; Deng, S.; Zhong, X.; Zhuang, G.; Wei, Z.; Wang, J. High-Throughput Screening of Hydrogen Evolution Reaction Catalysts in MXene Materials. *J. Phys. Chem. C* **2020,** *124*, 13695-13705.

(188) Gu, Y.; Wei, B.; Legut, D.; Fu, Z.; Du, S.; Zhang, H.; Francisco, J. S.; Zhang, R. Single Atom-Modified Hybrid Transition Metal Carbides as Efficient Hydrogen Evolution Reaction Catalysts. *Adv. Funct. Mater.* **2021,** *31*, 2104285.

(189) Hong, Y.-L.; Liu, Z.; Wang, L.; Zhou, T.; Ma, W.; Xu, C.; Feng, S.; Chen, L.; Chen, M.-L.; Sun, D.-M. Chemical vapor deposition of layered two-dimensional $MoSi_2N_4$ materials. *Science* **2020,** *369*, 670-674.

(190) Chen, J.; Tang, Q. The Versatile Electronic, Magnetic and Photo-electro Catalytic Activity of a New 2D MA2Z4 Family. *Chem. Eur. J.* **2021,** *27*, 9925-9933.

(191) Liu, Y.; Ji, Y.; Li, Y. Multilevel Theoretical Screening of Novel Two-Dimensional MA_2Z_4 Family for Hydrogen Evolution. *J. Phys. Chem. Lett.* **2021,** *12*, 9149-9154.

(192) Gao, G.; Jiao, Y.; Ma, F.; Jiao, Y.; Waclawik, E.; Du, A. Metal-free graphitic carbon nitride as mechano-catalyst for hydrogen evolution reaction. *J. Catal.* **2015,** *332*, 149-155.

(193) Shao, L.; Sun, H.; Miao, L.; Chen, X.; Han, M.; Sun, J.; Liu, S.; Li, L.; Cheng, F.; Chen, J. Facile preparation of NH_2-functionalized black phosphorene for the electrocatalytic hydrogen evolution reaction. *J. Mater. Chem. A* **2018,** *6*, 2494-2499.

(194) Li, W.; Li, M.; Li, J.; Liang, J.; Adair, K. R.; Hu, Y.; Xiao, Q.; Cui, X.; Li, R.; Brandys, F. Phosphorene Nanosheets Exfoliated from Low-Cost and High-Quality Black Phosphorus for Hydrogen Evolution. *ACS Appl. Nano Mater.* **2020,** *3*, 7508-7515.

(195) Cai, Y.; Gao, J.; Chen, S.; Ke, Q.; Zhang, G.; Zhang, Y.-W. Design of phosphorene for hydrogen evolution performance comparable to platinum. *Chem. Mater.* **2019,** *31*, 8948-8956.

(196) Lu, J.; Zhang, X.; Liu, D.; Yang, N.; Huang, H.; Jin, S.; Wang, J.; Chu, P. K.; Yu, X.-F. Modulation of phosphorene for optimal hydrogen evolution reaction. *ACS Appl. Mater. Interfaces* **2019,** *11*, 37787-37795.

(197) Ryder, C. R.; Wood, J. D.; Wells, S. A.; Yang, Y.; Jariwala, D.; Marks, T. J.; Schatz, G. C.; Hersam, M. C. Covalent functionalization and passivation of exfoliated black phosphorus via aryl diazonium chemistry. *Nat. Chem.* **2016,** *8*, 597-602.

(198) Zhou, W.; Dong, L.; Tan, L.; Tang, Q. Enhancing the Surface Reactivity of Black Phosphorus on Hydrogen Evolution by Covalent Chemistry. *J. Phys. Chem. C* **2021,** *125*, 7581-7589.

(199) Jin, R.; Li, G.; Sharma, S.; Li, Y.; Du, X. Toward Active-Site Tailoring in Heterogeneous Catalysis by Atomically Precise Metal Nanoclusters with Crystallographic Structures. *Chem. Rev.* **2021,** *121*, 567-648.

(200) Olga, L.-A.; Kacprzak, K. A.; Akola, J.; Hkkinen, H. Quantum size effects in ambient CO oxidation catalysed by ligand-protected gold clusters. *Nat. Chem.* **2010,** *2*, 329-334.

(201) Aikens, C. M. Origin of Discrete Optical Absorption Spectra of $M_{25}(SH)_{18}^-$ Nanoparticles (M = Au, Ag). *J. Phys. Chem. C* **2008,** *112*, 19797-19800.

(202) Yang, H.; Wang, Y.; Edwards, A. J.; Yan, J.; Zheng, N. High-yield synthesis and crystal structure of a green Au_{30} cluster co-capped by thiolate and sulfide. *Nat. Chem.* **2014,** *50*, 14325-14327.

(203) Kwak, K.; Choi, W.; Tang, Q.; Kim, M.; Lee, Y.; Jiang, D.-E.; Lee, D. A molecule-like $PtAu_{24}(SC_6H_{13})_{18}$ nanocluster as an electrocatalyst for hydrogen production. *Nat. Commun.* **2017,** *8*, 14723.

(204) Hu, G.; Tang, Q.; Lee, D.; Zili, W.; Jian, D.-E. Metallic Hydrogen in Atomically Precise Gold Nanoclusters. *Chem. Mater.* **2017,** *29*, 4840-4847.

(205) Choi, W.; Hu, G.; Kwak, K.; Kim, M.; Jiang, D.-E.; Choi, J.-P.; Lee, D. Effects of metal-doping on hydrogen evolution reaction catalyzed by MAu_{24} and M_2Au_{36} nanoclusters (M= Pt, Pd). *ACS Appl. Mater. Inter.* **2018,** *10*, 44645-44653.

(206) Chen, J.; Zhang, Q.-F.; Bonaccorso, T. A.; Williard, P. G.; Wang, L.-S. Controlling gold nanoclusters by diphospine ligands. *J. Am. Chem. Soc.* **2014,** *136*, 92-95.

(207) Naveen, M. H.; Khan, R.; Bang, J. H. Gold Nanoclusters as Electrocatalysts: Atomic Level Understanding from Fundamentals to Applications. *Chem. Mater.* **2021,** *33*, 7595-7612.

(208) Deng, C.; Li, F.; Tang, Q. Electrocatalytic Oxygen Reduction Reaction over the $Au_{22}(L^8)_6$ Nanocluster with Promising Activity: A DFT Study. *J. Phys. Chem. C* **2019,** *123*, 27116-27123.

(209) Wu, Z.; Hu, G.; Jiang, D.-E.; Mullins, D. R.; Zhang, Q.-F.; Allard Jr, L. F.; Wang, L.-S.; Overbury, S. H. Diphosphine-protected Au_{22} nanoclusters on oxide supports are active for gas-phase catalysis without ligand removal. *Nano Lett.* **2016,** *16*, 6560-6567.

(210) Hu, G.; Wu, Z.; Jiang, D.-E. Stronger-than-Pt hydrogen adsorption in a Au_{22} nanocluster for the hydrogen evolution reaction. *J. Mater. Chem. A* **2018,** *6*, 7532-7537.

(211) Takano, S.; Hasegawa, S.; Suyama, M.; Tsukuda, T. Hydride Doping of Chemically Modified Gold-Based Superatoms. *Acc. Chem. Res.* **2018,** *51*, 3074-3083.

(212) Yuan, S.-F.; Li, J.-J.; Guan, Z.-J.; Lei, Z.; Wang, Q.-M. Ultrastable hydrido gold nanoclusters with the protection of phosphines. *Chem. Commun.* **2020,** *56*, 7037-7040.

(213) Dong, J.; Gao, Z. H.; Zhang, Q. F.; Wang, L. S. The Synthesis, Bonding, and Transformation of a Ligand-Protected Gold Nanohydride Cluster. *Angew. Chem. Int. Ed.* **2021,** *60*, 2424-2430.

(214) Li, Y.; Li, S.; Nagarajan, A. V.; Liu, Z.; Nevins, S.; Song, Y.; Mpourmpakis, G.; Jin, R. Hydrogen Evolution Electrocatalyst Design: Turning Inert Gold into Active Catalyst by Atomically Precise Nanochemistry. *J. Am. Chem. Soc.* **2021,** *143*, 11102-11108.

(215) Zhu, J.; Hu, L.; Zhao, P.; Lee, L. Y. S.; Wong, K.-Y. Recent Advances in Electrocatalytic Hydrogen Evolution Using Nanoparticles. *Chem. Rev.* **2020,** *120*, 851-918.

(216) Tan, T. L.; Wang, L.-L.; Zhang, J.; Johnson, D. D.; Bai, K. Platinum nanoparticle during electrochemical hydrogen evolution: adsorbate distribution, active reaction species, and size effect. *ACS Catal.* **2015,** *5*, 2376-2383.

(217) Zalineeva, A.; Baranton, S.; Coutanceau, C.; Jerkiewicz, G. Octahedral palladium nanoparticles as excellent hosts for electrochemically adsorbed and absorbed hydrogen. *Sci. Adv.* **2017,** *3*, e1600542.

(218) Corona, B.; Howard, M.; Zhang, L.; Henkelman, G. Computational screening of core@ shell nanoparticles for the hydrogen evolution and oxygen reduction reactions. *J. Chem. Phys.* **2016,** *145*, 244708.

(219) Trindell, J. A.; Duan, Z.; Henkelman, G.; Crooks, R. M. Well-Defined Nanoparticle Electrocatalysts for the Refinement of Theory. *Chem. Rev.* **2020,** *120*, 814-850.

(220) Sun, T.; Xu, L.; Wang, D.; Li, Y. Metal organic frameworks derived single atom catalysts for electrocatalytic energy conversion. *Nano Res.* **2019,** *12*, 2067-2080.

(221) Wang, A.; Li, J.; Zhang, T. Heterogeneous single-atom catalysis. *Nat. Rev. Chem.* **2018,** *2*, 65-81.

(222) Cui, X.; Li, W.; Ryabchuk, P.; Junge, K.; Beller, M. Bridging homogeneous and heterogeneous catalysis by heterogeneous single-metal-site catalysts. *Nat. Catal.* **2018,** *1*, 385-397.

(223) Zhuo, H.-Y.; Zhang, X.; Liang, J.-X.; Yu, Q.; Xiao, H.; Li, J. Theoretical understandings of graphene-based metal single-atom catalysts: stability and catalytic performance. *Chem. Rev.* **2020,** *120*, 12315-12341.

(224) Zhao, Y.; Zhou, H.; Chen, W.; Tong, Y.; Zhao, C.; Lin, Y.; Jiang, Z.; Zhang, Q.; Xue, Z.; Cheong, W.-C.; Jin, B.; Zhou, F.; Wang, W.; Chen, M.; Hong, X.; Dong, J.; Wei, S.; Li, Y.; Wu, Y. Two-Step Carbothermal Welding To Access Atomically Dispersed Pd^{-1} on Three-Dimensional Zirconia Nanonet for Direct Indole Synthesis. *J. Am. Chem. Soc.* **2019,** *141*, 10590-10594.

(225) Yao, Y.; Hu, S.; Chen, W.; Huang, Z.-Q.; Wei, W.; Yao, T.; Liu, R.; Zang, K.; Wang, X.; Wu, G.; Yuan, W.; Yuan, T.; Zhu, B.; Liu, W.; Li, Z.; He, D.; Xue, Z.; Wang, Y.; Zheng, X.; Dong, J.; Chang, C.-R.; Chen, Y.; Hong, X.; Luo, J.; Wei, S.; Li, W.-X.; Strasser, P.; Wu, Y.; Li, Y. Engineering the electronic structure of single atom Ru sites via compressive strain boosts acidic water oxidation electrocatalysis. *Nat. Catal.* **2019,** *2*, 304-313.

(226) Wang, X.; Li, Z.; Qu, Y.; Yuan, T.; Wang, W.; Wu, Y.; Li, Y. Review of Metal Catalysts for Oxygen Reduction Reaction: From Nanoscale Engineering to Atomic Design. *Chem* **2019,** *5*, 1486-1511.

(227) Liu, J. Catalysis by Supported Single Metal Atoms. *ACS Catal.* **2017,** *7*, 34-59.

(228) Fan, L.; Liu, P. F.; Yan, X.; Gu, L.; Yang, Z. Z.; Yang, H. G.; Qiu, S.; Yao, X. Atomically isolated nickel species anchored on graphitized carbon for efficient hydrogen evolution electrocatalysis. *Nat. Commun.* **2016,** *7*, 10667.

(229) Liang, H.-W.; Brueller, S.; Dong, R.; Zhang, J.; Feng, X.; Muellen, K. Molecular metal-N-x centres in porous carbon for electrocatalytic hydrogen evolution. *Nat. Commun.* **2015,** *6*, 1-8.

(230) Luo, W.; Wang, Y.; Cheng, C. Ru-based electrocatalysts for hydrogen evolution reaction: Recent research advances and perspectives. *Mater. Today Phys.* **2020,** *15*, 100274.

(231) Lei, Y.; Wang, Y.; Liu, Y.; Song, C.; Li, Q.; Wang, D.; Li, Y. Designing Atomic Active Centers for Hydrogen Evolution Electrocatalysts. *Angew. Chem. Int. Ed.* **2020,** *59*, 20794-20812.

(232) Li, L.; Chang, X.; Lin, X.; Zhao, Z.-J.; Gong, J. Theoretical insights into single-atom catalysts. *Chem. Soc. Rev.* **2020,** *49*, 8156-8178.

(233) Chen, Y.; Ji, S.; Chen, C.; Peng, Q.; Wang, D.; Li, Y. Single-atom catalysts: synthetic strategies and electrochemical applications. *Joule* **2018,** *2*, 1242-1264.

(234) Wang, Y.; Wang, D.; Li, Y. Rational Design of Single-Atom Site Electrocatalysts: From Theoretical Understandings to Practical Applications. *Adv. Mater.* **2021,** *33*, 2008151.

(235) Qu, Y.; Chen, B.; Li, Z.; Duan, X.; Wang, L.; Lin, Y.; Yuan, T.; Zhou, F.; Hu, Y.; Yang, Z.; Zhao, C.; Wang, J.; Zhao, C.; Hu, Y.; Wu, G.; Zhang, Q.; Xu, Q.; Liu, B.; Gao, P.; You, R.; Huang,

W.; Zheng, L.; Gu, L.; Wu, Y.; Li, Y. Thermal Emitting Strategy to Synthesize Atomically Dispersed Pt Metal Sites from Bulk Pt Metal. *J. Am. Chem. Soc.* **2019,** *141*, 4505-4509.

(236) Cheng, N.; Stambula, S.; Wang, D.; Banis, M. N.; Liu, J.; Riese, A.; Xiao, B.; Li, R.; Sham, T.-K.; Liu, L.-M.; Botton, G. A.; Sun, X. Platinum single-atom and cluster catalysis of the hydrogen evolution reaction. *Nat. Commun.* **2016,** *7*, 13638.

(237) Zuo, Q.; Liu, T.; Chen, C.; Ji, Y.; Gong, X.; Mai, Y.; Zhou, Y. Ultrathin Metal-Organic Framework Nanosheets with Ultrahigh Loading of Single Pt Atoms for Efficient Visible-Light-Driven Photocatalytic H_2 Evolution. *Angew. Chem. Int. Ed.* **2019,** *58*, 10198-10203.

(238) Zhang, L.; Han, L.; Liu, H.; Liu, X.; Luo, J. Potential-Cycling Synthesis of Single Platinum Atoms for Efficient Hydrogen Evolution in Neutral Media. *Angew. Chem., Int. Ed.* **2017,** *56*, 13694-13698.

(239) Ye, S.; Luo, F.; Zhang, Q.; Zhang, P.; Xu, T.; Wang, Q.; He, D.; Guo, L.; Zhang, Y.; He, C.; Ouyang, X.; Gu, M.; Liu, J.; Sun, X. Highly stable single Pt atomic sites anchored on aniline-stacked graphene for hydrogen evolution reaction. *Energy Environ. Sci.* **2019,** *12*, 1000-1007.

(240) Li, D.; Li, X.; Chen, S.; Yang, H.; Wang, C.; Wu, C.; Haleem, Y. A.; Duan, S.; Lu, J.; Ge, B.; Ajayan, P. M.; Luo, Y.; Jiang, J.; Song, L. Atomically dispersed platinum supported on curved carbon supports for efficient electrocatalytic hydrogen evolution. *Nat. Energy* **2019,** *4*, 512-518.

(241) Cao, L.; Luo, Q.; Liu, W.; Lin, Y.; Liu, X.; Cao, Y.; Zhang, W.; Wu, Y.; Yang, J.; Yao, T.; Wei, S. Identification of single-atom active sites in carbon-based cobalt catalysts during electrocatalytic hydrogen evolution. *Nat. Catal.* **2019,** *2*, 134-141.

(242) Moschkowitsch, W.; Lori, O.; Elbaz, L. Recent Progress and Viability of PGM-Free Catalysts for Hydrogen Evolution Reaction and Hydrogen Oxidation Reaction. *ACS Catal.* **2022,** *12*, 1082-1089.

(243) Ouyang, T.; Chen, A.-N.; He, Z.-Z.; Liu, Z.-Q.; Tong, Y. Rational design of atomically dispersed nickel active sites in beta-Mo_2C for the hydrogen evolution reaction at all pH values. *Chem. Commun.* **2018,** *54*, 9901-9904.

(244) Jiang, K.; Siahrostami, S.; Zheng, T.; Hu, Y.; Hwang, S.; Stavitski, E.; Peng, Y.; Dynes, J.; Gangisetty, M.; Su, D.; Attenkofer, K.; Wang, H. Isolated Ni single atoms in graphene nanosheets for high-performance CO_2 reduction. *Energy Environ. Sci.* **2018,** *11*, 893-903.

(245) Gong, M.; Wang, D.-Y.; Chen, C.-C.; Hwang, B.-J.; Dai, H. A mini review on nickel-based electrocatalysts for alkaline hydrogen evolution reaction. *Nano Res.* **2016,** *9*, 28-46.

(246) Ling, T.; Zhang, T.; Ge, B.; Han, L.; Zheng, L.; Lin, F.; Xu, Z.; Hu, W.-B.; Du, X.-W.; Davey, K.; Qiao, S.-Z. Well-Dispersed Nickel- and Zinc-Tailored Electronic Structure of a Transition Metal Oxide for Highly Active Alkaline Hydrogen Evolution Reaction. *Adv. Mater.* **2019,** *31*, 1807771.

(247) Jiang, H.; Liu, Y.; Li, W.; Li, J. Co Nanoparticles Confined in 3D Nitrogen-Doped Porous Carbon Foams as Bifunctional Electrocatalysts for Long-Life Rechargeable Zn-Air Batteries. *Small* **2018,** *14*, 1703739.

(248) Chen, Z.; Wu, R.; Liu, Y.; Ha, Y.; Guo, Y.; Sun, D.; Liu, M.; Fang, F. Ultrafine Co

Nanoparticles Encapsulated in Carbon-Nanotubes-Grafted Graphene Sheets as Advanced Electrocatalysts for the Hydrogen Evolution Reaction. *Adv. Mater.* **2018,** *30*, 1802011.

(249) Shi, Q.; Wang, Y.; Wang, Z.; Lei, Y.; Wang, B.; Wu, N.; Han, C.; Xie, S.; Gou, Y. Three-dimensional (3D) interconnected networks fabricated via in-situ growth of N-doped graphene/carbon nanotubes on Co-containing carbon nanofibers for enhanced oxygen reduction. *Nano Res.* **2016,** *9*, 317-328.

(250) Yu, F.; Yu, L.; Mishra, I. K.; Yu, Y.; Ren, Z. F.; Zhou, H. Q. Recent developments in earth-abundant and non-noble electrocatalysts for water electrolysis. *Mater. Today Phys.* **2018,** *7*, 121-138.

(251) Kong, D.; Cha, J. J.; Wang, H.; Lee, H. R.; Cui, Y. First-row transition metal dichalcogenide catalysts for hydrogen evolution reaction. *Energy Environ. Sci.* **2013,** *6*, 3553-3558.

(252) Fung, V.; Hu, G.; Wu, Z.; Jiang, D.-E. Descriptors for hydrogen evolution on single atom catalysts in nitrogen-doped graphene. *J. Phys. Chem. C* **2020,** *124*, 19571-19578.

(253) Zhao, Y.; Ling, T.; Chen, S.; Jin, B.; Vasileff, A.; Jiao, Y.; Song, L.; Luo, J.; Qiao, S.-Z. Non-metal Single-Iodine-Atom Electrocatalysts for the Hydrogen Evolution Reaction. *Angew. Chem. Int. Ed.* **2019,** *58*, 12252-12257.

(254) Lee, J.; Farha, O. K.; Roberts, J.; Scheidt, K. A.; Nguyen, S. T.; Hupp, J. T. Metal–organic framework materials as catalysts. *Chem. Soc. Rev.* **2009,** *38*, 1450-1459.

(255) Zhu, B.; Zou, R.; Xu, Q. Metal–organic framework based catalysts for hydrogen evolution. *Adv. Energy Mater.* **2018,** *8*, 1801193.

(256) Shen, K.; Chen, X.; Chen, J.; Li, Y. Development of MOF-Derived Carbon-Based Nanomaterials for Efficient Catalysis. *ACS Catal.* **2016,** *6*, 5887-5903.

(257) Zhao, S.-N.; Song, X.-Z.; Song, S.-Y.; Zhang, H.-j. Highly efficient heterogeneous catalytic materials derived from metal-organic framework supports/precursors. *Coord. Chem. Rev.* **2017,** *337*, 80-96.

(258) Wang, W.; Xu, X.; Zhou, W.; Shao, Z. Recent Progress in Metal-Organic Frameworks for Applications in Electrocatalytic and Photocatalytic Water Splitting. *Adv. Sci.* **2017,** *4*, 1600371.

(259) Mahmood, A.; Guo, W.; Tabassum, H.; Zou, R. Metal-Organic Framework-Based Nanomaterials for Electrocatalysis. *Adv. Energy Mater.* **2016,** *6*, 1600423.

(260) Wang, H.; Zhu, Q.-L.; Zou, R.; Xu, Q. Metal-Organic Frameworks for Energy Applications. *Chem* **2017,** *2*, 52-80.

(261) Wang, J.; Fan, Y.; Qi, S.; Li, W.; Zhao, M. Bifunctional HER/OER or OER/ORR catalytic activity of two-dimensional $TM_3(HITP)_2$ with TM= Fe–Zn. *J. Phys. Chem. C* **2020,** *124*, 9350-9359.

(262) Dhakshinamoorthy, A.; Asiri, A. M.; Garcia, H. 2D metal–organic frameworks as multifunctional materials in heterogeneous catalysis and electro/photocatalysis. *Adv. Mater.* **2019,** *31*, 1900617.

(263) Clough, A. J.; Yoo, J. W.; Mecklenburg, M. H.; Marinescu, S. C. Two-dimensional metal–organic surfaces for efficient hydrogen evolution from water. *J. Am. Chem. Soc.* **2015,** *137*, 118-

121.

(264) Ji, Y.; Dong, H.; Liu, C.; Li, Y. Two-dimensional π-conjugated metal–organic nanosheets as single-atom catalysts for the hydrogen evolution reaction. *Nanoscale* **2019,** *11*, 454-458.

(265) Wang, J.; Wang, J.; Qi, S.; Zhao, M. Stable multifunctional single-atom catalysts resulting from the synergistic effect of anchored transition-metal atoms and host covalent–organic frameworks. *J. Phys. Chem. C* **2020,** *124*, 17675-17683.